THE ROLE OF THE CELL CYCLE IN *KARLODINIUM VENEFICUM* TOXICITY: TOOLS AND PREDICTIONS FROM THE LABORATORY

by

Erik L. J. E. Broemsen

A dissertation submitted to the faculty of
The University of North Carolina at Charlotte
in partial fulfillment of the requirements
for the degree of Doctor of Philosophy in
Biology

Charlotte

2023

Approved by:

_____
Dr. Matthew W. Parrow

_____
Dr. Allen R. Place

_____
Dr. Adam M. Reitzel

_____
Dr. Sandra Clinton

_____
Dr. Xiuxia Du

ABSTRACT

ERIK L. J. E. BROEMSEN. The Role of the Cell Cycle in Karlodinium veneficum Toxicity: Tools and Predictions From the Laboratory. (Under the direction of Dr. MATTHEW W. PARROW)

The toxic dinoflagellate *Karlodinium veneficum* forms blooms in estuaries worldwide. These blooms are often associated with severe fish mortalities that are largely caused by production of karlotoxins. The toxicity of these blooms can vary between bloom events and within blooms over time. Laboratory experiments also indicate production of these toxins is inversely related to growth rate, and is light dependent. Additionally, cell cycle studies have found G1 phase of the cell cycle to occur during daylight hours and growth limited cells to arrest in G1 phase. These data suggest a model of karlotoxin biosynthesis that closely corresponds to the cell cycle, wherein rapidly dividing cells have relatively low cellular karlotoxin content while slowly dividing cells arrest in G1 phase proceed through multiple light/dark cycles and light dependent karlotoxin synthesis cycles leading to increased cellular toxicity. Application of this model to field populations of *K. veneficum* may explain the variable toxicity of natural blooms. However, this requires optimization of methods for measuring *in situ* growth rates. The goals of this dissertation were to 1) optimize methodologies for measuring *in situ* growth rates of *K. veneficum*, 2) to evaluate the synchrony of karlotoxin synthesis and the cell cycle, and 3) evaluate the influence of mixotrophic nutrition on cell cycle synchrony. To achieve these goals we optimized image cytometry, a quantitative fluorescence microscopy technique, for cell cycle analysis of *K. veneficum* and demonstrated its feasibility as a technique for estimating *in situ* growth rates following

the cell cycle method. We also determined the duration of cytokinesis, an important component of determining *in situ* growth rates using the mitotic index technique that in the case of *K. veneficum* must be determined in the laboratory. Lastly, we evaluated the synchrony between karlotoxin synthesis and the cell cycle and the effects of mixotrophic nutrition on cell cycle synchrony in laboratory cultures. This work established a set of tools for measuring *in situ* growth rates in *K. veneficum* blooms, demonstrated synchrony between karlotoxin synthesis and G1 phase of the cell cycle, and determined that the *K. veneficum* cell cycle remains synchronous under mixotrophic nutrition. The work described in this dissertation sets the ground work for future field studies that will seek to explain the source of karlotoxin variability observed in natural blooms.

DEDICATION

This dissertation is dedicated to my parents, Edward and Linda Broemsen. Thank you for giving me that which you never received. Without it I would not have had what it takes.

ACKNOWLEDGEMENTS

First I would like to thank my advisor Dr. Matthew Parrow for starting my career in science and guiding me through this great endeavor, especially for the hard parts. I would also like to thank my committee members Dr. Allen Place, Dr. Adam Reitzel, Dr. James Oliver, Dr. Sandra Clinton, and Dr. Xiuxia Du for their advice, encouragement, and enthusiasm for science. A special thanks to Dr. Sandra Clinton for joining my committee at short notice.

Additional appreciation is extended to my labmate John Ramsby for his assistance with the intense sampling schedules my experiments required, they would have been nearly impossible without your help.

I must also acknowledge the emotional support, and scientific discussions afforded to me by the friends, graduate students, post doctoral fellows, and faculty that I have had the pleasure of meeting and getting to know during my time here at UNC Charlotte.

A final note of appreciation to the National Oceanic and Atmospheric Administration, National Centers for Coastal Ocean Science ECOHAB Program for providing the funding for this project and supporting me.

TABLE OF CONTENTS

LIST OF TABLES

CHAPTER 2

CHAPTER 3

CHAPTER 4

LIST OF FIGURES

CHAPTER 1

CHAPTER 2

CHAPTER 4

CHAPTER 1

INTRODUCTION

1.1 The history of *Karlodinium veneficum*

Figure 1.1 Toxic dinoflagellate *Karlodinium veneficum*. Scale bar = 10 µm

First discovered in the 1950s, *Karlodinium veneficum* (Figure 1) was originally found in estuary environments on three separate continents, each described independently by different authors (Ballantine, 1956; Braarud, 1957; Hulburt, 1957). The earliest work began with Dr. Mary Parke's isolation of two *Gymnodinium* species from Plymouth Sound, UK in 1949 and 1950. Both of these isolates were originally intended as potential oyster feed, however, observations of toxicity associated with one isolate were soon reported (Bainbridge, 1953; Marshall and Orr, 1955). Formal description would follow in 1956 by Dorothy Ballantine, naming the new species *Gymnodinium vitiligo* and *Gymnodinium veneficum*. Ballantine would note the most significant difference between these species was the potent toxicity of *G. veneficum* (Ballantine, 1956). Meanwhile, also in 1950, the research vessel HDMS Galathea would weigh anchor in Walvis Bay, Namibia during a red water event, coincident with a fish mortality event several days prior (Steemann Nielsen and Jensen, 1957). This region had historically been the site of yearly mass fish mortality events since 1837 (Copenhagen and Fisheries, 1953; Place et al., 2012). During the stayover Professor Einer Steeman Nielsen collected formalin fixed water samples, which were provided to Dr. Trygve Braarud for analysis. These samples were dominated by a

novel species of gymnodinoid dinoflagellate, *G. galatheanum* (Braarud, 1957). While in North America, Hulburt (1957) described a similar novel unarmored dinoflagellate naming it *Gyrodinium estuariale*, however, noting its similarity to *G. vitiligo* and *G. veneficum*. Another similar UK species, *Woloszynskia micra*, would be described by Leadbeater and Dodge (1966), and subsequently renamed to *G. micrum* (Loeblich A, 1970). Then later Bjørnland and Tangen (1979) would isolate another similar gymnodinoid from blooms in the Oslofjord, Norway. However, the authors refrained from assigning identity to this Norwegian isolate due to its marked similarity to these other species, arguing the need to account for pigmentation in the previous descriptions. All of these species would eventually be consolidated under *K. veneficum* in the early 2000s when the genus *Gymnodinium* was shown to be polyphyletic; necessitating the creation of the new genus *Karlodinium* (Daugbjerg et al., 2000; Bergholtz et al., 2006).

Despite the early observations of culture toxicity and associations with fish kills *K. veneficum* was not considered a concerning harmful algal bloom (HAB) species until the 1990s (Nielsen and Strømgren, 1991; Nielsen, 1993; Paulmier et al., 1995; Nielsen, 1996; Glibert and Terlizzi, 1999). Annual fish killing blooms in Alfacs Bay, Spain were first documented in 1994. These events were attributed to *Gy. corsicum*, a species name now considered synonymous with *K. veneficum* (Paulmier et al., 1995; Garcés et al., 2006). The first documented North American *K. veneficum* associated fish kill occurred in July 1996 at the HyRock Fish Farm, Princess Anne, MD. Two additional fish kill events would occur here in 1997 and 1999, eventually leading to closure of the farm due to lost revenue (Glibert and Terlizzi, 1999; Deeds et al., 2002; Place et al., 2012). This event would lead to investigations into the toxic potential of *K. veneficum*, and the toxic

compounds would eventually be purified from an isolate originating from the 1996 bloom (Deeds et al., 2002). Another fish kill associated *K. veneficum* bloom would occur a few years later in a residential retention pond in Mount Pleasant, SC (Kempton et al., 2002; Lewitus et al., 2003). Bloom sample filtrates from this event would demonstrate high hemolytic activity and HPLC purified fractions would have high ichthyotoxicity. The purified fractions would have similar properties to toxins, now known as karlotoxins, purified from the HyRock isolate of *K. veneficum* (CCMP 1975). These observations provided strong evidence that *K. veneficum* was playing a major role in fish mortality events in North America. Outside the U.S. the first documented *K. veneficum* bloom producing karlotoxins would occur in the Swan River Estuary near Perth, Western Australia during the austral autumn of 2005 (Adolf et al., 2015). Toxic *K. veneficum* blooms had become recurrent events starting in 2002 but lacked Karlotoxin analysis prior to 2005. Measurements from this bloom revealed Karlotoxin concentrations high enough to result in larval fish death within four hours. Since 2005, the ability to produce Karlotoxin has been verified in several European strains, including the original Plymouth isolate described by Ballantine (1956) and Norwegian strains described by Bjørnland and Tangen (1979), as well as in several strains from the East China Sea (Cai et al., 2016; Adolf et al., 2020).

1.2 Overview of karlotoxins

The first reports of *K. veneficum* toxicity indicated that karlotoxins were active against a broad range of animals (Bainbridge, 1953; Marshall and Orr, 1955; Abbott and

Ballantine, 1957). The most extensive of these studies tested animal survival against either whole cultures or culture supernatants, finding that all animals tested died within five days, apart from several species of polychaetes able to survive indefinitely (Abbott and Ballantine, 1957). These authors further aimed to elucidate the mode of action of the toxin and developed a bio – assay, informed from their survival screenings. The sensitivity and rapid death of Goby fish (*Gobius virescens* and *Gobius niger)* when immersed in culture lead to their selection in this assay and were used to determine an "approximate lethal concentration" based on time to death. This allowed testing of compounds that might assist with determining the karlotoxin mode of action. Interestingly, the authors found that addition of cholesterol in this assay could confer complete protection from death at high doses and prolong time to death at low doses. Additional experiments conducted in this study using crude toxin extracts and isolated tissues, particularly nerve tissue and frog skin, demonstrated that tissue exposed to karlotoxin had lost action potential and increased sodium permeability. The authors hypothesized that the toxin killed by action against the nervous system via depolarization of excitable cell membranes but conceded that their conclusions were preliminary and further work awaited purification of the associated toxin.

It would be almost 50 years later that these toxins would finally be purified and characterized (Deeds et al., 2002; Kempton et al., 2002; Bachvaroff et al., 2008; Van Wagoner et al., 2008; Peng et al., 2010). Initial purifications would note a difference in UV absorption maxima of karlotoxins purified from Chesapeake Bay strains and South Carolina strains (Deeds et al., 2002; Kempton et al., 2002). These differences would prove to be consistent amongst other isolates based on their geographic origin, with

karlotoxins found in the Chesapeake Bay designated as Karlotoxin 1 (KmTx 1), and those found south of the Chesapeake Bay designated as Karlotoxin 2 (KmTx 2; Deeds et al., 2004). Elucidation of the molecular structure of these compounds would reveal they are polyketide toxins similar in structure to amphidinols (Figure 2; Van Wagoner et al., 2008; Peng et al., 2010; Deeds et al., 2015). The hairpin – like structures feature three distinct regions: a polyol arm, a hinge region, and a lipophilic arm. The spectral differences observed between KmTx 1 and KmTx 2 turned out to be due to chlorination of the terminal diene of the KmTx 2 lipophilic arm (Peng et al., 2010). Other differences include an 18 carbon long lipophilic arm in KmTx 1, which is two carbons longer than KmTx 2 and accounts for the tenfold greater potency of KmTx 1 (Place et al., 2012). At least 19 karlotoxin congeners have thus far been described from isolates around the globe, including from the original Plymouth Sound strain (PLY103) and newer strains from the East China Sea (Place et al., 2012; Cai et al., 2016; Krock et al., 2017; Adolf et al., 2020).

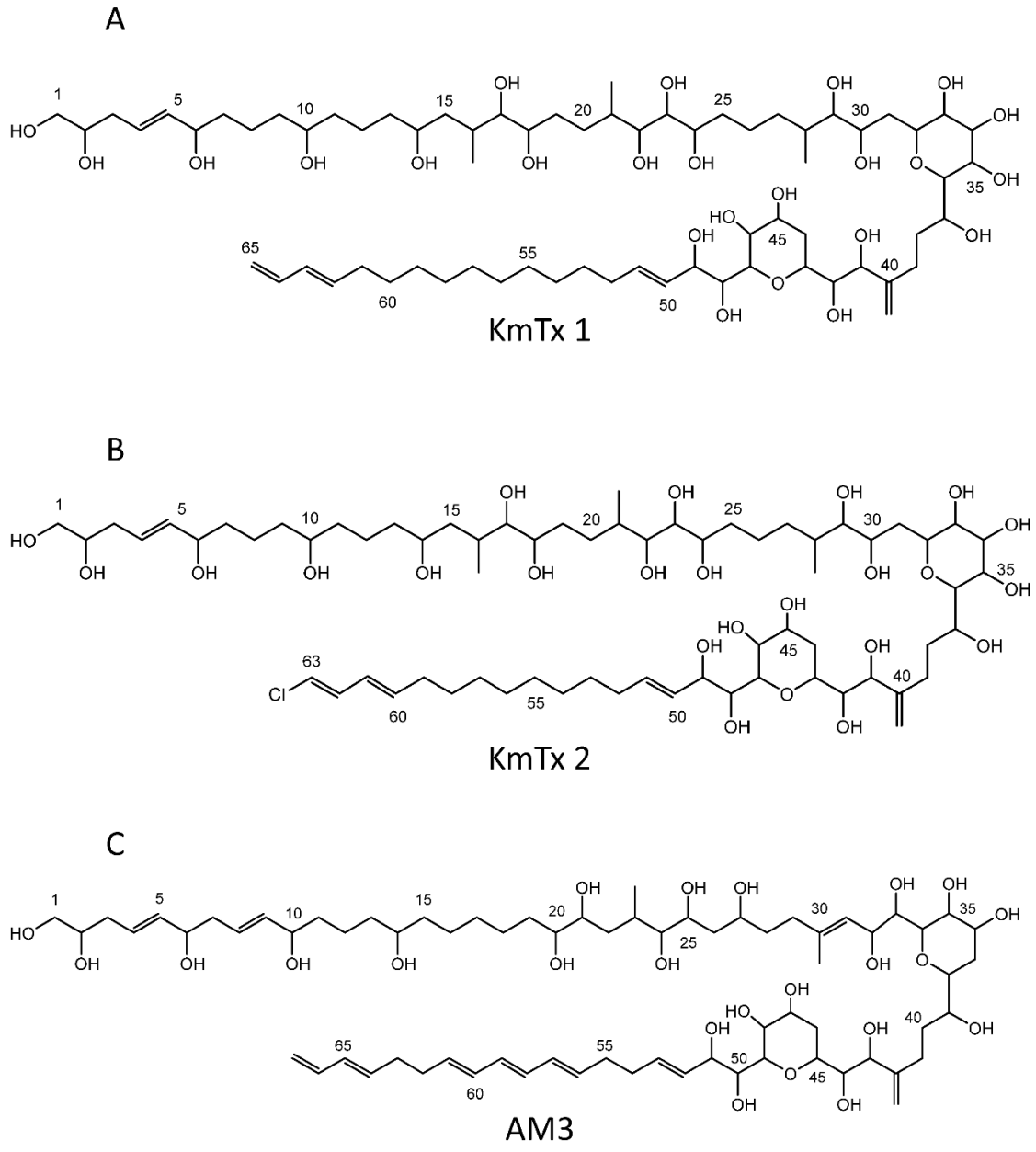

Figure 1.2 Illustration of structural similarities of (A) karlotoxin 1 (KmTx 1), (B) karlotoxin 2 (KmTx 2), and (C) amphidinol 3 (AM3). Figure adapted from Deeds et al., 2015*.

*Reprinted from Aquatic Toxicology, 159, Jonathan R. Deeds, Robert E. Hoesch, Allen R. Place, Joseph P.Y. Kao, The cytotoxic mechanism of karlotoxin 2 (KmTx 2) from *Karlodinium veneficum* (Dinophyceae), 148-155, 2015, with permission from Elsevier.

Karlotoxins are known to be hemolytic, cytotoxic, and ichthyotoxic with fish death ultimately resulting from respiratory failure (Abbott and Ballantine, 1957; Nielsen, 1993; Deeds et al., 2002; Deeds et al., 2006). (Abbott and Ballantine, 1957) suspected that this is due to disruption of action potential in the nervous system via increased membrane ionic permeability. However, histological examination of juvenile Zebra fish (*Danio rerio*) exposed to lethal and sublethal concentrations of KmTx 2 found gill tissues to be the only site of injury (Deeds et al., 2006). Exceptionally high dose exposures of larval Zebra fish to KmTx 2, however, exhibited indiscriminate cellular swelling, and sloughing/lysis of all epithelial surfaces, supporting a cellular mechanism similar to that proposed by Abbott and Ballantine (1957). This mechanism dictates that because intracellular protein concentrations are high, the increased membrane ionic permeability created by Karlotoxins will lead to increased ionic influx. This results in movement of water through osmosis causing cells to then swell and lyse. Such a mechanism could be mediated and lysis inhibited by balancing the extracellular and intracellular osmotic pressure with the addition of extracellular osmolytes. Such mediation was observed by Deeds et al. (2015), where Rainbow Trout (*Oncorhynchus mykiss*) erythrocytes were co – incubated with KmTx 2 and osmolytes ranging in molecular weight from 342.3 g mol^{-1} to 10,000 g mol^{-1} had reduced lysis, with higher molecular weight osmolytes conferring greater protection. Furthermore, through the use of microfluorometric measurement of fluorescent ion indicators and the whole – cell patch – clamp technique increases in cell membrane permeability to Na^{+}, Ca^{+}, and Mn^{2+} following exposure to KmTx 2 were observed. While this is clear evidence that karlotoxins target cell membranes and cause

changes in membrane ionic permeability that led to osmolysis it does not explain the molecular mechanism for these changes.

Like karlotoxins, similarly structured amphidinols also increase membrane permeability (Paul et al., 1995; Houdai et al., 2004). In fact, experiments using phospholipid liposomes have shown this permeability to be modulated based on the liposomal sterol content; with permeability enhanced by greater sterol percentages (Paul et al., 1995; Morsy et al., 2008). Surface plasmon resonance studies have also shown that liposomal sterols enhance the binding efficiency of amphidinols to liposomes (Swasono et al., 2010). Similar interactions between sterols and karlotoxins have also been reported. The original work of Abbott and Ballantine (1957) showed that the addition of ethanol dissolved cholesterol inhibited the toxicity of *K. veneficum* cultures. More recently Deeds and Place (2006) demonstrated that cholesterol and ergosterol both had inhibitory effects on KmTx 2 – induced hemolysis of Rainbow Trout erythrocytes and that the addition of gymnodinosterol, a membrane sterol found abundant in *K. veneficum*, failed to inhibit hemolysis. This suggests that in these hemolysis assays cholesterol and ergosterol bind and sequester KmTx 2 away from the erythrocyte membranes, while gymnodinosterol does not interact with the toxin. These findings along with observations of KmTx 2 – induced lysis of *Oxyrrhis marina*, a co – occurring heterotrophic dinoflagellate lacking gymnodinosterol, and immunity of *K. veneficum* to KmTx 2 suggests a mechanism of cytotoxicity likely similar to that proposed by amphidinols, especially given their structural and behavioral similarities. This mechanism would propose that karlotoxins interact and bind to certain membrane sterols (4 – desmethyl sterols) to form pores that

allow the influx of extracellular ions which leads to cellular osmolysis. However, due to the lack of interaction with gymnodinosterol *K. veneficum* is immune to the effects of the toxin. Such a model is illustrated in Waters et al. (2015), where nuclear magnetic resonance studies were used to identify cholesterol binding sites on KmTx 2 (Figure 3).

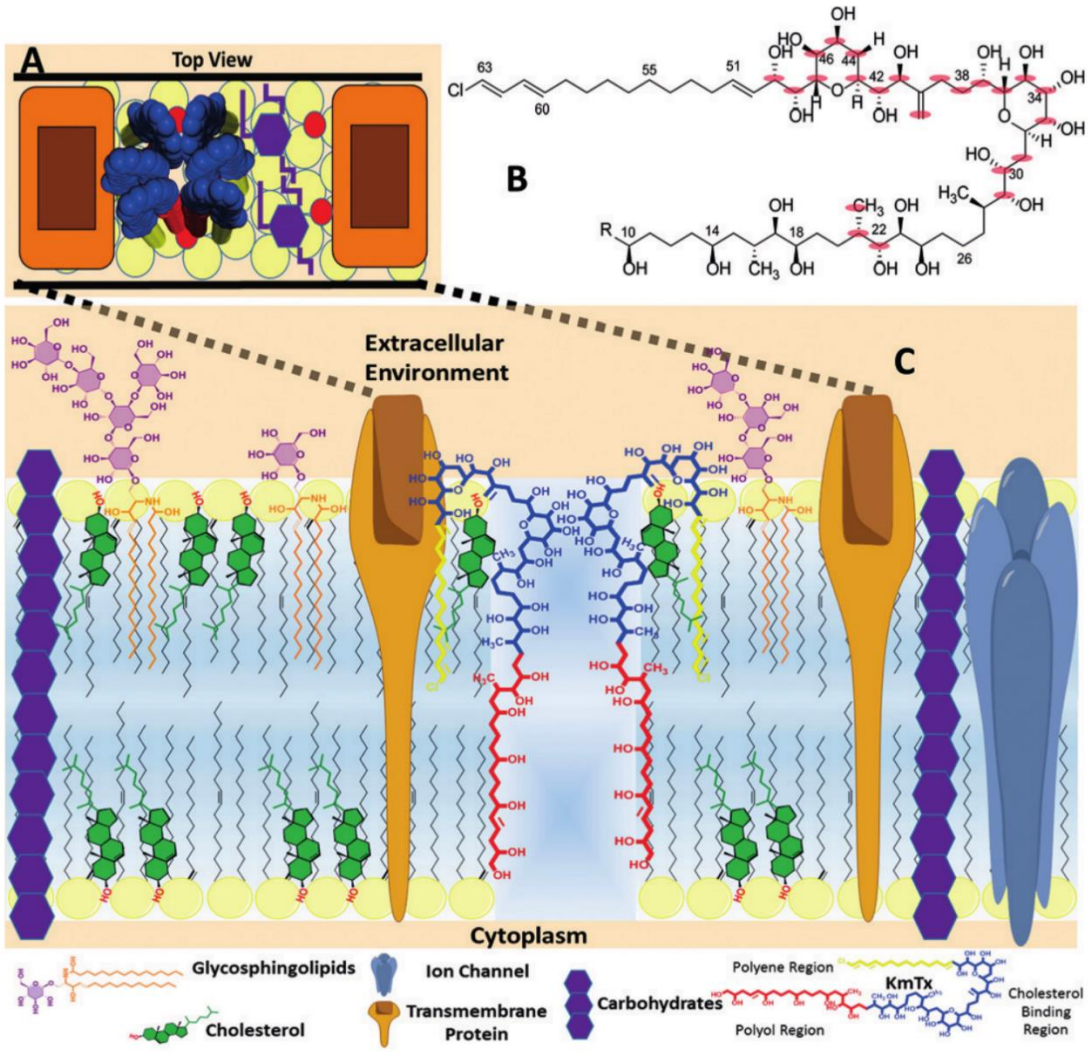

Figure 1.3 Graphical representation of proposed model of mechanism of action for KmTx. (A) Top-down view of pore formed in cell membrane from multiple KmTx and cholesterol molecules. (B) KmTx atoms(highlighted in red) involved in cholesterol interactions. (C) Side view of KmTx/cholesterol pore formed in cell membrane. Figure adapted from Waters et al., 2015*.

*Reprinted from Angewandte Chemie International Edition, 54, Amanda L. Waters, Joonseok Oh, Allen R. Place, and Mark T. Hamann, Stereochemical studies of the karlotoxin class using NMR spectroscopy and DP4 chemical-shift analysis: Insights into their mechanism of action, 15705-15710, 2015, with permission from John Wiley & Sons, Inc.

1.3 Ecology, and Ecophysiology of *K. veneficum*

While populations of *K. veneficum* can be found in estuaries around the globe, those that reside within the Chesapeake Bay have been a source of significant insight into the ecology and ecophysiology of this species. Early field studies found this organism present year-round and widely distributed throughout the Chesapeake Bay (Marshall, 1980; Li et al., 2000b). Populations were generally restricted to salinities between 7 and 18 psu and cell densities of *K. veneficum* correlated positively with concentrations of cryptophyte microalgae (Li et al., 2000b). *Karlodinium veneficum* cells observed in these field studies often contained orange fluorescent inclusions, indicative of phagocytosis of phycoerythrin – containing cryptophyte prey (Li et al., 1996). These studies were the first indication of mixotrophy (i.e., simultaneous autotrophic and heterotrophic nutrition) in *K. veneficum*. This is a common trait amongst dinoflagellates, especially HAB species, and has been proposed as a potential mechanism for triggering bloom development (Smayda, 1997; Stoecker, 1999; Burkholder et al., 2008; Jeong et al., 2010). Often blooms of *K. veneficum* in the Baltimore Inner Harbor are preceded by blooms of cryptophytes. One such bloom occurring in 2007 grew from 21,000 *K. v.* mL^{-1} to over 750,000 *K. v.* mL^{-1} following a cryptophyte bloom three days prior. This rapid increase in *K. veneficum* density was likely in part a result of advection, but increased growth rates due to mixotrophic nutrition undoubtedly played a role. This is apparent in that the percentage of *K. veneficum* cells containing orange fluorescent inclusions spiked from 13 % to 138 % over the course of the cryptophyte bloom, underscoring the importance of mixotrophy in *K. veneficum* bloom initiation (Adolf et al., 2008). These correlations between

cryptophyte and *K. veneficum* blooms in the Chesapeake Bay appear to be a long-term phenomenon. Lin et al. (2018), performing cross – correlational analysis between nutrients, prey abundance, and *K. veneficum* abundance found that together nutrient concentrations and prey abundance could explain up to 46 % of the variance in *K. veneficum* density between the years 2002 and 2011.

Documented prey of *K. veneficum* include diatoms, haptophytes, cryptophytes, and metazoans (Li et al., 1996; Place et al., 2012; Yang et al., 2020). However, cryptophytes are the preferred prey type and phagocytosis of which can increase growth rates by two-to-three-fold relative to phototrophic rates (Li et al., 1999; Adolf et al., 2006b; Calbet et al., 2011). Estimates of the nutritional contribution of cryptophytes suggest that they can supplement as much as 10 % of C, 11 % of N, and 17 % of P required for *K. veneficum* reproduction (Li et al., 2001). Laboratory experiments indicate that cryptophyte ingestion is stimulated by light and nutrient depletion, with the highest rates when P:N ratios were below the Redfield ratio (Li et al., 2000a). Mixotrophy has also been shown to be facilitated by karlotoxins. Adolf et al. (2006a) observed two-to-three-fold increases in rates of prey ingestion when prey cells were co – incubated with *K. veneficum* cells in media containing 25 ng mL^{-1} exogenous KmTx 2. Insight into this effect was provided by Sheng et al. (2010) using digital holographic microscopy, where slowing and immobilization of prey was exposed upon their exposure to toxic strains of *K. veneficum* or purified karlotoxins. Exposure of prey to non – toxic *K. veneficum* strains did not lead to altered swimming patterns. This suggests that karlotoxins facilitate phagocytosis by stunning prey cells prior to ingestion. Interestingly, karlotoxins also have anti – grazing properties, offering toxic strains of *K. veneficum* protection from

grazing by copepods and heterotrophic dinoflagellates that otherwise feed well on non – toxic strains (Delgado and Alcaraz, 1999; Adolf et al., 2007; Waggett et al., 2008).

Little is known about the regulatory and biosynthetic pathways responsible for karlotoxin production, but wide variation in cellular toxin content has been observed between and within cultured strains and bloom events. Comparison of cellular toxin content from cultures and bulk water from *K. veneficum* associated fish kill events indicate a severe degree of variation, with cellular karlotoxin content of bulk water being as much as 10-fold higher (5 – 12 pg $cell^{-1}$) than cultured isolates (0.1 - 1 pg $cell^{-1}$; Deeds et al., 2004). Bachvaroff et al. (2009) also reported significant differences in not only cellular toxin quotas but also differences in karlotoxin congener profiles between isolates; even those isolated from the same water source. Differences in karlotoxin quotas and profiles can also be influenced by environmental conditions. Cultures grown under N or P deplete conditions have been observed to increase cellular karlotoxin quotas by as much as 15-fold, revealing an inverse relationship between toxicity and growth rate. Furthermore, NH_4 as a sole nitrogen source has been observed to alter the ratio of KmTx 3: KmTx1 produced by the Chesapeake Bay strain CCMP 1974 (Adolf et al., 2009). There have also been reports of interactive effects between CO_2 and phosphate concentrations on karlotoxin levels, where conditions with elevated CO_2 and limited phosphate result in more toxic cultures (Fu et al., 2010). Furthermore, karlotoxin has been found to be light dependent and synthesis of which begins with glycolate, a photorespiration byproduct. Also, of importance is the lack of N or P in the molecular structure of karlotoxin (Adolf et al., 2020). These observations suggest that limiting environments, where N or P are unbalanced with the growth needs of *K. veneficum*, are

likely to slow or arrest cell division without impediment to karlotoxin biosynthesis allowing cellular accumulation of karlotoxins.

1.4 Cell Cycle and Toxicity

Few studies have investigated the relationship between the cell cycle and toxin synthesis in HAB species. Those existing studies have observed toxin synthesis taking place during discrete periods of the cell cycle. Saxitoxin production in *Alexandrium fundyense* was found to occur during the first eight hours of the light cycle coinciding with hours during which culture populations occupied G1 phase of the cell cycle, and stopped once cells began entering S phase (Taroncher-Oldenburg et al., 1997). In the case of *Prorocentrum lima*, which produces a suite of diarrhetic shellfish poisoning (DSP) toxins, dinophysistoxin – 4 (DTX4) is produced during G1 phase and early S phase, while okadaic acid (OA) and dinophysistoxin – 1 (DTX1) production occurs during late S phase and G2 + M phase (Pan et al., 1999). Another DSP dinoflagellate, *Dinophysis acuminata*, produced DTX1, OA, and pectenotoxin – 2 throughout G1 phase and S phase (Jia et al 2019). While the hemolytic toxicity of the HAB prymnesiophyte *Chrysocromulina polylepsis* was greatest during hours occupied by G1 phase (Eschbach et al., 2005). Such observations have yet to be made for *K. veneficum.* However, cell cycle studies indicate a strong synchrony with the diel cycle (Adolf et al., 2020). In logarithmically growing phototrophic cultures, small cohorts of cells (15 – 45 %) enter S phase every 24 hours in the late hours of the light phase. Approximately four to five hours later this cohort enters G2 + M phase which then requires another five hours for

completion with the resultant daughter cells re – entering G1 phase before the end of the dark period. Those cells not entering S phase in a single 24-hour period remain in G1 phase until the next light period. Upon entry into stationary phase cells then arrest in G1 phase. These observations demonstrate a strict restriction of S and G2 + M phases to dark periods with well defined durations and relegation of G1 phase predominantly to the light phase with a variable duration dependent on growth conditions.

Considering these cell cycle patterns together with observations of increased toxicity under growth limiting nutrient stress and the light dependence of karlotoxin synthesis suggests the existence of an inverse relationship between cellular proliferation rates and accumulation of cellular karlotoxin. A relationship such that growth limited cells arrest in G1 phase for multiple diel cycles, undergo multiple cycles of light dependent karlotoxin synthesis, and become increasingly toxic (Adolf et al., 2020). Such a model may explain the variable toxicity observed in natural systems (Deeds et al., 2004). However, this model has yet to be tested for *K. veneficum*, requiring specific adaptations and refinement of techniques for measuring *in situ* growth rates of this species. Furthermore, given the prevalence of mixotrophy in natural systems and its impact on growth rates it must be determined if the mixotrophic cell cycle remains synchronized with the diel cycle. The increased growth rates observed in mixotrophic experiments can only be explained by either compression of the duration of one or more cell cycle phases or the decoupling of the cell cycle from the diel cycle (Adolf et al., 2020).

1.5 Measuring Growth Rates *in situ*

In order to measure *in situ* growth rates of natural phytoplankton populations it is necessary to account for losses and gains due to factors such as ocean advection, predator grazing, general cell lysis, and sinking. Therefore, net growth rate calculations based on changes in cell number cannot be used. Indirect methods such as bottle incubations and molecular techniques exist, but are subject to limits from bottle effects, expense, and expertise (Rivkin and Seliger, 1981; Videau, 1987; Lin et al., 1995; Liu et al., 2005; Richardson et al., 2006). Alternatively, cell cycle based methods offer simpler and more direct approaches. The basis of these techniques relies on the identification and measurement of the frequency of cells, in a given sample, that are actively undergoing cell division. This can be based on morphological observation and determination of the frequency of cells in terminal stage(s) of cell division, known as the mitotic index technique, or based on the distribution of cells in different stages of the cell cycle, determined from quantitative fluorometric measurement of nuclear DNA content, also known as the cell cycle method (McDuff and Chisholm, 1982; Carpenter and Chang, 1988). The most accurate use of these techniques requires knowledge of the durations of these terminal stages being quantified. *A priori* knowledge of these durations is rare and is typically carried out by determining *in situ* the time interval between two consecutive terminal stages of cell division. An example with the mitotic index technique would be the time interval between the peak maxima of the time distributions of binucleated cells and paired cells, while for the cell cycle method it would be the time interval between the peak maxima of the frequency of S phase cells and G2 + M phase cells. Unfortunately, in

the case of *K. veneficum* the only morphologically obvious stage of cell division is the paired cell (i.e., dividing cell) stage as cytokinesis and karyokinesis occur simultaneously (Leadbeater and Dodge, 1967). However, the determination of the duration of this stage can be carried out in the laboratory with asynchronous cultures growing in steady state (McDuff and Chisholm, 1982). Alternatively, the cell cycle method would not be as hindered due to the fact that the *K. veneficum* cell cycle exhibits discrete G1, S and G2 + M phases, allowing partitioning of cells into these stages based on nuclear DNA content. However, the preferred method of fluorescent quantification of nuclear DNA content, flow cytometry, would face challenges analyzing natural populations of *K. veneficum* that can exist within complex assemblages of phototrophic, heterotrophic, and mixotrophic protists of varying and potentially overlapping cell size and DNA content. Moreover, mixotrophic microalgae such as *K. veneficum* can contain non – nuclear DNA within phagocytic food vacuoles, which flow cytometry could not distinguish from nuclear DNA. Therefore, microscope-based methods, such as image cytometry, offer the best solution as they allow visual selection and measurement of fluorescently stained nuclei in single cells.

1.6 Project Goals

The aims of this present work were to 1) optimize methodologies for measuring *in situ* growth rates of natural populations of *K. veneficum* (Chapters 1 and 2), 2) determine if, in laboratory cultures, karlotoxin synthesis is correlated with phases of the cell cycle

(Chapter 3), and 3) determine the influence of mixotrophic nutrition on synchrony between the diel and cell cycles (Chapter 3).

The specific aim of chapter 1 was to optimize image cytometry methods for DNA quantification and cell cycle analysis of microalgae, specifically *K. veneficum*. Image cytometry is a microscope based technique wherein a high resolution digital camera is used to capture images of many cells with fluorescently stained DNA in a single field of view. These images are then processed via image analysis software in order to quantify the DNA content of each cell in the image. This process allows, either manually or automatically, the selection and/or exclusion of user designated cells. A useful function for analyzing complex mixed samples such as is found in the environment. These analyses can then be used to determine the cell cycle distribution of the selected population analyzed in a time series of samples, and subsequently calculate an *in situ* growth rate based on the cell cycle method of Carpenter and Chang (1988). The tools and methods described in this chapter are of much utility for coastal management entities and testing of the model for predicting *K. veneficum* bloom toxicity described above.

In chapter 2 our specific aims were to determine the duration of mitosis and assess the variability of this value across a range of environmentally relevant temperatures and geographically distinct strains. These aims are necessary for the utility of the mitotic index technique of McDuff and Chisholm (1982). This technique is a technically simpler alternative to the cell cycle method of Carpenter and Chang (1988) requiring only a simple light microscope and the knowledge of how to identify dividing cells of *K. veneficum*.

Chapter 3 aimed to determine correlations between karlotoxin synthesis and cell cycle phases, as well as to determine the influence of mixotrophic nutrition on cell cycle synchrony. This study served as a laboratory controlled test of our proposed model for prediction of *K. veneficum* bloom toxicity, and functions as a range – finding study for any future studies to test the model in the field. Additionally, insight into how mixotrophic nutrition influences cell cycle synchrony is important for our understanding of the role of mixotrophy in bloom development.

CHAPTER 2

*QUANTITATIVE NUCLEAR DNA CONTENT AND CELL CYCLE ANALYSIS OF A MIXOTROPHIC DINOFLAGELLATE BY IMAGE CYTOMETRY

Erik L. J. E. Broemsen, Allen R. Place, Matthew W. Parrow

*Reprinted with permission from **Broemsen, E.L.J.E., Place, A.R., Parrow, M.W.**, 2021. Quantitative nuclear DNA content and cell cycle analysis of a mixotrophic dinoflagellate by image cytometry. Limnol. Oceanogr. Methods 19(4), 253-266.

Abstract

The goal of this work was to develop and demonstrate the utility of microscope-based image cytometry (ICM) as a method for quantifying nuclear DNA content and cell cycle phase distribution in microalgae both in culture and in natural blooms, as an alternative to flow cytometry (FCM). To do so, aliquots from the same samples of the dinoflagellate *Karlodinium veneficum* were examined using both ICM and FCM. Image cytometry specimen preparation and data acquisition methods were optimized to improve precision and agreement between the two techniques. Accuracy and precision of DNA measurements by ICM were significantly higher using the DNA fluorophore DAPI compared to SYBR® Green I. Milli-Q H2O was found to be superior to Tris-EDTA as a staining and slide preparation solution for ICM analyses. Lower-powered objective magnification (10x, 20x) in image acquisition for ICM produced higher precision in nuclear DNA measurements. Overall precision of ICM analysis of DAPI-stained

Karlodinium veneficum cells was comparable to FCM, with respective 1C DNA peak coefficients of variation as low as 6.2 %. Cell cycle distributions of mid-log culture samples analyzed by both ICM and FCM were in agreement (Two-way ANOVA; $p = 0.93$); while distributions analyzed in a field sample were similar but not identical (Z-test; $p < 0.001$). Overall, the results show the feasibility of image cytometry as a useful tool for microalgal cell cycle analysis, with the potential for more flexible application to mixotrophic/phagotrophic species and complex field populations.

Introduction

The measurement of phytoplankton growth rates in the field is important for understanding how populations respond to environmental factors during blooms. Several methods have been described for determining species-specific *in situ* growth rates of phytoplankton in natural blooms, all of which calculate rates based on the frequency of dividing cells, or the frequency of cells within two consecutive terminal stages of cell division and the duration of time between those stages (McDuff & Chisholm, 1982, Carpenter & Chang, 1988, Vaulot, 1992, Chang & Dam, 1993). The cell cycle method described by Carpenter and Chang (1988) provides one of the most accurate approaches based on its use of cell cycle phases S and G2 + M as the consecutive terminal stages. This approach provides advantages over other methods, which rely on morphological identification of proliferation stages (e.g., cells undergoing cytokinesis or binucleated cells) and *a priori* knowledge of the duration of these stages (Litaker et al., 2002). The cell cycle method requires neither of these, but instead depends upon quantitative

determination of cellular DNA content and assignment of cells in the population to G1, S, or G2 + M phases.

Fluorescent quantification of cellular DNA content by flow cytometry (FCM) is the gold standard for cell cycle analysis. However, mixotrophic microalgae such as *Karlodinium veneficum* that consume other phytoplankton cells may contain significant non-nuclear DNA in phagocytic food vacuoles, along with their organellar DNA in mitochondria and plastids. Flow cytometry cannot distinguish cytoplasmic from nuclear DNA when analyzing whole cells. Furthermore, natural field populations of microalgae typically exist in a complex assemblage of phototrophic, heterotrophic, and mixotrophic protists that can overlap in cell size and DNA content, making a target species difficult to separate out for cell cycle analysis by FCM, particularly when the target species is not numerically dominant in the community. These factors have limited the use of FCM for cell cycle analysis of field populations of microalgae, with notable exceptions (Boucher et al., 1991, Vaulot & Partensky, 1992, Liu et al., 1998), and provided the impetus for using microfluorometry instead (Vaulot & Partensky, 1992, Yamaguchi, 1992, Liu et al., 1997, Garcés et al., 1998, Garcés et al., 1999, Gisselson et al., 1999, Van Dolah & Leighfield, 1999, Garcés & Masó, 2001). Microfluorometry is a microscope slide-based technique wherein a light microscope equipped with a fluorescence spectrophotometer is used to allow visual selection and quantitative measurement of stained DNA fluorescence of nuclei in single cells, one cell at a time. A closable aperture allows the operator to optically exclude non-target cells and cytoplasmic DNA. However, this method is time consuming as it requires measurement of one cell at a time, which typically results in only 200- 300 cells being measured and relatively high coefficients of variation (CV;

coefficient of variation = [peak SD ÷ mean] ×100) on the fluorescence peaks for G1 and G2 phases (Cetta & Anderson, 1990, Garcés et al., 1998, Garcés et al., 1999, Garcés & Masó, 2001).

An alternative approach to measuring DNA fluorescence by microfluorometry is image cytometry (ICM). This slide-based technique uses a linear charge-coupled device (CCD) camera mounted on a light microscope to acquire digital images of fields of view containing multiple cells with fluorescently stained DNA. These images are then processed with image analysis software to measure fluorescence intensity of all user or software-selected nuclei present in the image. Non-target cells and even non-nuclear DNA in target cells can be simply ignored by manual or software-trained selection of the nuclei of interest. This technique offers all the advantages of microfluorometry over flow cytometry for complex cells and samples, with added advantages such as faster data collection and digital storage of the original data (images).

ICM has been used extensively in biomedical research, where it has been shown to have comparable utility for cell cycle analysis as FCM (Galbraith et al., 1991, Wang et al., 1995, Maciorowski et al., 1997, Lamas et al., 2003, Bocsi et al., 2004). Variants of ICM have also been used for cell cycle analysis of two dinoflagellate species (Bhaud et al., 1991, Gisselson et al., 1999) and genome size estimation in *Thalassiosira* spp. diatoms (Von Dassow et al., 2008) and multicellular red algae (Kapraun & Freshwater, 2012, Salvador Soler et al., 2014). However, estimates of precision in measurements, such as 1C DNA peak CV's have rarely accompanied these non-biomedical studies, and overall little effort has been made to optimize methodology and provide comparison to established methods such as FCM on non-clinical cells such as microalgae.

The bloom forming toxic dinoflagellate *K. veneficum* is found in temperate and subtropical coastal seas around the world, where it is responsible for major fish kill events (Deeds et al., 2002, Kempton et al., 2002, Lim et al., 2014). The toxins produced by *K. veneficum,* karlotoxins, have been characterized and can be quantified in cultures and field samples (Deeds & Place, 2006, Bachvaroff et al., 2008, Van Wagoner et al., 2008). Previous studies have shown toxicity of blooms to vary widely, and culture-based studies have observed an inverse relationship between growth rates and toxicity (Deeds et al., 2004, Adolf et al., 2009). While this relationship has yet to be observed in nature, it could explain the variable toxicity observed between *K. veneficum* blooms, and within blooms over time. In order to investigate the relationship between growth rates and toxicity in field blooms, we propose ICM as a useful tool for measuring *in situ* growth using the cell cycle technique. Here we present an optimized methodology for performing ICM based cell cycle analysis of *K. veneficum* with direct comparison to FCM analysis. Furthermore, we apply these methods to field samples collected during a 2016 bloom of *K. veneficum* in the Baltimore Inner Harbor, MD to demonstrate the feasibility of applying cell cycle analysis to natural bloom populations of mixotrophic microalgae.

Materials and procedures

Cultures

Strain 2010 IH was clonally isolated in 2010 and identified as *K. veneficum* from the Baltimore Inner Harbor by co-author Place's laboratory based on morphology and

identical ITS sequence match to other North American *K. veneficum* isolates. Cultures were maintained at 20 °C in 15 ppt EH-1 enriched artificial seawater with 1 mM Hepes, modified from Berges et al. (2001). Illumination was provided by daylight deluxe fluorescent bulbs on a 12h: 12h L: D schedule with a 100 μE m^{-2} s^{-1} intensity.

Sample preparation

Samples were prepared for ICM and FCM analyses by fixing 50 mL of mid-log *K. veneficum* culture in 5 % formalin and 0.1 % Tween 80 (final concentrations) overnight at 4 °C. Following fixation cells were pelleted at 3,000 g for 10 min, resuspended in 50 mL of 70 % methanol, and incubated overnight in darkness at 4 °C. Methanol extracted cells were then pelleted at 2,000 g for 10 minutes and resuspended in 1 mL TE (10 mM Tris-HCl and 1 mM EDTA) with 0.1 % Tween 80.

Microscope instrumentation

All microscopy and ICM was performed with a Zeiss Axio Observer A1 inverted microscope (Carl Zeiss Microscopy GmbH, Jena Germany) equipped with 10x (NA 0.45), 20x (NA 0.8), and 40x (NA 0.95) Plan Apochromat objectives. Epifluorescence excitation was provided by an HBO 103 W/2 mercury short-arc lamp and excitation and emission wavelengths were selected using either a Zeiss filter set 10 (excitation: 450-490 nm, emission: 515-565 nm, beam splitter: 510 nm) or a Zeiss filter set 49 (excitation: 365 nm, emission: 445/50 nm, beam splitter: 395 nm). Images were captured with a Zeiss

Axiocam 506 monochromatic CCD camera with a 2752 x 2208 pixel resolution and a 14-bit pixel depth controlled by Zeiss Zen 2.6 software with image analysis package. Camera exposure times were set initially by autoexposure to a randomly selected field of view for each slide analyzed and the exposure time reduced incrementally until the intensity of all pixels within the image fell within the pixel depth of the image histogram in the Zen 2.6 acquisition software. This ensured utilization of the full dynamic range of the camera.

Image calibration

Even with careful alignment and an apochromatic epi-light train, the mercury arc lamp did not provide a totally even intensity field of excitation light across the entire field of view (e.g., higher excitation intensity in the center compared to the edges). In order to correct for this effect within fluorescent images, each pixel was normalized using a shading reference image. This image was acquired from epi-illumination of a thin film of 10 % fluorescein dissolved in 100 mM $NaHCO_3$ mounted between a microscope slide and a # 1.5 coverslip sealed with clear nail polish, following Model & Burkhardt (2001) and Varga et al. (2004). A new shading reference was acquired for each imaging session following a 15 minute warm up period for the mercury lamp. Exposure time for the shading reference was automatically selected with the “auto exposure” feature. The shading correction was acquired with the “shading correction” feature on the Zen 2.6 image acquisition tab and applied automatically at the time of acquisition for each image. Flow-Check™ Fluorospheres (Beckman Coulter, Fullerton, CA) were used to verify

image calibrations and compare precision of fluorescence measurements between FCM and ICM. A drop of fluorosphere solution was placed on a silicone grease rimmed 25 mm x 25 mm # 1.5 coverslip and mounted to a microscope slide. The slide was placed on the microscope stage with coverslip facing down and fluorospheres allowed to settle on coverslip surface prior to imaging. All imaging sessions were conducted in a darkened room. The microscope light path was directed 100% to the camera, and fields of view were selected in a grid fashion using low-light brightfield displayed on the computer screen. To capture fluorescence images, transmitted light was blocked and epi-illumination triggered for immediate image acquisition.

Image analysis

Images of fluorescently stained cells and fluorosphere standards were analyzed with Zen 2.6 image analysis package. Images were framed for analysis such that the entirety of the image was used and any nuclei touching the edges of the image were excluded from analyses. Images were automatically segmented and fluorescent objects detected by defining the threshold for foreground pixels using the Otsu algorithm and adjacent touching objects were separated using the watershed method (Otsu, 1979, Malpica et al., 1997). Non-target fluorescent objects were then excluded from subsequent analyses based on area (number of pixels x scaling factor; μm^2) of the object such that only objects between 15 μm^2 and 160 μm^2 (i.e., equivalent circular diameters between 4 µm and 14 µm) were included. Parameters recorded for each target fluorescent object in each image were area, Feret ratio (the ratio of the minimum and maximum distances

between two parallel lines tangent to the object perimeter), and Integrated fluorescence intensity (sum of pixel values).

Methods optimization

In order to optimize ICM methodology several factors in sample preparation and instrumentation were considered and compared. These factors included selection of nucleic acid dye (SYBR® Green I [Lonza Rockland, Rockland, ME] vs 4′, 6 – diamidino – 2 – phenylindole; DAPI), cell resuspension/slide preparation buffer (TE buffer vs Milli-Q H_2O), and microscope objective magnification power (10x vs 20x vs 40x) used in image acquisition. Genome size estimation and 1C DNA peak CV's, as determined by ICM and FCM, served as metrics for comparison and method selection.

For dye comparison, cell suspensions were diluted to 1 x 10^5 cells mL^{-1} in TE buffer with 1 x 10^5 calf thymocyte nuclei as a genome size standard (7.4 pg DNA $nucleus^{-1}$, Biosure, Grass Valley, CA) and stained with either SYBR® Green (5x and 20x concentrations, diluted from 10,000x stock concentration) or DAPI (1 μg mL^{-1}) fluorescent nucleic acid dyes (final concentrations) (Vinogradov, 1998). For each cell suspension 20 μL was aliquoted onto a poly-D-lysine coated coverslip (Electron Microscopy Sciences, Hatfield, PA) and allowed to fully air dry. Coverslips were then mounted onto microscope slides with 10 μL Vectashield® antifade (Vector Laboratories, Burlingame, CA) and sealed with clear nail polish. Slides were then subject to ICM analysis and remaining suspensions were analyzed by FCM with a BD LSRFortessa™ flow cytometer (BD Biosciences, San Jose, California) equipped with 405 nm and 488

nm 50 mW solid-state lasers following methods of Kremp & Parrow (2006). Suspensions stained with DAPI were analyzed using the 405 nm laser for excitation and fluorescence emissions were detected at 450 nm. SYBR® Green I stained suspensions were analyzed with the 488 nm laser and fluorescence emissions were detected at 530 nm.

Selection of optimal cell resuspension/slide preparation buffer and objective power were combined into one set of comparisons. *Karlodinium veneficum* cells were harvested and prepared as above and diluted to 1 x 10^5 cells mL^{-1} in either TE or Milli-Q H2O and stained with 1 μg mL^{-1} DAPI. Slides were prepared as above and ICM analysis was performed on images captured with 10x, 20x, and 40x objectives. Coefficients of variation on 1C DNA peaks (G1 phase cells) were compared to determine optimal buffer and magnification power for ICM.

Comparing ICM and FCM for cell cycle analysis

Titrations to determine optimal dye concentration were carried out by comparative genome size estimation between ICM and FCM using calf thymocyte nuclei as a genome size standard. Samples were diluted in Milli-Q H_2O to 2.6 x 10^5 *K. veneficum* cells mL^{-1}, calf thymocyte nuclei were added to a concentration of 1 x 10^5 calf thymocyte nuclei mL^{-1}, and stained with 1 μg mL^{-1}, 2 μg mL^{-1}, and 4 μg mL^{-1} DAPI (final concentrations). For ICM, 20 μL of each cell suspension was aliquoted onto a poly-D-lysine-coated coverslip and allowed to air dry. Dried coverslips were mounted onto microscope slides with 10 μL of Vectashield® antifade mounting medium (Vector Laboratories, Burlingame, CA) and sealed with clear nail polish. Remaining cell

suspensions were directly used for FCM analysis with a BD LSRFortessa™ flow cytometer. Genome sizes and associated error were calculated from single cytometry experiments without replication. *Karlodinium veneficum* was assumed to be haplontic in life cycle (Adolf et al., 2020), and so the signal mean of the lowest measured DNA fluorescence peak of flagellate cells was assumed to represent 1C DNA (1N, G1 cell cycle phase) following Kremp & Parrow (2006). Genome sizes were determined by multiplying the mean fluorescence ratio of 1C DNA *K. veneficum* cells: calf thymocyte nuclei by the 2C value of *Bos taurus*.

For cell cycle analysis a single culture was harvested at mid-log and prepared as described above. In triplicate this cell suspension was diluted in Milli-Q H_2O to 2.6 x 10^5 *K. veneficum* cells mL^{-1} and genome size standards were added at 1 x 10^5 calf thymocyte nuclei mL^{-1}; the suspension was then stained with DAPI (1 μg mL^{-1}). Microscope slides were prepared as described above and the remaining cell suspensions were subjected to FCM analysis as above. ICM and FCM DNA histograms from replicate samples were deconvoluted to estimate cell cycle phase distributions using FlowJo V10.6 (FlowJo, Ashland, Oregon).

Field samples were collected during a *K. veneficum* dominated mixed species algal bloom occurring in the Baltimore Inner Harbor, MD on June 3rd, 2016. Bloom samples were fixed with 5 % formalin and 0.1 % Tween 80 and processed identically to culture samples. Following dilution into Milli-Q H_2O and prior to staining with DAPI (1 μg mL^{-1}), cells were passed through a 35 μm Nitex® mesh in order to remove larger plankton and debris. Following DAPI staining, the cell suspension was mounted on poly-D-lysine coated coverslips as described above. Images used for ICM analysis were

collected with the 20x objective. The remaining cell suspension was subjected to FCM analysis and the presumptive *K. veneficum* population was gated using forward scatter vs side scatter gates established from culture samples of *K. veneficum*, as in Van Dolah et al. (2008).

Data collection methods and statistics

All images were saved as Zeiss proprietary file format (.CZI). Following image analysis, all data were exported as comma delimited .CSV file format and data from multiple fields of view were concatenated together using Windows 10 command prompt. Concatenated data were imported directly into FlowJo, which automatically converted the .CSV files into Flow Cytometry Standard (.FCS) file format. In order to maintain comparability between FCM and ICM measurements, the number of events analyzed by either method were restricted to comparable quantities. This was achieved by randomly subsampling analyses to equal number of events by using the FlowJo utilities plugin tool DownSample, or by stopping FCM analyses at the first 2500 events. Peak means, CV's, and proportions of cell cycle phases were determined using FlowJo following the Watson-Pragmatic model for phase deconvolution (Watson et al., 1987). ICM versus FCM data were compared by Two-way ANOVA in GraphPad Prism 6 (GraphPad Software, San Diego, California). Calculation of confidence intervals and Z-test statistics were performed in Microsoft® Excel® software 2013 (Microsoft Corporation, Redmond, Washington).

Assessment

Precision of quantitative fluorescence measurements

Precise measurement of DNA content by ICM was significantly impacted by uneven sample illumination provided by the epifluorescence light source. The effect of this uneven illumination is shown in Figures 1A - D, where the homogenous film of 10 % fluorescein was epi-illuminated by the microscope mercury arc lamp. Regions of brighter (center) pixels and more dim (edges) pixels illustrate the positional effect such a pattern had on the fluorescence intensity of uncorrected images (Fig. 1A). This was also evident in the 2.5 dimensional projection of the image (Fig. 1C), where the pixel intensity (i.e., fluorescence) was visualized on the Z-axis. Flatfield correction of this uneven illumination pattern (Fig. 1B and 1D) was carried out by normalizing data images using the methods described above. Statistical analysis also supported the necessity of flatfield correction: mean pixel intensity of a representative uncorrected image of 10 % fluorescein had a fluorescence intensity of 11299.0 ± 1771.1 gray-levels resulting in a fluorescence peak CV of 15.7 %. Upon flatfield correction mean pixel intensity of the same image increased to 15071.9 ± 184.0 gray-levels with a corresponding peak CV of 1.2 %. Fluorescence intensity of Flow-Check™ fluorospheres (n = 1373) was analyzed by both FCM (Fig. 2A) and ICM with (Fig. 2B) and without (Fig. 2C) flatfield correction. Peak CV's for ICM with and without correction resulted in CVs of 2.1 % and 11.7 %, respectively. Peak CV's for FCM analyzed fluorospheres was 1.8 %.

Methods optimization

Not all SYBR® Green I and DAPI staining treatments produced equivalent DNA histograms within and between ICM and FCM analyses (Fig. 3). The lowest ICM CV for the internal calf thymocyte nuclei DNA standard was 8.1 % when stained with the 20x concentration of SYBR® Green I (Table 1). The lowest FCM CV for the calf thymocyte nuclei was 2.5 % when stained with DAPI. The CVs for calf thymocyte nuclei were lower for FCM analyses than ICM with the exception of the 20x Concentration of SYBR® Green I. The lowest ICM and FCM *K. veneficum* 1C DNA peak CVs were 5.8 % and 3.3 %, respectively, when stained with DAPI. The highest was 16.6 % with 20x SYBR® Green I staining. As with the calf thymocyte nuclei CVs, *K. veneficum* 1C DNA peak CVs were lowest when analyzed by FCM, with the exception of the 20x SYBR® Green I concentration. Furthermore, genome size estimations only agreed between the SYBR® Green I FCM and DAPI ICM analyses, while the DAPI FCM genome size estimation was not in agreement with any SYBR® Green I analyses or the DAPI ICM analysis.

Both objective magnification and slide preparation solution had significant effects on DNA measurement precision in ICM (Fig. 4). Coefficients of variation for both Milli-Q H2O and TE buffer increased with objective magnification power (respective coefficients of correlation, r = 0.99 and 0.97). The CVs for data collected with the 10x objective were similar for Milli-Q H_2O and TE buffer (5.4 % and 5.5 %, respectively), however, as objective magnification increased the disparity between Milli-Q H_2O and TE buffer CVs increased (Fig. 4). Additionally, CVs for cells resuspended in TE buffer were

greater than those in Milli-Q H2O. The effect of magnification and slide preparation solution was also apparent in the number of images needed to capture comparable numbers of cells between the comparisons. The number of images required to reach the target sample size increased with magnification due to smaller fields of view, and was also higher for slides prepared with TE buffer compared to Milli-Q H2O at each magnification (Fig. 4). This was caused by salt precipitation from the TE buffer during slide preparation, which caused the cells to settle on the coverslip in slightly different focal planes.

Fluorescent dye titrations

Titrations revealed that as concentrations of DAPI increased, estimated genome sizes decreased for FCM, with the highest estimate at 12.6 ± 0.8 pg DNA cell^{-1} and the lowest at 7.7 ± 1.4 pg DNA cell^{-1} (Fig. 5). Additionally, FCM CVs for *K. veneficum* 1C DNA peaks increased with DAPI concentrations from 5.3 % to 16.7 %. Calf thymocyte nuclei CVs remained low only increasing at the highest DAPI concentration (5.6 % at 4 µg mL^{-1}).

Unlike FCM, ICM-based genome size measurements for *K. veneficum* varied by less than 1.0 pg DNA cell^{-1} across the different DAPI concentration treatments (Fig. 5). Image cytometry CVs for *K. veneficum* 1C DNA peaks remained below 10 % at all concentrations, but did increase with increasing DAPI concentrations (6.2 %, 7.5 %, and 9.3 % at 1 µg mL^{-1}, 2 µg mL^{-1}, and 4 µg mL^{-1}, respectively). Calf thymocyte nuclei CVs were only below 10 % at the lowest concentration of DAPI tested (8.3 % at 1 µg mL^{-1}).

Optimal DAPI concentration for cell cycle analysis (1 µg mL^{-1}) was chosen from the above titrations where genome size estimation was in closest agreement between ICM and FCM and CVs were the lowest. This optimal concentration was determined empirically for the cell concentrations used in this study (2.6 x 10^5 *K. veneficum* cells mL^{-1} and 1 x 10^5 calf thymocyte nuclei mL^{-1}).

Cell cycle deconvolution of DNA histograms

Cell cycle analysis of culture samples stained with 1 µg mL^{-1} DAPI were in agreement between the FCM and ICM data, and G1 peak CVs were comparable between the two methods (Fig. 6, Table 2). The ICM average *K. veneficum* G1 peak CV was 6.4 ± 1.1 %, while the FCM average *K. veneficum* G1 peak CV was 5.2 ± 0.4 %. These CVs were not significantly different (p-value = 0.16). Increasing the event total to 10,000 events for FCM analyses resulted in a reduction of *K. veneficum* G1 peak CV to 4.7 ± 0.1 % (data not shown). The average CVs for the calf thymocyte nuclei within the dinoflagellate sample analyzed by ICM were 12.8 ± 1.7 %, and the average FCM CVs were 3.3 ± 0.6 % which were significantly different (p-value < 0.01). Two-way ANOVA indicated no statistical difference in cell cycle phase distributions between the two methods of analysis (p-value = 0.93). Additionally, the statistical test revealed that differences between cell cycle phases (i.e., G1 vs S vs G2 + M) were significant (p-value < 0.001) and there were no significant interactions between cytometry method and cell cycle phase (p-value = 0.07).

Comparative cell cycle analysis of the natural bloom sample by ICM versus FCM demonstrated some significant differences. Apparent precision in measuring G1-phase DNA content was significantly better for FCM analysis (G1 peak CV = 6.4 %) than ICM analysis (G1 peak CV = 10.3 %). However, deconvolution of cell cycle phases was successful for both methods (Fig. 7). Deconvolution of ICM data estimated 85.5 ± 1.1 % of the *K. veneficum* cells to be in G1 phase, 1.0 ± 0.3 % in S-phase, and 13.5 ± 1.0 % in G2 + M-phase. This contrasted with deconvolution of FCM data that estimated 73.9 ± 1.3 % of the *K. veneficum* cells to be in G1 phase, 5.2 ± 0.7 % to be in S-phase, and 20.9 ± 1.2 % to be in G2 + M-phase. Comparison of corresponding cell cycle phase frequencies revealed significant differences between ICM and FCM (Z-test, p-value < 0.001). Additionally, DNA indices (G2 mean: G1 mean) for the two data sets were not in agreement; with an ICM DNA index of 1.9 and an FCM DNA index of 1.6.

Discussion

ICM has been used in a very limited number of phytoplankton and fungal studies (Gisselson et al., 1999, Kullman & Teterin, 2006, Von Dassow et al., 2008), these have generally lacked detailed methods and give little information on quantitative precision. However, ICM has been extensively utilized and optimized for clinical research (Poulin et al., 1994a, Poulin et al., 1994b, Wang et al., 1995, Maciorowski et al., 1997, Varga et al., 2004, Roukos et al., 2015). Such studies largely informed the methods developed here. Overall, ICM data obtained here for the dinoflagellate *K. veneficum*, were of equivalent or higher quality in terms of DNA peak CV's as those reported in clinical

studies on human cells where CVs ranged from 3.5 % to 16.4 % (Lamas et al., 2003 and references above).

The CVs for *K. veneficum* 1C DNA peaks were comparable between both methods (ICM and FCM) and other ICM studies, which range from 3.4 % to 16.6 % (Poulin et al., 1994a, Poulin et al., 1994b, Wang et al., 1995, Maciorowski et al., 1997, Lamas et al., 2003). In Maciorowski et al. (1997), where fixation and slide mounting methods were compared; the best CV attained was 6.1 % which is only slightly better than CVs reported here (human peripheral blood lymphocytes, 1C DNA = 3.5 pg DNA, n = 200). Poulin et al. (1994b) achieved CVs as low as 3.4 % in ethanol fixed propidium iodide stained human adenocarcinoma cells (n = 1000). In comparison to previous phytoplankton studies, the CVs reported here using ICM are comparable to other studies using microfluorometry (3.6 % - 9.1 %) (Chang & Carpenter, 1988, Cetta & Anderson, 1990, Yamaguchi, 1992) and FCM (7.3 % -12.1 %) (Parrow & Burkholder, 2003a, Parrow & Burkholder, 2003b, Figueroa et al., 2010). *Karlodinium veneficum* genome size estimations determined by ICM in this study (13.8 ± 2.3 pg DNA cell^{-1} to 14.6 ± 1.5 pg DNA cell^{-1}) are also comparable to those reported for other North American strains, which ranged from 11.2 ± 0.6 pg DNA cell^{-1} to 16.9 pg DNA cell^{-1} (LaJeunesse et al., 2005, Adolf et al., 2020). Interestingly, DAPI titrations revealed fluorescence intensity ratios between *K. veneficum* nuclei and calf thymocyte nuclei were less perturbed by increasing dye concentrations when analyzed by ICM as opposed to FCM. The effect of DAPI concentration on mean fluorescence intensity and CVs have previously been reported (Yamaguchi, 1992, Wen et al., 2001). Wen et al. (2001), using FCM, observed increases in both CVs and mean fluorescence intensity of trout red blood cell standards

and mouse cell lines with increased DAPI concentrations. This was attributed to oversaturation of DAPI and was reversible by dilution of cell suspensions in DAPI free buffer. Additionally, they observed an effect of staining buffer pH on CVs for mouse cell lines, concluding pH = 6 to be optimal for DAPI staining. Yamaguchi (1992), using microfluorometry to study the cell cycle of *Gymnodinium nagasakiense* (= *Karenia mikimotoi*), also observed effects of DAPI concentration on both CVs and mean fluorescence intensity. The differences observed in this current study between ICM and FCM in terms of stain type and concentration are likely due to the unavoidable differences between ICM and FCM sample preparation. Samples prepared for ICM were fully dried onto coverslips. This may lead to altered hydration states of DNA and DAPI or SYBR Green I molecules, possibly leading to conformational changes that alter dye binding chemistry and/or fluorescence yield.

The determined CVs of the calf thymocyte nuclei standards in ICM were higher than FCM, which may be explained by the different morphological dimensions of *K. veneficum* cells (8 – 12 μm, Place et al., 2012) versus calf thymocyte nuclei (~ 5 μm, Hess & Lagg, 1958), when stained and analyzed together as internal standards in ICM images. This was supported by the observation that when calf thymocyte nuclei were analyzed alone by ICM, CVs were as low as 6.2 % (data not shown). As previously reported in Lockett et al. (1992) and Varga et al. (2004) the z-axis distance from the optimal focal plane of fluorescent objects has a significant impact on the precision of fluorescence measurement in ICM. This effect is largely influenced by the focal depth of the objective used, which is inversely proportional to the square of the numerical aperture (Waters, 2009). In the case of the objective used here (20x, NA = 0.8) the theoretical

focal depth is approximately 1.6 μm which is less than the difference in diameters of the *K. veneficum* cells and calf thymocyte nuclei. Therefore, collecting images in the optimal focal plane for *K. veneficum* cells inevitably resulted in suboptimal focus for the calf thymocyte nuclei, which increased their CV's as compared to FCM. Likewise, use of high ionic strength buffer in slide preparation was found to exacerbate focal plane differences, as salt precipitation during sample drying resulted in specimens being distributed amongst multiple focal planes, which increased CV's in ICM. The method described here minimizes the effects of multiple focal planes by using poly-D-lysine coated coverslips and a low ionic strength resuspension/slide preparation solution (i.e., Milli-Q H_2O), thereby reducing the number of out of focus specimens. Lastly, increasing objective magnification and NA was observed to contribute to increases in fluorescent measurement error in ICM, due to decreasing focal depth for reasons given above. Therefore, a compromise must be made in selecting the appropriate magnification that facilitates user discrimination of non-target taxa while also attaining the highest practical level of precision in DNA fluorescence measurement. In this study, the 20x objective was found to be a good compromise that allowed easy discrimination of *K. veneficum* cells from other similarly sized taxa, which would prove more difficult with a lower powered (e.g., 10x) objective.

At this time, we know of no epifluorescence light source and/or optics system that can deliver a completely flat, uniform field of epi-illumination across a microscope field of view, at all magnifications. Therefore, flatfield correction was found to be necessary for precision in ICM using widefield fluorescence microscopy (Lockett et al., 1992, Model & Burkhardt, 2001). Following flatfield correction, precision of fluorescence

intensity measurements via ICM for both microsphere and nuclear DNA standards improved significantly and became comparable to that of FCM analysis. Coefficients of variation obtained herein on fluorosphere standards were 2.1%, consistent with previous ICM studies where such CVs ranged from 2 % to 3.9 % (Lockett et al., 1992, Poulin et al., 1994a, Poulin et al., 1994b, Varga et al., 2004). All of these studies used a flatfield correction method similar to that used here, although Poulin et al. (1994a), additionally improved CV's of fluorosphere standards from 2.7% to 2% by setting the field aperture of the epi-source to half stop, thereby reducing the effects of glare, but reducing the useable frame of the CCD camera to one quarter of its original size. This would have had the disadvantage of significantly impacting the speed of data acquisition.

Using methods optimized here, ICM was shown to be equivalent to FCM for determining DNA content and cell cycle phase distribution in cultured *K. veneficum*, with no significant differences found between identical samples analyzed using the two different platforms. This clearly demonstrates the comparability of ICM to FCM for cell cycle analysis, in agreement with clinical studies comparing ICM to FCM for cell cycle/ploidy analysis of human lymphocyte cells, as well as tumors from lung and breast cancer patients (Montironi et al., 1993, Yamamoto et al., 1994, Chan et al., 2011). Unlike culture samples, *K. veneficum* cell cycle phase distributions in the field bloom sample were less close in agreement between ICM and FCM estimates. This was likely a result of variation introduced during sample preparation that caused increased cell clumping during slide preparation (Fig. 8) as compared to the culture samples. Unlike culture samples, the field sample had been in storage for a long period of time (years) before analysis. This may have caused the observed increased cell clumping, which had the

effect in ICM of distributing many/most cells through slightly different focal planes, which increased error in DNA fluorescence measurements for reasons given above. This problem should be correctable in the future through timelier sample analysis and/or increased physical disaggregation steps. Clumped cells were automatically excluded from analysis in FCM via gated size exclusion, and the method allowed a much larger volume of sample to be analyzed to gradually collect data from (relatively rare) non-clumped cells. The exclusion gates in ICM could have also been adjusted for a higher degree of exclusion, but changing such parameters mid-experiment was against the goals of this study. Overall, ICM appeared to slightly overestimate the percentage of G1 phase cells in bloom samples, and thus underestimated S and G2 + M phase cells as compared to FCM. This was likely caused by the higher G1 CV in the ICM DNA histogram, which the cell cycle model accommodated with a wider Gaussian fit, thereby overlapping a portion of the S-phase population. While the ICM G1 peak CV (10.3 %) was higher than the FCM CV (6.4 %) for the field samples, it nevertheless fell within an acceptable range (< 15 %) (Boucher et al., 1991, Veldhuis et al., 1997, Ormerod et al., 1998, Parrow & Burkholder, 2003a). Furthermore, CVs are typically not reported for field data on bloom cell cycle phase distribution (Vaulot & Partensky, 1992, Garcés et al., 1998, Garcés et al., 1999, Garcés & Masó, 2001). Even if the case, overestimation of the percentage of G1 phase cells when determining *in situ* growth rates would only result in a lower (i.e. more conservative) estimate of specific growth rates (μ).

This study demonstrates that ICM can be an effective technique for performing nuclear genome size estimations and cell cycle analysis of microalgal taxa in culture and natural bloom populations including phagotrophic species and complex field assemblages

which present particular problems for FCM. As with other quantitative fluorescence microscopy methods, several important factors need to be considered for acquiring precise measurements in ICM (Waters, 2009): 1) uniformity of illumination or image correction, 2) careful selection of a fluorochrome with regards to binding specificity, quantum yield, and Stoke's shift, 3) saturation of fluorochrome binding, 4) fluorescence fading, 5) characteristics of the microscope objective such as magnification and numerical aperture, and 6) signal to noise ratio and linearity of the camera used to capture images. These factors were critical to the development of the methods optimized here for *K. veneficum,* and future studies should carefully consider other factors such as cell concentration and stain incubation time when determining optimal dye concentrations (Kremp & Parrow, 2006, Darzynkiewicz, 2011).

Theoretical advantages of ICM over classical microfluorometry include much more rapid data acquisition and data archiving as images. Potential advantages over flow cytometry include reduced instrumentation costs and maintenance, ability to visually select cells of interest by morphology, and ability to measure nuclear DNA while ignoring cytoplasmic DNA (or vice versa). Data collection and processing in ICM can proceed rapidly, with the data from the bloom sample in this study collected as only 15 images with an average of 77.1 cells analyzed per image. Data on cultured samples was collected as ~ 11 images per replicate, with an average of~ 235 cells per image using the 20x objective. Analysis of the images was rapid and automatically performed by the trained image analysis software. The rate of processing was primarily slowed by user curation to manually remove non-target nuclei (e.g. other phytoplankton with similar genome sizes, intracellular food vacuoles containing ingested nuclei) from the analyses.

Application in field samples was aided by the ability to use morphological identification in brightfield images that were cross-referenced to their respective fluorescent images being analyzed (Fig. 8).

Although this study made use of a commercially available image analysis software package (Zen 2.6), other image analysis tools are available that could be also be utilized in ICM. Wiesmann et al. (2015) reviewed 15 free image analysis software tools, and ranked them based on usability and functionality. Of these, CellProfiler was specifically designed for high-throughput image analysis (Kamentsky et al., 2011). This software allows user designed analysis pipelines that can be utilized to analyze hundreds of images automatically. This could significantly improve data collection speeds as compared to Zen 2.6, which required analysis of a single image at a time.

With the methods and tools described by this study and references within, ICM can be adopted from clinical research into ecological field studies to measure cell cycle progression and *in situ* growth rates of natural bloom populations of complex assemblages and/or phagotrophic/mixotrophic microalgae. Furthermore, multiparameter fluorescence studies are possible with ICM (Galbraith et al., 1991). The application of multiparameter fluorescence would be useful for investigating the cell cycle progression in relation to other labelled biomarkers, including those labelled using immunofluorescence and fluorescence *in situ* hybridization. This could be useful for studies of other biotic factors influencing bloom formation, maintenance, and decline such as co-occurrence of intracellular parasites like *Amoebophrya* that have been implicated in the demise of *K. veneficum* blooms (Place et al., 2012). One such a study was previously performed during an *Alexandrium fundyense* bloom using an Imaging

FlowCytobot modified specifically for measuring cellular DNA content (Brosnahan et al., 2014). This type of study was complicated by instrumentation expense, necessary expertise, and the inability to ignore cytoplasmic/vacuolar DNA. Image cytometry offers a cost effective, accessible, alternative platform for cell cycle and other quantitative fluorescence-based studies of both cultured mixotrophic/phagotrophic microalgae and complex natural field populations.

Acknowledgments

This research was supported by the National Oceanic and Atmospheric Administration, National Centers for Coastal Ocean Science ECOHAB Program, grant number NA15NOS4780180. The authors acknowledge the assistance of Dr. Saddef Haq in obtaining the Baltimore Harbor bloom sample. The authors would like to extend appreciation to Richard Riese of Biosure® Inc. for assistance with cytometry DNA standards. This paper is ECOHAB contribution No. 969, No. 5887 from the University of Maryland Center for Environmental Science, and No. 20-013 from the Institute of Marine and Environmental Technology.

References

Adolf, J. E., Bachvaroff, T. R. & Place, A. R. 2009. Environmental modulation of karlotoxin levels in strains of the cosmopolitan dinoflagellate, *Karlodinium veneficum* (Dinophyceae). *J. Phycol.* **45**:176-92.

Adolf, J. E., Parrow, M. W. & Place, A. R. 2020. *Karlodinium veneficum*: Still blooming and toxic sixty-two years later. *In*: Subba Rao, V. D. [Ed.] *Dinoflagellates.* Nova Science Publishers, Inc., pp. 355 - 402.

Bachvaroff, T. R., Adolf, J. E., Squier, A. H., Harvey, H. R. & Place, A. R. 2008. Characterization and quantification of karlotoxins by liquid chromatography-mass spectrometry. *Harmful Algae* **7**:473-84.

Berges, J. A., Franklin, D. J. & Harrison, P. J. 2001. Evolution of an artificial seawater medium: Improvements in enriched seawater, artificial water over the last two decades. *J. Phycol.* **37**:1138-45.

Bhaud, Y., Salmon, J.-M. & Soyer-Gobillard, M.-O. 1991. The complex cell cycle of the dinoflagellate protoctist *Crypthecodinium cohnii* as studied *in vivo* and by cytofluorimetry. *J. Cell Sci.* **100**:675-82.

Bocsi, J., Varga, V. S., Molnár, B., Sipos, F., Tulassay, Z. & Tárnok, A. 2004. Scanning fluorescent microscopy analysis is applicable for absolute and relative cell frequency determinations. *Cytometry Part A* **61A**:1-8.

Boucher, N., Vaulot, D. & Partensky, F. 1991. Flow cytometric determination of phytoplankton DNA in cultures and oceanic populations. *Mar. Ecol. Prog. Ser.* **71**:75-84.

Brosnahan, M. L., Farzan, S., Keafer, B. A., Sosik, H. M., Olson, R. J. & Anderson, D. M. 2014. Complexities of bloom dynamics in the toxic dinoflagellate *Alexandrium fundyense* revealed through DNA measurements by imaging flow cytometry coupled with species-specific rRNA probes. *Deep Sea Res. Part II Top. Stud. Oceanogr.* **103**:185-98.

Carpenter, E. J. & Chang, J. 1988. Species-specific phytoplankton growth rates via diel DNA synthesis cycles. I. Concept of the method. *Mar. Ecol. Prog. Ser.* **43**:105-11.

Cetta, C. M. & Anderson, D. M. 1990. Cell cycle studies of the dinoflagellates *Gonyaulax polyedra* Stein and *Gyrodinium uncatenum* Hulburt during asexual and sexual reproduction. *J. Exp. Mar. Biol. Ecol.* **135**:69-83.

Chan, L. L., Zhong, X., Qiu, J., Li, P. Y. & Lin, B. 2011. Cellometer Vision as an alternative to flow cytometry for cell cycle analysis, mitochondrial potential, and immunophenotyping. *Cytometry Part A* **79A**:507-17.

Chang, J. & Carpenter, E. J. 1988. Species-specific phytoplankton growth rates via diel DNA synthesis cycles. II. DNA quantification and model verification in the dinoflagellate *Heterocapsa triquetra*. *Mar. Ecol. Prog. Ser.* **44**:287-96.

Chang, J. & Dam, H. G. 1993. The influence of grazing on the estimation of phytoplankton growth rate via cell cycle analysis: experimental and modeling evidence. *Limnol. Oceanogr.* **34**:202-12.

Darzynkiewicz, Z. 2011. Critical aspects in analysis of cellular DNA content. *Curr. Protoc. Cytom.* **56**:7.2.1-7.2.8.

Deeds, J. R., Kibler, S. R., Tester, P. A. & Place, A. R. 2004. Geographic strain variation in toxin production in *Karlodinium micrum* (Dinophyceae) from Southeastern United States. *In*: Steidinger, K. A., Landsberg, J. H., Tomas, C. R. & Vargo, G. A. [Eds.] *Harmful Algae 2002.* IOC-UNESCO, Florida, pp. 145-47.

Deeds, J. R. & Place, A. R. 2006. Sterol-specific membrane interactions with the toxins from *Karlodinium micrum* (Dinophyceae) — a strategy for self-protection? *Afr. J. Mar. Sci.* **28**:421-25.

Deeds, J. R., Terlizzi, D. E., Adolf, J. E., Stoecker, D. K. & Place, A. R. 2002. Toxic activity from cultures of *Karlodinium micrum* (=*Gyrodinium galatheanum*)

(Dinophyceae)—a dinoflagellate associated with fish mortalities in an estuarine aquaculture facility. *Harmful Algae* **1**:169-89.

Figueroa, R. I., Garcés, E. & Bravo, I. 2010. The use of flow cytometry for species identification and life-cycle studies in dinoflagellates. *Deep Sea Res. Part II Top. Stud. Oceanogr*. **57**:301-07.

Galbraith, W., Wagner, M. C. E., Chao, J., Abaza, M., Ernst, L. A., Nederlof, M. A., Hartsock, R. J., Taylor, D. L. & Waggoner, A. S. 1991. Imaging cytometry by multiparameter fluorescence. *Cytometry* **12**:579-96.

Garcés, E., Delgado, M., Masó, M. & Camp, J. 1998. Life history and *in situ* growth rates of *Alexandrium taylori* (Dinophyceae, Pyrrophyta). *J. Phycol.* **34**:880-87.

Garcés, E., Delgado, M., Masó, M. & Camp, J. 1999. *In situ* growth rate and distribution of the ichthyotoxic dinoflagellate *Gyrodinium corsicum* Paulmier in an estuarine embayment (Alfacs Bay, NW Mediterranean Sea). *J. Plankton Res.* **21**:1977-91.

Garcés, E. & Masó, M. 2001. Phytoplankton potential growth rate versus increase in cell numbers estimation of cell lysis. *Mar. Ecol. Prog. Ser.* **212**:297-300.

Gisselson, L.-Å., Granéli, E. & Carlsson, P. 1999. Using cell cycle analysis to estimate *in situ* growth rate of the dinoflagellate *Dinophysis acuminata*: drawbacks of the DNA quantification method. *Mar. Ecol. Prog. Ser.* **184**:55-62.

Hess, E. L. & Lagg, S. E. 1958. Calf thymus composition: a comparison of differential centrifugation and chemical fractionation procedures. *J. Biophys. Biochem. Cytol.* **4**:717-25.

Kamentsky, L., Jones, T. R., Fraser, A., Bray, M.-A., Logan, D. J., Madden, K. L., Ljosa, V., Rueden, C., Eliceiri, K. W. & Carpenter, A. E. 2011. Improved structure, function and compatibility for CellProfiler: modular high-throughput image analysis software. *Bioinformatics* **27**:1179-80.

Kapraun, D. F. & Freshwater, D. W. 2012. Estimates of nuclear DNA content in red algal lineages. *AoB Plants* **2012**:pls005-pls05.

Kempton, J. W., Lewitus, A. J., Deeds, J. R., Law, J. M. & Place, A. R. 2002. Toxicity of *Karlodinium micrum* (Dinophyceae) associated with a fish kill in a South Carolina brackish retention pond. *Harmful Algae* **1**:233-41.

Kremp, A. & Parrow, M. W. 2006. Evidence for asexual resting cysts in the life cycle of the marine peridinoid dinoflagellate, *Scrippsiella hangoei*. *J. Phycol.* **42**:400-09.

Kullman, B. & Teterin, W. 2006. Estimation of fungal genome size: comparison of image cytometry and photometric cytometry. *Folia Cryptogam. Est.* **42**:43-56.

LaJeunesse, T. C., Lambert, G., Andersen, R. A., Coffroth, M. A. & Galbraith, D. W. 2005. *Symbiodinium* (Pyrrhophyta) genome sizes (DNA content) are smallest among dinoflagellates. *J. Phycol*. **41**:880-86.

Lamas, E., Chassoux, D., Decaux, J.-F. o., Brechot, C. & Debey, P. 2003. Quantitative fluorescence imaging approach for the study of polyploidization in hepatocytes. *J. Histochem. Cytochem.* **51**:319-30.

Lim, H. C., Leaw, C. P., Tan, T. H., Kon, N. F., Yek, L. H., Hii, K. S., Teng, S. T., Razali, R. M., Usup, G., Iwataki, M. & Lim, P. T. 2014. A bloom of *Karlodinium australe* (Gymnodiniales, Dinophyceae) associated with mass mortality of cage-cultured fishes in West Johor Strait, Malaysia. *Harmful Algae* **40**:51-62.

Litaker, R. W., Warner, V. E., Rhyne, C., Duke, C. S., Kenney, B. E., Ramus, J., Tester, P. A. 2002. Effect of diel and interday variations in light on the cell division pattern and *in situ* growth rates of the bloom-forming dinoflagellate *Heterocapsa triquetra*. *Mar. Ecol. Prog. Ser.* **232:**63-74.

Liu, H., Campbell, L., Landry, M. R., Nolla, H. A., Brown, S. L. & Constantinou, J. 1998. *Prochlorococcus* and *Synechococcus* growth rates and contributions to production

in the Arabian Sea during the 1995 Southwest and Northeast Monsoons. *Deep Sea Res. Part II Top. Stud. Oceanogr.* **45**:2327-52.

Liu, H., Nolla, H. A. & Campbell, L. 1997. *Prochlorococcus* growth rate and contribution to primary production in the equatorial and subtropical North Pacific Ocean. *Aquat. Microb. Ecol.* **12**:39-47.

Lockett, S. J., Jacobson, K. & Herman, B. 1992. Quantitative precision of an automated, fluorescence-based image cytometer. *Anal. Quant. Cytol. Histol.* **14**:187-202.

Maciorowski, Z., Veilleux, C., Gibaud, A., Bourgeois, C. A., Klijanienko, J., Boenders, J. & Vielh, P. 1997. Comparison of fixation procedures for fluorescent quantitation of DNA content using image cytometry. *Cytometry* **28**:123-29.

Malpica, N., de Solórzano, C. O., Vaquero, J. J., Santos, A., Vallcorba, I., García-Sagredo, J. M. & del Pozo, F. 1997. Applying watershed algorithms to the segmentation of clustered nuclei. *Cytometry* **28**:289-97.

McDuff, R. E. & Chisholm, S. W. 1982. The calculation of *in situ* growth rates of phytoplankton populations from fractions of cells undergoing mitosis: A clarification. *Limnol. Oceanogr.* **27**:783-88.

Model, M. A. & Burkhardt, J. K. 2001. A standard for calibration and shading correction of a fluorescence microscope. *Cytometry* **44**:309-16.

Montironi, R., Diamanti, L., Santinelli, A., Magi Galluzzi, C., Scarpelli, M., Giannulis, I. & Mangili, F. 1993. Computed cell cycle and DNA histogram analyses in image cytometry in breast cancer. *J. Clin. Pathol.* **46**:795-800.

Ormerod, M. G., Tribukait, B. & Giaretti, W. 1998. Consensus report of the task force on standardisation of DNA flow cytometry in clinical pathology. DNA Flow Cytometry Task Force of the European Society for Analytical Cellular Pathology. *Anal. Cell. Pathol.* **17**:103-10.

Otsu, N. 1979. A threshold selection method from gray-level histograms. *IEEE Trans. Syst. Man Cybern.* **9**:62-66.

Parrow, M. W. & Burkholder, J. M. 2003a. Estuarine heterotrophic cryptoperidiniopsoids (Dinophyceae): Life cycle and culture studies. *J. Phycol.* **39**:678-96.

Parrow, M. W. & Burkholder, J. M. 2003b. Reproduction and sexuality in *Pfiesteria shumwayae* (Dinophyceae). *J. Phycol.* **39**:697-711.

Place, A. R., Bowers, H. A., Bachvaroff, T. R., Adolf, J. E., Deeds, J. R. & Sheng, J. 2012. *Karlodinium veneficum*—The little dinoflagellate with a big bite. *Harmful Algae* **14**:179-95.

Poulin, N., Harrison, A. & Palcic, B. 1994a. Quantitative precision of an automated image cytometric system for the measurement of DNA content and distribution in cells labeled with fluorescent nucleic acid stains. *Cytometry* **16**:227-35.

Poulin, N. M., Matthews, J. B., Skov, K. A. & Palcic, B. 1994b. Effects of fixation method on image cytometric measurement of DNA content and distribution in cells stained for fluorescence with propidium iodide. *J. Histochem. Cytochem.* **42**:1149-56.

Roukos, V., Pegoraro, G., Voss, T. C. & Misteli, T. 2015. Cell cycle staging of individual cells by fluorescence microscopy. *Nat. Protoc.* **10**:334.

Salvador Soler, N., Gómez Garreta, A., Ribera Siguan, M. A. & Kapraun, D. F. 2014. Nuclear DNA content variation in life history phases of the Bonnemasoniaceae (Rhodophyta). *PLOS ONE* **9**:e86006.

Van Dolah, F. M. & Leighfield, T. A. 1999. Diel phasing of the cell-cycle in the Florida red tide dinoflagellate, *Gymnodinium breve*. *J. Phycol.* **35**:1404-11.

Van Dolah, F. M., Leighfield, T. A., Kamykowski, D., Kirkpatrick, G. J. 2008. Cell cycle behavior of laboratory and field populations of the Florida red tide dinoflagellate, *Karenia brevis*. *Cont. Shelf Res.* **28**:11-23.

Van Wagoner, R. M., Deeds, J. R., Satake, M., Ribeiro, A. A., Place, A. R. & Wright, J. L. C. 2008. Isolation and characterization of karlotoxin 1, a new amphipathic toxin from *Karlodinium veneficum*. *Tetrahedron Lett.* **49**:6457-61.

Varga, V. S., Bocsi, J., Sipos, F., Csendes, G., Tulassay, Z. & Molnár, B. 2004. Scanning fluorescent microscopy is an alternative for quantitative fluorescent cell analysis. *Cytometry Part A* **60A**:53-62.

Vaulot, D. 1992. Estimate of phytoplankton division rates by the mitotic index method: The fmax approach revisited. *Limnol. Oceanogr*. **37**:644-49.

Vaulot, D. & Partensky, F. 1992. Cell cycle distributions of prochlorophytes in the north western Mediterranean Sea. *Deep Sea Res. A* **39**:727-42.

Veldhuis, M. J. W., Cucci, T. L. & Sieracki, M. E. 1997. Cellular DNA content of marine phytoplankton using two new fluorochromes: Taxonomic and ecological implications. *J. Phycol.* **33**:527-41.

Vinogradov, A. E. 1998. Genome size and GC-percent in vertebrates as determined by flow cytometry: The triangular relationship. *Cytometry* **31**:100-09.

Von Dassow, P., Petersen, T. W., Chepurnov, V. A. & Armbrust, E. V. 2008. Inter- and intraspecific relationships between nuclear DNA content and cell size in selected members of the centric diatom genus *Thalassiosira* (Bacillariophyceae). *J. Phycol.* **44**:335-49.

Wang, N., Pan, Y., Heiden, T. & Tribukait, B. 1995. Fluorescence image cytometry for measurement of nuclear DNA content in surgical pathology. *Cytometry* **22**:323-29.

Waters, J. C. 2009. Accuracy and precision in quantitative fluorescence microscopy. *J. Cell Biol.* **185**:1135-48.

Watson, J. V., Chambers, S. H. & Smith, P. J. 1987. A pragmatic approach to the analysis of DNA histograms with a definable G1 peak. *Cytometry* **8**:1-8.

Wen, J., Krishan, A. & Thomas, R. A. 2001. NASA/American Cancer Society high-resolution flow cytometry project – II. Effect of pH and DAPI concentration on dual parametric analysis of DNA/DAPI fluorescence and electronic nuclear volume. *Cytometry* **43**:12-15.

Wiesmann, V., Franz, D., Held, C., Münzenmayer, C., Palmisano, R. & Wittenberg, T. 2015. Review of free software tools for image analysis of fluorescence cell micrographs. *J. Microsc.* **257**:39-53.

Yamaguchi, M. 1992. DNA synthesis and the cell cycle in the noxious red-tide dinoflagellate *Gymnodinium nagasakiense*. *Mar. Biol.* **112**:191-98.

Yamamoto, T., Horiguchi, H., Kamma, H., Noro, M., Ogata, T., Inage, Y., Akaogi, E., Mitsui, K., Hori, M. & Isobe, M. 1994. Comparative DNA analysis by image cytometry and flow cytometry in non-small cell lung cancer. *Jap. J. Cancer Res.* **85**:1171-77.

Table 2.1 Comparison of precision and genome size estimation by ICM and FCM using SYBR® Green I (5x and 20x concentrations) and DAPI (1 μg mL^{-1}) nucleic acid dyes. Genome size standard deviations propagated from % CVs of calf thymocyte nuclei (CTN) and *K. veneficum* 1C DNA peaks (n = 2500 events). Highlighted genome estimations were in agreement with reports from other North American strains (LaJeunesse et al., 2005, Adolf et al., 2020).

Dye (Concentration)	Analysis Method	CTN (% CV)	*K. v.* G1 (% CV)	*K. v.* 1C/ CTN	*K. v.* Genome Size Estimation (pg DNA $cell^{-1}$ ± SD)
SYBR® Green (5x)	FCM	5.0	7.3	2.3	17.0 ± 1.5
	ICM	16.3	9.4	4.8	35.5 ± 3.9
SYBR® Green (20x)	FCM	8.7	16.6	2.4	17.8 ± 1.6
	ICM	8.1	7.9	3.2	23.7 ± 2.6
DAPI (1 μg mL^{-1})	FCM	2.5	3.3	1.6	11.8 ± 0.5
	ICM	9.4	5.8	2.5	18.5 ± 2.0

Table 2.2 Cell cycle statistics. Mean percentage of cell cycle phases G1, S, and G2 with mean % CVs of *K. veneficum* G1 phase and the calf thymocyte nuclei (CTN) internal DNA standard from triplicate samples analyzed by ICM and FCM. Errors are SD.

	% G1	% S	% G2	*K.v.* G1 % CV	CTN % CV
ICM	80.0 ± 1.2	9.7 ± 2.6	10.2 ± 1.5	6.4 ± 1.1	12.8 ± 1.7
FCM	77.3 ± 0.6	7.9 ± 3.5	14.4 ± 4.1	5.2 ± 0.4	3.3 ± 0.6

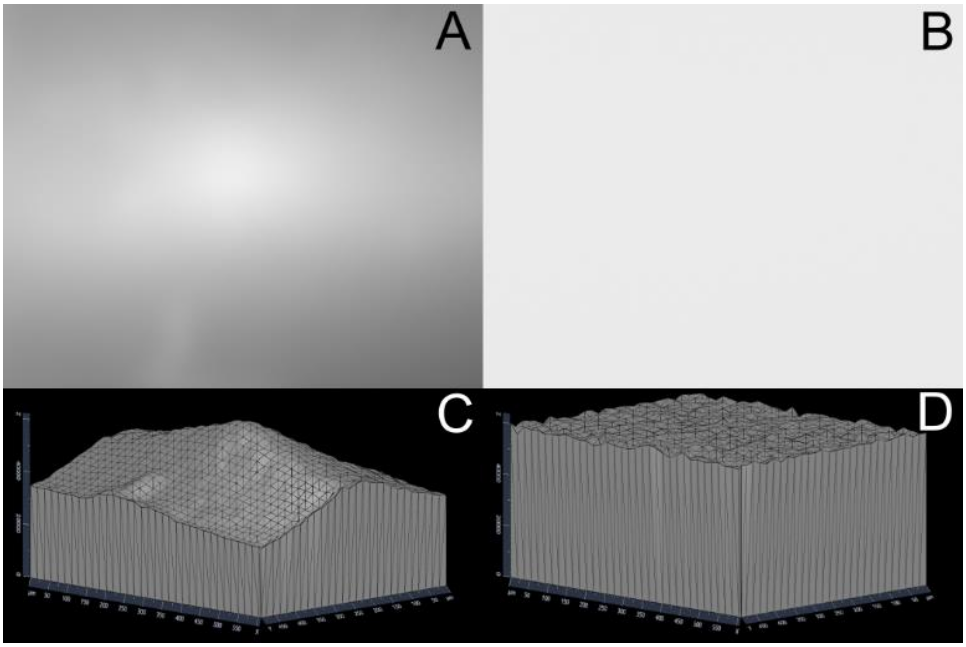

Figure 2.1 Field of view captured from an epifluorescence illuminated film of fluorescein. Fluorescence patterns before (A) and after (B) flatfield correction, with respective 2.5 dimensional representations (C and D). Z-axis in 2.5 dimensional representations indicate pixel gray level. X and Y axes indicate X/Y position within field of view.

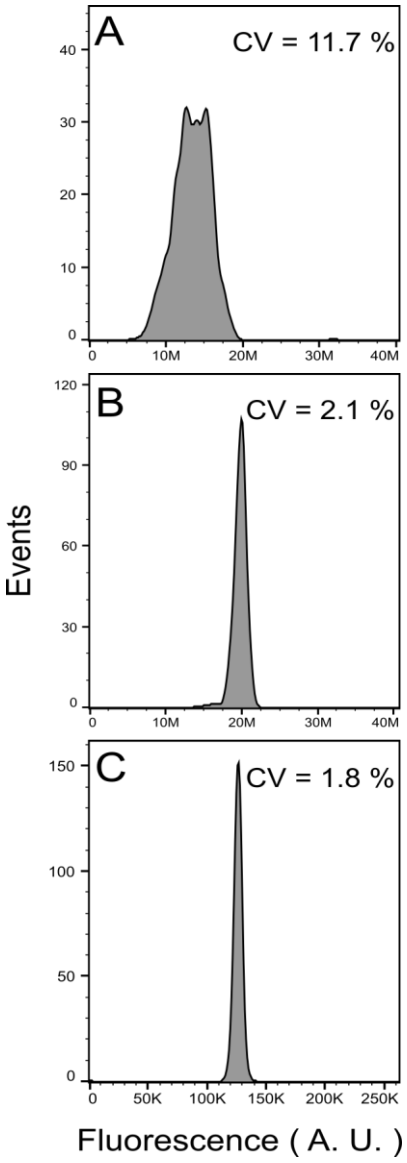

Figure 2.2 Fluorescence histograms of Flow-Check™ fluorospheres (n = 1373 events), analyzed by image cytometry prior to flatfield correction (A), after flatfield correction (B), and by flow cytometry (C).

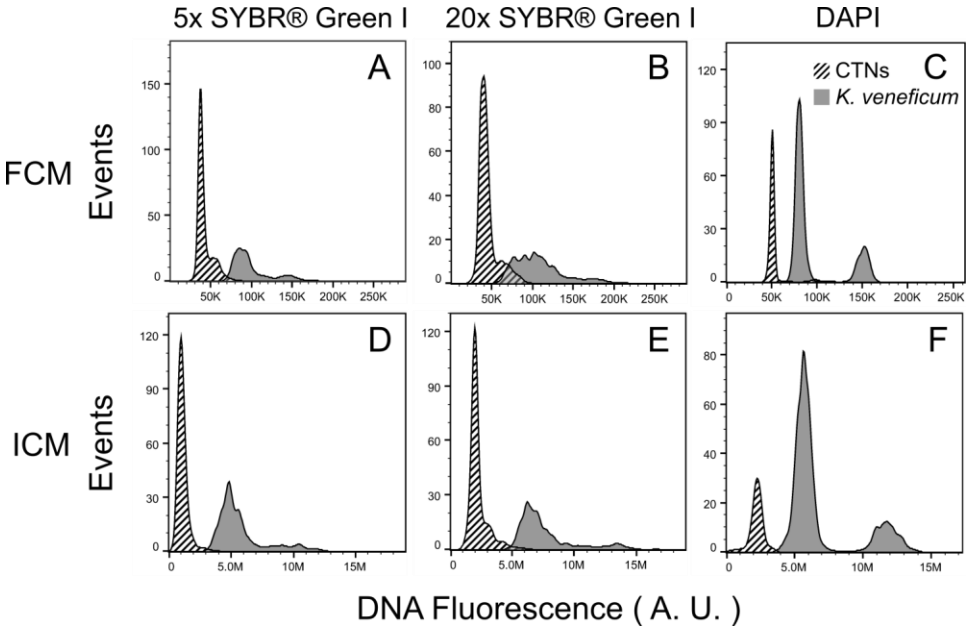

Figure 2.3 Comparison of FCM (A-C) and ICM (D-F) DNA histograms stained with 5x SYBR® Green I (A and D), 20x SYBR® Green I (B and E), and 1 μg mL^{-1} DAPI (C and F). Calf thymocyte nuclei (CTNs; diagonal stripe fill) used as genome size standards for estimating *K. veneficum* (solid gray fill) 1C DNA content (n = 2500 events). Higher magnitude values on the X-axis scale of ICM histograms are due to greater dynamic range for the CCD camera as compared to the FCM photomultiplier tubes.

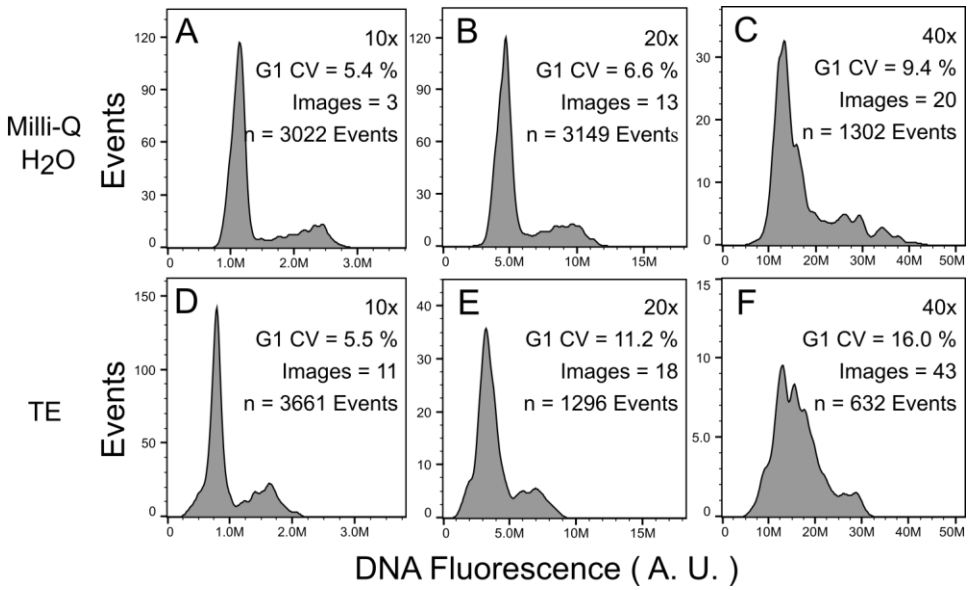

Figure 2.4 Crosswise comparison of the effects of objective magnification (10x, 20x, 40x) and cell resuspension/slide preparation solution (Milli-Q H_2O versus TE) on 1C DNA peak CV's measured by ICM. Scales of X-axes vary due to differences in number of pixels per nucleus as a factor of magnification.

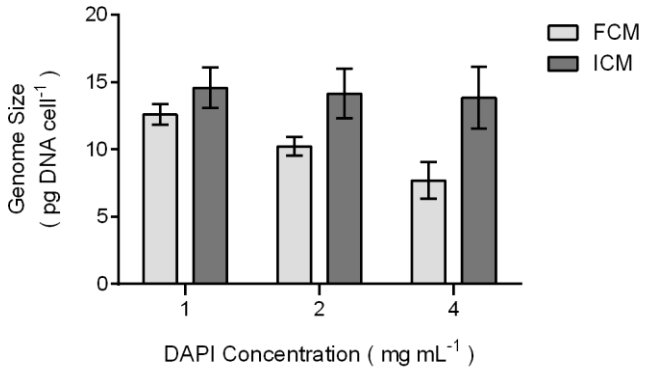

Figure 2.5 The effect of DAPI concentration on genome size estimation for *K. veneficum*, as measured by FCM (light gray) versus ICM (dark gray). Error bars represent ± 1 SD, which were propagated from % CVs of calf thymocyte nuclei and *K. veneficum* 1C DNA peaks (n = 2500 events).

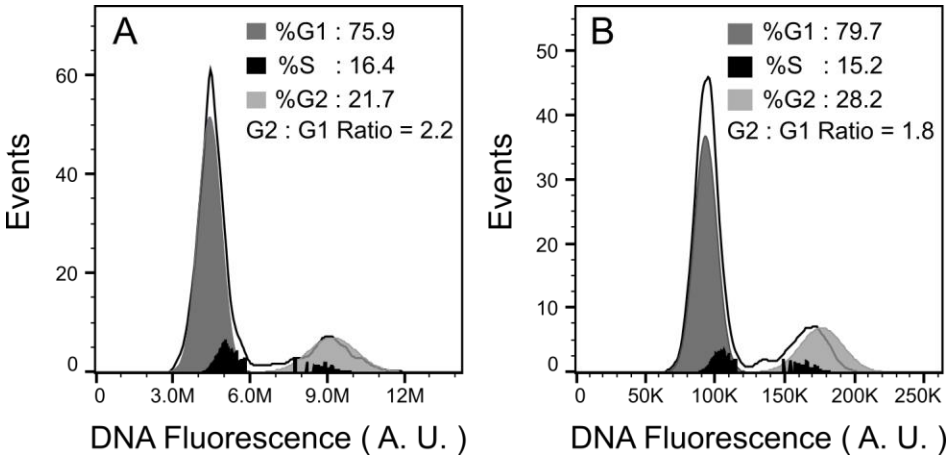

Figure 2.6 Representative DNA histograms from ICM (A) and FCM (B) analysis of the same culture replicate fitted to Watson-Pragmatic cell cycle model. Overlay of Watson Pragmatic cell cycle model is shown, where the proportion of G1-phase is represented with dark gray shading, S-phase is represented with black shading, and G2-phase is represented by light gray shading (n = 2500 events). Deconvolved percentages do not account for population overlaps between G1 and S phases or S and G2 + M phases. X-axis scale differences due to the dynamic range of the CCD camera (ICM) versus photomultiplier tube (FCM).

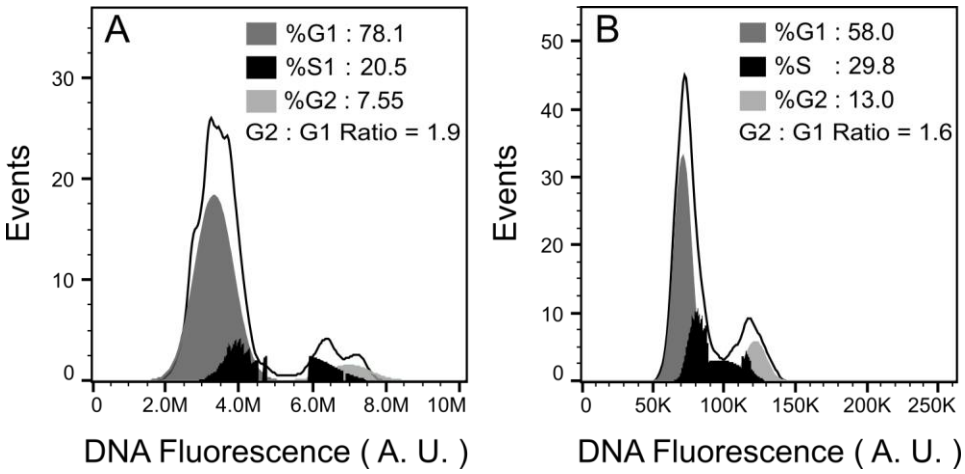

Figure 2.7 Representative DNA histograms from a natural bloom sample; Watson-Pragmatic deconvolution of ICM (A) and FCM (B) collected data (n = 1157 events). Deconvolved percentages do not account for population overlaps between G1 and S phases or S and G2 + M phases. X-axis scale differences due to the dynamic range of the CCD camera (ICM) versus photomultiplier tube (FCM).

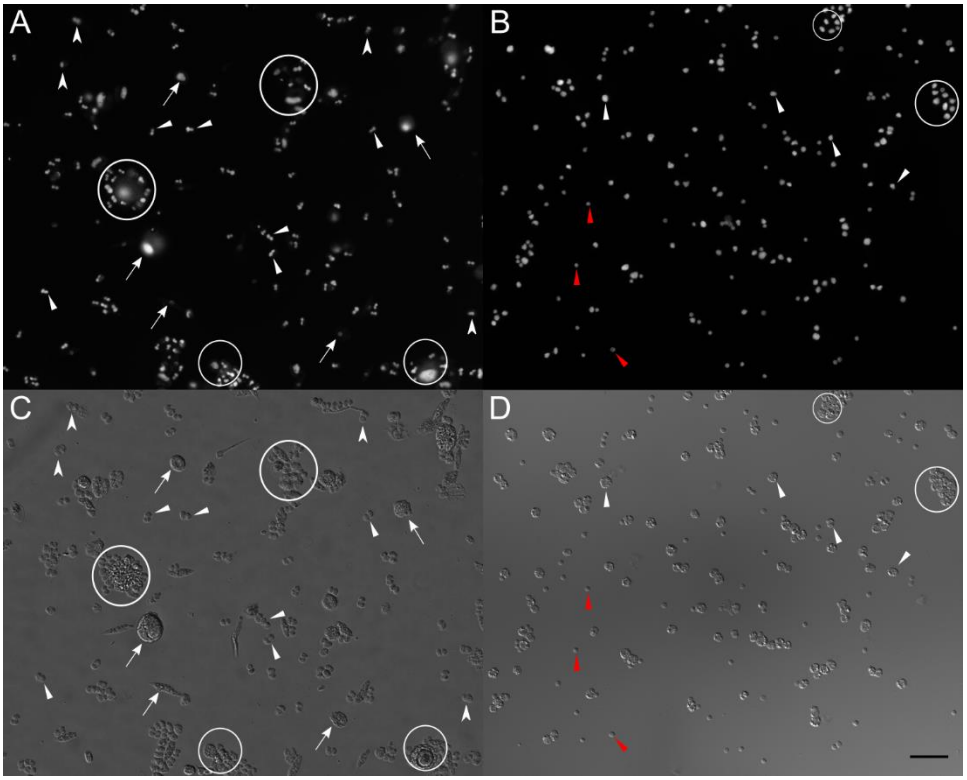

Figure 2.8 Matching epifluorescence (A and B) and brightfield (C and D) images from a *K. veneficum* bloom sample (A and C) and culture (B and D) used for ICM analysis. Calf thymocyte nuclei (red arrowheads) included in *K. veneficum* culture sample as internal DNA standard. In focus *K. veneficum* cells (white arrowheads) and non-target taxa (arrows) are identified using the brightfield image and included/excluded from analysis of the epifluorescence image. Cell clumping (white circles) and out of focus *K. veneficum* cells (notched arrowheads) contributed to the variability of ICM measurements. All images captured at 20x objective magnification. Scale bar = 50 μm.

CHAPTER 3

DIVISION TIME (T_D) FOR *IN SITU* GROWTH MEASUREMENTS DEMONSTRATES THERMAL ECOTYPES OF *KARLODINIUM VENEFICUM*

Erik L. J. E. Broemsen, Allen R. Place, Matthew W. Parrow

Abstract

The toxic dinoflagellate *Karlodinium veneficum* forms fish killing blooms in temperate estuaries worldwide. These blooms have variable toxicity which may be related to bloom stage and *in situ* growth rates of the constituent *K. veneficum* cells. Measurement of *in situ* growth rates is challenging and methods such as the mitotic index technique require knowledge of the dynamics of cell division. In order to better understand these dynamics we determined the duration of cell division (t_d) in four geographically distinct laboratory strains of *K. veneficum* at three different environmentally relevant temperatures. The results demonstrated that the t_d value for each strain, growing at strain-specific optimal temperatures temperatures, was 1.6 ± 0.1 h. This value corresponded to a range of growth rates from 0.17 ± 0.08 d-1 to 0.62 ± 0.07 d-1. Equivalent values of t_d spread across four geographically distinct laboratory strains and a nearly fourfold range of growth rates implies that 1.6 h represents the t_d value of *K. veneficum*. Additionally, temperature conditions yielding this value for t_d and the highest growth rates varied among strains, indicating cold-adapted (Norway), warm-adapted (Florida, USA), and eurythermally-adapted (Maryland, USA) strains. These differences have been apparently retained in culture over many years, indicating a conserved genetic

basis that suggests distinct thermal ecotypes of the morphospecies *K. veneficum*. This knowledge together with the first estimate of t_d for *K. veneficum* will be useful in future field studies aimed at correlating bloom toxicity with *in situ* growth rate using the mitotic index technique.

Introduction

Karlodinium veneficum is a relatively small (~10 µm) bloom forming dinoflagellate that is responsible for major fish kill events in coastal regions around the world (Place et al., 2012; Adolf et al., 2020). The hemolytic and cytotoxic compounds produced by *K. veneficum*, known as karlotoxins (KmTx), have been characterized and can be quantified in culture and in naturally occurring blooms (Bachvaroff et al., 2008; Van Wagoner et al., 2008). Interestingly, KmTx cell quotas can vary between strains and bloom events, with differences between strains varying by as much as 100-fold and single bloom events varying comparably over time (Bachvaroff et al., 2009; Adolf et al., 2015). Furthermore, Deeds et al. (2004) observed a tenfold higher cellular KmTx quota in natural samples than in clonal isolates. Relative to total cell carbon, KmTx content is estimated to vary between 1.2 % and 3.3 %, depending on light and CO2 availability (Adolf et al., 2020; Coyne et al., 2021). Variable toxicity has also been observed under mixotrophic conditions. In cultures pulse fed with the cryptophyte Storeatula major, cellular toxicity was observed to decrease during mixotrophic growth periods, however, this was attributed to increased cellular division rates (Adolf et al., 2020). In contrast, Lin et al. (2017) observed that toxicity (via Crassostrea virginica larval mortality) increased

during mixotrophic growth. Exploring the source of this variation, Adolf et al. (2009) found an inverse correlation between KmTx cell quotas and cellular growth rates, wherein nutrient limited cultures in stationary phase had significantly higher cellular KmTx quotas than those in log phase. This was similar to observations of saxitoxin content in phosphorous limited *Alexandrium tamarensis* cultures (Boyer et al. 1987). This observation could explain the variable toxicity observed in natural blooms, where the most toxic blooms could simply be old, non-growing populations that are essentially in stationary phase. However, actually determining that is challenged by the difficulty of measuring actual, *in situ* growth rates in natural systems.

Measuring *in situ* growth rates has long been a challenge for phytoplankton ecologists. Unfortunately, simple measurement of the change in cell number over time cannot account for the effects of predation and losses due to general cell lysis and convection, or advection of new cells into the area (Garcés and Masó, 2001). A variety of incubation and molecular methods exist that attempt to account for these effects (Rivkin and Seliger, 1981; Videau, 1987; Lin et al., 1995; Liu et al., 2005; Richardson et al., 2006). However, these methods are hampered by potential bottle effects, equipment expense, and the need for high degrees of technical expertise. Alternatively, a more direct approach is to measure the mitotic index, or fraction of dividing cells, in samples from the environment. As early as the 1970s researchers have been using the mitotic index to calculate *in situ* growth rates (Swift and Durbin, 1972; Elbrächter, 1973). The simplest approach is to use fmax, whereby the maximum observed frequency of dividing cells (i.e. mitotic index) is used as the direct estimate the *in situ* growth rate. The disadvantage of

this formula is that it only provides the lower bound estimate for the *in situ* growth rate (Antia et al., 1990). The more reliable formula is that of McDuff and Chisholm (1982):

$$\mu = \frac{1}{nt_d} \sum_{i=1}^{n} ln(1 + f_i) \quad (1)$$

Where μ is the specific growth rate in days-1, fi is the fraction of cells undergoing division (i.e. mitotic index) in sample i, n is the number of samples collected in a 24 hr period, and t_d is the duration of mitosis. This final parameter is critical to the utility of this formula, and is the major weakness of this method as the value of t_d varies between species and must be empirically determined (Weiler and Eppley, 1979; Chisholm, 1981; Rubin, 1981; Videau and Partensky, 1990). Several assumptions about t_d are required for the implementation of this method, these assumptions are: 1) t_d is the same for all cells within a population, 2) t_d is constant for given environmental conditions, and 3) all cells in a population are active (Campbell and Carpenter 1986; Vaulot 1994). It is also important to note that selection of an appropriate sampling interval relative to t_d can have significant impact on the accuracy of specific growth rate estimation. A detailed discussion of this relationship can be found in McDuff and Chisholm (1982).

Ideally, t_d is determined from the same samples used for calculating the *in situ* growth rate by determining the time interval between the peak maxima of the time distributions of two consecutive stages indicative of progression through a terminal phase of the cell cycle. These consecutive stages can be stages of the same terminal phase such as binucleated cells (mitosis) followed by paired cells (subsequent cytokinesis) (Braunwarth and Sommer, 1985), or a combination of pre and post-division stages such

as paired cells in cytokinesis and subsequent newly divided cells (Reguera et al., 2003). Unfortunately, neither of these approaches are feasible with *K. veneficum* because it lacks two morphologically distinct consecutive stages when dividing. The simple morphology offers only a single distinct stage: paired (i.e. in cytokinesis) cells, to mark progression through the cell cycle. Furthermore, nuclear division occurs simultaneously with cytokinesis in *K. veneficum*, precluding the use of binucleated cells as a possible stage of cell division (Leadbeater and Dodge, 1967). Therefore, the value of t_d for *K. veneficum* must be determined empirically in the lab and its variability assessed. In such cases, as addressed by McDuff and Chisholm (1982), this is most easily done with cultures that are undergoing fully asynchronous cell division/growth and have steady state values for μ and fi, wherein Equation 1 above reduces to:

$$\mu = \frac{1}{t_d} \ln(1 + f) \qquad (2)$$

If fully asynchronous growth is achieved, μ and f become constants, and t_d can be solved for. The goal of this study was to do so, and for the first time determine t_d for *K. veneficum* for use in measuring *in situ* growth using the mitotic index technique. Furthermore, to assess potential variability, the t_d of four geographically distinct strains of *K. veneficum* was determined at three different environmentally relevant temperatures. In doing so, strain and temperature specific differences were found that are proposed to represent distinct thermal ecotypes for *K. veneficum*.

Methods

Strains and culture maintenance

Four strains of *K. veneficum* were selected based on origin from distinct geographic regions and represent isolates from subtropic, temperate, and subarctic zones. Strains CCMP 426 (origin: Florida Everglades, Florida), CCMP 1975 (origin: Lower Chesapeake, Hyrock Fish Farm, Princess Anne, Maryland), and CCMP 416 (origin: inner Oslofjord, Norway) were obtained from the National Center for Marine Algae and Microbiota (NCMA), while strain 2010 IH, was isolated by co-author Place's lab from the Baltimore Inner Harbor (Upper Chesapeake; Broemsen et al., 2021). Additionally strain CCMP 2936, isolated from the Delaware Inland Bays, was included in this study to test the accuracy of growth rate estimates of the mitotic index technique using the estimated t_d determined here. Prior to experimentation all strains were maintained on a 12:12 h L:D schedule with 30 µmole photons m-2 s-1 illumination provided by daylight deluxe fluorescent bulbs at 20 °C in 15 ppt EH-1 enriched artificial seawater with 1mM Hepes, modified from Berges et al. (2001).

Experimental design

K. veneficum naturally exhibits synchronous cell division when grown under an alternating light:dark cycle (Adolf et al., 2020). In order to induce asynchronous cell division and to calculate steady state values for µ and fi each strain was grown under

constant illumination. The variability of t_d as a function of temperature was assessed by growing asynchronous cultures at 15 °C, 20 °C, and 25 °C with 95 μmole photons m-2 s-1 light intensity. All cultures were acclimated to these growth conditions for at least two weeks by serial transfer prior to splitting the culture into triplicate for the experiment. Once triplicate cultures reached mid-log cell densities, 27 hours of hourly sampling commenced for cell cycle analysis, cell density, and mitotic index.

Unfortunately, strain CCMP 416 did not maintain growth under constant illumination during the two-week acclimation period. Therefore, it was grown under a 12:12 L:D schedule with all other conditions identical to the other strains. This scenario was addressed by McDuff and Chisholm (1982), where they reference experiments carried out by Rubin (1981) demonstrating that t_d values for *Alexandrium tamarense* grown at optimal temperature under 12:12 L:D and constant illumination are the same.

Mitotic index and cell density

Samples collected for mitotic index and cell density measurements were fixed with 1 % acidic Lugol's solution. The mitotic index and cell densities were determined simultaneously from a minimum of 100 cells counted by transect on a Palmer-Maloney counting chamber (Wetzel and Likens, 1991). Mitotic index was calculated as the fraction of paired (dividing) cells (Figure 1) per the total number of cells counted per sample. Note: the morphology of gamete fusion differs from that of cell division in *K. veneficum* (Adolf et al. 2020), so such events (if occurring) can be distinguished, as in Brosnahan et al. (2015).

Cell cycle analysis

While monitoring the mitotic index throughout the sampling period will indicate the degree of cell division synchrony, it provides little information about other phases of the cell cycle. Therefore, flow cytometric cell cycle analysis was performed in order to verify that growth under constant illumination desynchronized the cell cycle in *K. veneficum*. For each time point 50 mL of culture was collected and fixed with 5% formalin and 0.1% Tween 80 (final concentrations) overnight at 4 °C. The fixed cells were then prepared for cell cycle analysis by centrifugation at 3000 g for 10 min, followed by resuspension in 50 mL of 70% methanol, and incubation at 4 °C in the dark overnight. After this overnight incubation cells were pelleted at 2000 g for 10 min and resuspended in 500 µL TE (10 mM Tris-HCl and 1 mM EDTA) with 0.1% Tween 80. These cell suspensions were then stained with 4', 6 – diamidino – 2 – phenylindole (DAPI) at a final concentration of 1 µg mL-1.

Cell cycle analysis was conducted on the stained cell suspensions using a BD LSRFortessa™ flow cytometer (BD Biosciences) equipped with a 405 nm 50 mW solid – state laser following methods of Kremp and Parrow (2006). Replicate DNA histograms were then deconvoluted using FlowJo V10.8 (FlowJo) to estimate cell cycle phase distributions.

Calculation of the duration of cytokinesis

Historically, t_d has been described in terms of mitosis because mitotic indices are often determined from the frequency of binucleated cells. However, for this study mitotic indices are determined by the frequency of dividing cells. As such herein we will refer to t_d as the duration of cytokinesis. Duration of cytokinesis was calculated for each strain at each temperature according to the equations of McDuff and Chisholm (1982) rearranged to solve for t_d. For strains exhibiting asynchronous cell division the simplified formula:

$$t_d = \frac{1}{\mu}\ln(1+f) \tag{3}$$

was used where μ was calculated from the slope of the linear regression of the cell density data transformed by the natural logarithm, and f was calculated by averaging the mitotic indices of all 27 time points. In the case of strain CCMP 416, grown on a 12:12 L:D schedule, the formula:

$$t_d = \frac{1}{n\mu}\sum_{i=1}^{n} ln(1+f_i) \tag{4}$$

was used. Because cell division for this strain was not asynchronous μ was calculated from cell density data from two time points that were 24 hours apart using the formula:

$$\mu = \frac{ln\,{}^{N_1}/_{N_0}}{T_1 - T_0} \quad (5)$$

where N1 and N0 are the cell densities at times T1 and T0, respectively.

Comparison of mitotic index and cell density growth rate estimates

In order to test the accuracy of the growth rate estimation, the mitotic index technique was used with the determined t_d and applied to strains 2010 IH and CCMP 2936. In this experiment, the strains were acclimated to a 12:12 L:D cycle at 25 °C over the course of two weeks by serial transfer. Following acclimation, cultures were split into triplicates and upon reaching midlog growth, and sampling commenced. Subsamples were collected and fixed with 1 % acidic Lugol's solution every two hours for 48 hours. Mitotic indices and cell density were determined for each time point as described above. Growth rates were calculated using equations 1 and 5, using the determined value for t_d (below), and compared.

Statistical Analyses

Calculation of mitotic indices, cell densities, μ, and error propagation were all carried out in Microsoft® Excel® software 2013 (Microsoft Corporation). All hypothesis testing and figure construction was carried out using GraphPad Prism™ 6 (GraphPad Software).

Results

Cell cycle analysis

In order to verify asynchronous growth of cultures grown under continuous illumination, cell cycle progression was monitored throughout the duration of the mid-log sampling. All strains grown under continuous illumination did not oscillate in cell cycle phase proportions over time (= asynchronous growth), and within strains the average percentage of each cell cycle phase varied little between 15 °C, 20 °C, and 25 °C (Figure 2).

Using the formulas of Slater et al. (1977) and the cell cycle phase distributions, durations of G1, S, and G2 + M phases were calculated for all asynchronously grown strains at each temperature (Figure 3). The durations for each cell cycle phase increased in length with decreases in growth rate (i.e. increased generation time), with G1 phase showing the greatest increases in duration for each strain. However, the proportion of the entire cell cycle duration occupied by each cell cycle phase remained mostly unchanged with temperature (Table 1; One - way ANOVA, all p – values ≥ 0.42).

Culture growth rate for t_d determination

All strains had significant positive growth at all temperatures, with the exceptions of strains CCMP 416 and CCMP 426 (Figures 4 and 5). Strain CCMP 416 (Norway) failed to grow during the two-week acclimation period at 25 °C (warmest temperature

tested). Alternatively, CCMP 426 (Florida, USA) completed acclimation to 15 °C (coldest temperature tested), but, failed to continue to grow following separation into replicate cultures (p – value = 0.16). Two – way ANOVA analysis indicated a significant interaction between strain and temperature (p – value < 0.0001). Multiple comparisons (Tukey corrected) within strains were carried out to determine optimal growth temperatures. For strains 2010 IH and CCMP 426 the optimal growth temperatures were 25 °C, and for strains CCMP 1975 and CCMP 416 it was 20 °C (Figure 5).

Mitotic index

For strains grown under continuous illumination, mitotic indices did not oscillate (Figure 6A - I). However, mitotic indices for strain CCMP 416, grown under 12:12 L:D oscillated, with the peak percentage of paired cells occurring during the dark period (Figure 6J and 6K). The average mitotic index during dark and light periods for CCMP 416 at 15 °C were 2.1 ± 0.2 % and 1.2 ± 0.1 %, respectively, and were significantly different from each other (T – test, p – value < 0.001). Similarly at 20 °C, dark and light periods had average frequencies of 2.3 ± 0.3 % and 1.3 ± 0.2 %, with the dark and light period mitotic indices being significantly different (T – test, p – value < 0.01).

Duration of cytokinesis

Mitotic indices and growth rates were used to calculate t_d for each strain and temperature (Figure 7). Two – way ANOVA comparison of t_d indicated a significant

interaction effect between strain and temperatures (p – value = 0.01). Analysis by Tukey's multiple comparisons within strains indicated significant differences occurred only within strain CCMP 426 at 15 °C where the culture growth rate was not significantly different from zero, causing an erroneously high estimation of t_d in that treatment (Figure 7).

To verify that a significant interaction was not due only to inclusion of strain CCMP 426 a two – way ANOVA analysis was conducted excluding all data from this strain. The interaction effect between strain and temperature remained significant (p – value < 0.01), and within strains comparisons indicated significant differences within 2010 IH and CCMP 416, but not strain CCMP 1975 (Figure 7). Differences identified within CCMP 416 corresponded to 25 °C where culture growth did not occur. One – way ANOVA comparison of the shortest estimated t_d for each strain indicated no significant difference between all strains including CCMP 426 (p – value = 0.94), and the determined mean value of t_d across all examined strains of *K. veneficum* was 1.6 ± 0.1 hours

Growth rate comparisons

Comparison of growth rates estimated by the mitotic index technique (μMI) using a t_d of 1.6 and cell density increase over time (μobs) was carried out using cultures of 2010 IH and CCMP 2936 grown under 12:12 L:D cycles. These cultures increased in cell density over the 48 hour sampling period (Figure 8A and 8B). Paired cell frequencies oscillated with a 24 hour period and peaks occurred near the middle of both dark periods

(Figure 8C and 8D). Growth rates calculated based on mitotic index versus cell density were the same for each of the two strains when calculated over the entire 48 h sampling period. (Figure 9A and 9B; 2010 IH p – value = 0.40, CCMP 2936 p – value = 0.16).

Discussion

Being able to measure the species-specific growth rate of harmful bloom forming phytoplankton *in situ* offers the opportunity to better monitor and model the impacts of these organisms. Laboratory experiments can contribute to this by providing insight into their ecophysiology. However, laboratory observations can be misleading as evidenced by Brosnahan et al. (2015), wherein *in situ* growth rates measured during a A. fundyense bloom in nature were ~2x greater than batch co-cultures or any rates previously observed in batch culture at comparable temperatures. Clearly the complexity of natural systems necessitates testing of laboratory observations in the field, and attempting to replicate the study of Brosnahan et al. (2015) in a *K. veneficum* bloom would be very valuable, especially since *K. veneficum* blooms are apparently impacted by sexual stages and *Amoebophyra* sp. infections, like *A. fundyense* (Brosnahan et al., 2015; Adolf et al., 2020). In the *K. veneficum,* the inverse relationship observed in the laboratory between toxicity and growth rate must also be confirmed in natural blooms, and hopefully the results from this study will aid in that (Adolf et al., 2009; 2020). The data presented here are the first estimate of t_d for *K. veneficum,* and the variable growth characteristics observed between strains in response to temperature indicates significant differences

between strains that correspond with distinct ecotypes adapted to the strains' original habitats.

Due to its simple division morphology, determination t_d for *K. veneficum* in the laboratory was ideally performed with asynchronously dividing cultures with steady state growth rates and frequencies of dividing cells (McDuff and Chisholm, 1982). As shown in Figures 2 and 6, all *K. veneficum* strains used in this study, with the exception of CCMP 416, were induced into asynchronous division by growth under continuous illumination. In a survey of tolerance to continuous illumination for 22 different phytoplankton species representing diatoms, dinoflagellates, coccolithophores, and cyanobacteria, Brand and Guillard (1981) found *Ceratium candelabrum* to be inhibited by continuous illumination, while most of the other dinoflagellates studied had variable responses to continuous illumination depending on the intensity of illumination. Leighfield and Van Dolah (2001) also observed that *Amphidinium operculatum* cultures failed to grow under continuous illumination, and speculated that expression of necessary genes phased to occur during dark periods (e.g. nitrate reductase) may limit growth when dark periods are absent. However, Paasche et al. (1984) showed that *K. veneficum* strain CCMP 416 (as strain KT-76D), had reduced nitrate assimilation rates during dark periods. This suggests that it is unlikely that nitrogen assimilation would be the limiting factor for growth under continuous illumination for CCMP 416, as nitrate reductase activity appears to be light dependent, which is also consistent with observations from many other microalgae (Dagenais-Bellefeuille and Morse, 2013; 2016). Alternatively, light to dark transitions may function as an entraining cue for cell division (Van Dolah et al., 1996), or dark periods may be important as times during which photosystem II repair

occurs (Li et al., 2016). However,, as mentioned by McDuff and Chisholm (1982) and as demonstrated in this present study (Figures 7 and 9), t_d does not vary between cultures grown under continuous illumination or periodic light cycles. We, therefore, expect that variable light (or nutrient) regimes will not alter t_d.

For those strains induced into asynchronous growth the durations of all cell cycle phases were observed to increase with decreasing growth rates (i.e. increasing generation time). The greatest change in phase duration was observed for the G1 phases, followed by the G2 + M phases, and the smallest changes were observed in the S phases. Past dinoflagellate and yeast cell cycle studies have made similar observations (Vanoni et al., 1984; Olson et al., 1986; Taroncher-Oldenburg et al., 1999), and this may be explained by temperature effects on first order enzyme kinetics where decreases in temperature reduce enzymatic activity (Vaulot, 1994). This was further supported by observations showing that the duration of each phase relative to the total length of the cell cycle was largely unchanged by temperature, an indication that the inhibitory effects were equal across all phases (Table 1). Furthermore, the average duration of G1, S, and G2 + M phases for these three strains grown under optimal temperatures were 26.7 ± 8.1 h, 2.7 ± 1.2 h, and 11.7 ± 7.4 h, respectively. This is consistent with durations calculated for S and G2 + M phases in previous *K. veneficum* cell cycle studies (Adolf et al., 2020).

Different optimal growth temperatures were observed between the strains examined in this study. This was most obvious for strains CCMP 416 (Norway) and CCMP 426 (Florida), which had significant growth inhibition at the warm and cold extremes of the tested temperature range, respectively. These observations were consistent with adaptation to the average temperatures of their original respective

habitats, where inner Oslofjord water temperatures rarely exceed 20 °C and Florida Everglades water temperatures rarely fall below 20 °C (Stabenau and Kotun, 2012; Lundsør et al., 2020). Similar to the results observed here for CCMP 416, Nielsen (1996) found CCMP 415 (as strain KT-76E, isolated simultaneously with CCMP 416 from the inner Oslofjord; Bjørnland and Tangen, 1979; Tengs et al., 2001) failed to grow at temperatures above 20 °C in 10 ppt K medium. However, when the salinity was increased to 14 ppt growth inhibition at warmer temperatures was alleviated. Additionally, CCMP 415 growth was observed to occur at temperatures as low as 7 °C regardless of salinity. From these experiments Nielsen concluded the optimal temperature and salinity for CCMP 415 was 21 °C and 23 ppt. However, this does not detract from the argument that these strains appeared optimally adapted to temperature regimes of their original habitats, especially considering that the highest growth rate for CCMP 426 (0.62 ± 0.07 day-1) was at 25 °C while that observed for CCMP 415 by Nielsen (1996) was 21 °C with a comparable rate. The temperate Chesapeake Bay strains were capable of growth at all three temperatures, consistent with the range of temperatures observed in the Chesapeake Bay (Ding and Elmore, 2015). Furthermore, the optimal growth temperature for strain 2010 IH (25 °C) was consistent with the temperatures (23 °C to 27 °C) measured during blooms of *K. veneficum* in the Baltimore Inner Harbor, where this strain was isolated (Adolf et al., 2008). In fact, the optimal growth temperatures for both Chesapeake Bay strains were well within the range of temperatures at which the majority of blooms occur in the Chesapeake Bay (Place et al., 2012).

Similar to the growth rate data, the estimated t_d values varied depending on the strain and temperature, with non-optimal temperatures dramatically decreasing growth

rate and thus erroneously increasing the estimated t_d. However, at growth-promoting temperatures, the t_d values estimated for each of the four examined strains could not be statistically distinguished, and indicate that the t_d for *K. veneficum* is 1.6 ± 0.1 hours. This average is on the lower end of t_d values calculated for past field and culture studies of other phytoplankton which ranged from 1 hour to 8 hours (Rubin, 1981; Videau and Partensky, 1990; Litaker et al., 2002; Reguera et al., 2003). The mean t_d for *K. veneficum* estimated here is also supported by the observation that the growth rate of strain CCMP 426 at 25 °C was twice that of the growth rate at 20 °C, while the average t_d values at the two temperatures differed by only 0.11 hours and were statistically indistinguishable (Figures 5 and 7; T – test, p – value = 0.62).

The variances observed in t_d among treatments was at first glance concerning, as pointed out in McDuff and Chisholm (1982) the mitotic index technique would be of limited utility if t_d was found to be highly variable or strictly a function of growth rate. However, when excluding the non – growing temperature treatments the values of t_d calculated here vary little; differing from one another only for two sub – optimal temperatures for a single strain (2010 IH; Tukey's multiple comparison, p – value < 0.01). This is despite significant geographic and phylogenetic differences (Tengs et al., 2001). Furthermore, exponential regression analysis of t_d vs specific growth rate shows that growth rate was a poor predictor of t_d (Figure 10; R2 = 0.48), an indication that t_d was not a function of growth rate. Given these observations and the fact that *K. veneficum* blooms are seasonal (Li et al 2015), most often occurring above 21 °C (Li et al., 2000, Li et al., 2015, Huang et al., 2019), and that all other t_d values determined here are indistinguishable across an ~ 4x range of growth rates (0.17 for CCMP 1975 at 15 °C to

0.62 for CCMP 426 at 25 °C) an average t_d of 1.6 ± 0.1 h calculated from the shortest values of each strain would be a conservative estimate of t_d for *K. veneficum*.

The variation in *K. veneficum* growth characteristics observed in this study adds to a long list of existing observations of intra-specific variability for this species. Bachvaroff et al. (2009) noted differences in toxin profiles based on geographical origin as well as variability in growth rates amongst 18 *K. veneficum* strains. Calbet et al. (2011) observed variation in several physiological and biochemical traits including growth rate, mixotrophic performance, and fatty acid composition for eleven Mediterranean *K. veneficum* strains isolated from the same bloom event. Phylogenetic analyses also indicate that Norwegian strains (CCMP 415 and CCMP 416) group closely to but distinctly separate from Chesapeake Bay strains based on both nuclear and plastid small subunit rDNA (Tengs et al., 2001). Furthermore, variability in growth characteristics and production of KmTx congeners have been reported between these same Norwegian strains (Adolf et al., 2020). Even significant differences in genome size have been reported among strains of *K. veneficum* (Adolf et al., 2020).

The need for evaluating intra-specific variability has long been emphasized in the field of phytoplankton ecology (Braarud, 1951; Wood and Leatham, 1992). However, the interpretation of such studies is tempered by the potential impact of evolutionary processes on long term laboratory culturing of microalgae (Lakeman et al., 2009). Calbet et al. (2011) counter this by asserting that strain variability in *K. veneficum* is likely a resilient trait, evidenced by the persistence of strain variability in their study following prolonged laboratory culturing. While the NCMA strains of *K. veneficum* used in this current study have been in culture for at least 25 years , the optimum growth temperatures

determined here do not reflect selection towards the temperatures reported by NCMA for culture maintenance (14 °C for CCMP 416 and CCMP 1975, 20 °C for CCMP 426; https://ncma.bigelow.org/, last accessed 6-2-2022). Furthermore, the t_d of 1.6 h shared by all strains in this study points towards a highly conserved genetic basis for the maximum speed at which the final stage of cell division can occur in *K. veneficum*. Given the established pervasiveness of strain variability and the variation in temperatures at which optimal growth rates occured for *K. veneficum*, it is evident that the strains studied here represent three distinct thermal ecotypes; a cold-adapted ecotype (CCMP 416), a eurythermal ecotype (CCMP 1975), and a warm-adapted ecotype (CCMP 426 and 2010 IH).

The utility of our estimate of t_d for measuring the specific growth rate of *K. veneficum* by counting only the fraction of dividing cells, not cell numbers, was apparent (Figure 9). Not only were both methods for growth rate estimation indistinguishable for strain 2010 IH, but also for strain CCMP 2936 for which t_d was not determined. While these cultures were grown under nutrient and light replete conditions, we expect that limitation of these would not have a significant impact on t_d or the accuracy of *in situ* growth rate estimation. Nutrient and light limitation can alter growth rates, however, the effect of this in many phytoplankton species is often observed to result in the extension of the duration of G1 phase of the cell cycle leaving G2 + M phase (within which cytokinesis occurs) unchanged (Olson et al 1986; Olson and Chisholm 1986; Vaulot 1994). Furthermore, *K. veneficum* cultures arrest in G1 during stationary phase when nutrient concentrations become limiting, resulting in an increased G1 phase duration (Adolf et al., 2020). Conversely, nutritional supplementation of *K. veneficum* via

mixotrophy has been observed to result in a reduced G1 phase duration while leaving other phases unchanged (unpublished data).

Considering the unlikely occurrence of blooms under suboptimal temperatures, and the apparent genetically conserved nature of our estimate of t_d, the value calculated here (1.6 h) should have broad applicability for determining *in situ* growth rates of natural populations of *K. veneficum*. At worst, use of this estimate in the formula of McDuff and Chisholm (1982) would provide an upper bound limit for *in situ* growth rates, which can then be contrasted with a lower bound limit estimated by the fmax approach (Antia et al., 1990; Vaulot, 1992). This may provide useful knowledge for future field studies to understand the relationship between toxicity and *in situ* growth rates of natural blooms, and may greatly benefit modeling and management efforts in fisheries impacted by *K. veneficum* blooms. The data presented here also identify three distinct thermal ecotypes of *K. veneficum*, further illustrating the complex evolutionary diversity within the *K. veneficum* morphospecies.

References

Adolf, J.E., Bachvaroff, T., Place, A.R., 2008. Can cryptophyte abundance trigger toxic *Karlodinium veneficum* blooms in eutrophic estuaries? Harmful Algae 8(1), 119-128.

Adolf, J.E., Bachvaroff, T.R., Deeds, J.R., Place, A.R., 2015. Ichthyotoxic *Karlodinium veneficum* (Ballantine) J Larsen in the Upper Swan River Estuary (Western Australia): Ecological conditions leading to a fish kill. Harmful Algae 48, 83-93.

Adolf, J.E., Bachvaroff, T.R., Place, A.R., 2009. Environmental modulation of karlotoxin levels in strains of the cosmopolitan dinoflagellate, *Karlodinium veneficum* (Dinophyceae). J. Phycol. 45(1), 176-192.

Adolf, J.E., Parrow, M.W., Place, A.R., 2020. *Karlodinium veneficum*: Still blooming and toxic sixty-two years later, In: Subba Rao, V.D. (Ed.), Dinoflagellates. Nova Science Publishers, Inc., pp. 355 - 402.

Antia, A.N., Carpenter, E.J., Chang, J., 1990. Species-specific phytoplankton growth rates via diel DNA synthesis cycles. III. Accuracy of growth rate measurement in the dinoflagellate *Prorocentrum minimum*. Mar. Ecol. Prog. Ser. 63, 273 - 279.

Bachvaroff, T.R., Adolf, J.E., Place, A.R., 2009. Strain variation in *Karlodinium veneficum* (Dinophyceae): Toxin profiles, pigments, and growth characteristics. J. Phycol. 45(1), 137-153.

Bachvaroff, T.R., Adolf, J.E., Squier, A.H., Harvey, H.R., Place, A.R., 2008. Characterization and quantification of karlotoxins by liquid chromatography-mass spectrometry. Harmful Algae 7(4), 473-484.

Berges, J.A., Franklin, D.J., Harrison, P.J., 2001. Evolution of an artificial seawater medium: Improvements in enriched seawater, artificial water over the last two decades. J. Phycol. 37(6), 1138-1145.

Bjørnland, T., Tangen, K., 1979. Pigmentation and morphology of a marine *Gyrodinium* (DINOPHYCEAE) with a major carotenoid different from peridinin and fucoxanthin. J. Phycol. 15, 457 - 463.

Boyer, G.L., Sullivan, J.J., Andersen, R.J., Harrison, P.J., Taylor, F.J.R., 1987. Effects of nutrient limitation on toxin production and composition in the marine dinoflagellate *Protogonyaulax tamarensis*. Mar. Biol. 96(1), 123-128.

Braarud, T., 1951. Taxonomical studies of marine dinoflagellates. Nytt magasin for naturvidenskapene 88, 43 - 48.

Brand, L.E., Guillard, R.R.L., 1981. The effects of continuous light and light intensity on the reproduction rates of twenty-two species of marine phytoplankton. J. Exp. Mar. Biol. and Ecol. 50, 119 - 132.

Braunwarth, C., Sommer, U., 1985. Analyses of the *in situ* growth rates of Cryptophyceae by use of the mitotic index technique. Limnol. Oceanogr. 30(4), 893-897.

Broemsen, E.L.J.E., Place, A.R., Parrow, M.W., 2021. Quantitative nuclear DNA content and cell cycle analysis of a mixotrophic dinoflagellate by image cytometry. Limnol. Oceanogr. Methods 19(4), 253-266.

Brosnahan, M.L., Velo-Suárez, L., Ralston, D.K., Fox, S.E., Sehein, T.R., Shalapyonok, A., Sosik, H.M., Olson, R.J., Anderson, D.M., 2015. Rapid growth and concerted sexual transitions by a bloom of the harmful dinoflagellate *Alexandrium fundyense* (Dinophyceae). Limnol. Oceanogr. 60(6), 2059-2078.

Calbet, A., Bertos, M., Fuentes-Grünewald, C., Alacid, E., Figueroa, R., Renom, B., Garcés, E., 2011. Intraspecific variability in *Karlodinium veneficum*: Growth rates, mixotrophy, and lipid composition. Harmful Algae 10(6), 654-667.

Campbell, L., Carpenter, E.J., 1986. Diel patterns of cell division in marine *Synechococcus* spp. (Cyanobacteria): use of the frequency of dividing cells technique to measure growth rate. Mar. Ecol. Prog. Ser. 32(2/3), 139-148.

Chisholm, S.W., 1981. Temporal patterns of cell division in unicellular algae. Can. Bull. Fish. Aquat. Sci. 210, 150 - 181.

Coyne, K.J., Salvitti, L.R., Mangum, A.M., Ozbay, G., Main, C.R., Kouhanestani, Z.M., Warner, M.E., 2021. Interactive effects of light, CO2 and temperature on growth and resource partitioning by the mixotrophic dinoflagellate, *Karlodinium veneficum*. PLOS ONE 16(10), e0259161.

Dagenais-Bellefeuille, S., Morse, D., 2013. Putting the N in dinoflagellates. Front. Microbiol. 4, 369.

Dagenais Bellefeuille, S., Morse, D., 2016. The main nitrate transporter of the dinoflagellate Lingulodinium polyedrum is constitutively expressed and not responsible for daily variations in nitrate uptake rates. Harmful Algae 55, 272-281.

Deeds, J.R., Kibler, S.R., Tester, P.A., Place, A.R., 2004. Geographic strain variation in toxin production in *Karlodinium micrum* (Dinophyceae) from Southeastern United States, In: Steidinger, K.A., Landsberg, J.H., Tomas, C.R., Vargo, G.A. (Eds.), Harmful Algae 2002, IOC-UNESCO, Florida, pp. 145-147.

Ding, H., Elmore, A.J., 2015. Spatio-temporal patterns in water surface temperature from Landsat time series data in the Chesapeake Bay, U.S.A. Remote Sens. Environ. 168, 335-348.

Elbrächter, M., 1973. Population dynamics of *Ceratium* in coastal waters of the Kiel Bay. Oikos 15, 43 - 48.

Garcés, E., Masó, M., 2001. Phytoplankton potential growth rate versus increase in cell numbers estimation of cell lysis. Mar. Ecol. Prog. Ser. 212, 297-300.

Huang, H.-L., Shao, Q.-W., Zhu, X.-J., Luo, J., Meng, R., Zhou, C.-X., Zhu, P., Zhu, Y.-F., Yan, X.-J., 2019. Distribution of *Karlodinium veneficum* in the coastal region of Xiangshan Bay in the East China Sea, as detected by a real-time quantitative PCR assay of ribosomal ITS sequence. Harmful Algae 81, 65-76.

Kremp, A., Parrow, M.W., 2006. Evidence for asexual resting cysts in the life cycle of the marine peridinoid dinoflagellate, *Scrippsiella hangoei*. J. Phycol. 42(2), 400-409.

Lakeman, M.B., von Dassow, P., Cattolico, R.A., 2009. The strain concept in phytoplankton ecology. Harmful Algae 8(5), 746-758.

Leadbeater, B., Dodge, J.D., 1967. An electron microscope study of nuclear and cell division in a dinoflagellate. Archiv für Mikrobiologie 57(3), 239-254.

Leighfield, T.A., Van Dolah, F.M., 2001. Cell cycle regulation in a dinoflagellate, *Amphidinium operculatum*: identification of the diel entraining cue and a possible role for cyclic AMP. J. Exp. Mar. Biol. Ecol. 262(2), 177-197.

Li, J., Glibert, P.M., Gao, Y., 2015. Temporal and spatial changes in Chesapeake Bay water quality and relationships to *Prorocentrum minimum, Karlodinium veneficum,* and CyanoHAB events, 1991–2008. Harmful Algae 42, 1-14.

Li, A., Stoecker, D.K., Coats, D.W., 2000. Spatial and temporal aspects of *Gyrodinium galatheanum* in Chesapeake Bay: distribution and mixotrophy. J. Plankton Res. 22(11), 2105-2124.

Li, G., Woroch, A.D., Donaher, N.A., Cockshutt, A.M., Campbell, D.A., 2016. A hard day's night: Diatoms continue recycling photosystem II in the dark. Front. Mar. Sci. 3.

Lin, C.H., Accoroni, S., Glibert, P.M., 2017. *Karlodinium veneficum* feeding responses and effects on larvae of the eastern oyster Crassostrea virginica under variable nitrogen:phosphorus stoichiometry. Aquat. Microb. Ecol. 79(2), 101-114.

Lin, S., Jeng, C., Carpenter, E.J., 1995. Growth characteristics of phytoplankton determined by cell cycle proteins: PCNA immunostaining of *Dunaliella tertiolecta* (Chlorophyceae). J. Phycol. 31(3), 388-395.

Litaker, R.W., Warner, V.E., Rhyne, C., Duke, C.S., Kenney, B.E., Ramus, J., Tester, P.A., 2002. Effect of diel and interday variations in light on the cell division pattern and *in situ* growth rates of the bloom-forming dinoflagellate *Heterocapsa triquetra*. Mar. Ecol. Prog. Ser. 232, 63-74.

Liu, J., Jiao, N., Hong, H., Luo, T., Cai, H., 2005. Proliferating cell nuclear antigen (PCNA) as a marker of cell proliferation in the marine dinoflagellate *Prorocentrum donghaiense* Lu and the green alga *Dunaliella salina* Teodoresco. J. Appl. Phycol. 17(4), 323-330.

Lundsør, E., Stige, L.C., Sørensen, K., Edvardsen, B., 2020. Long-term coastal monitoring data show nutrient-driven reduction in chlorophyll. J. Sea Res. 164, 101925.

McDuff, R.E., Chisholm, S.W., 1982. The calculation of *in situ* growth rates of phytoplankton populations from fractions of cells undergoing mitosis: A clarification. Limnol. Oceanogr. 27(4), 783-788.

Needham, D.M., Fuhrman, J.A., 2016. Pronounced daily succession of phytoplankton, archaea and bacteria following a spring bloom. Nat. Microbiol. 1(4), 16005.

Nielsen, M.V., 1996. Growth and chemical composition of the toxic dinoflagellate *Gymnodinium galatheanum* in relation to irradiance, temperature and salinity. Mar. Ecol. Prog. Ser. 136, 205 - 211.

Olson, R.J., Chisholm, S.W., 1986. Effects of light and nitrogen limitation on the cell cycle of the dinoflagellate *Amphidinium carteri*. J. Plankton Res. 8(4), 785-793.

Olson, R.J., Vaulot, D., Chisholm, S.W., 1986. Effects of environmental stresses on the cell cycle of two marine phytoplankton species. Plant Physiol. 80, 918 - 925.

Paasche, E., Bryceson, I., Tangen, K., 1984. Interspecific variation in dark nitrogen uptake by dinoflagellates. J. Phycol. 20, 394 - 401.

Place, A.R., Bowers, H.A., Bachvaroff, T.R., Adolf, J.E., Deeds, J.R., Sheng, J., 2012. *Karlodinium veneficum*—The little dinoflagellate with a big bite. Harmful Algae 14, 179-195.

Reguera, B., Garcés, E., Pazos, Y., Bravo, I., Ramilo, I., González-Gil, S., 2003. Cell cycle patterns and estimates of *in situ* division rates of dinoflagellates of the genus *Dinophysis* by a postmitotic index. Mar. Ecol. Prog. Ser. 249, 117-131.

Richardson, T.L., Pinckney, J.L., Walker, E.A., Marshalonis, D.M., 2006. Photopigment radiolabelling as a tool for determining *in situ* growth rates of the toxic dinoflagellate *Karenia brevis* (Dinophyceae). Eur. J. Phycol. 41(4), 415-423.

Rivkin, R.B., Seliger, H.H., 1981. Liquid scintillation counting for 14C uptake of single algal cells isolated from natural samples. Limnol. Oceanogr. 26(4), 780-785.

Rubin, C.G., 1981. Measurements of *in situ* growth rates of *Gonyaulax tamarensis*: The New England red tide organism, Department of Civil Engineering. Massachusetts Institute of Technology, p. 54.

Slater, M.L., Sharrow, S.O., Gart, J.J., 1977. Cell cycle of *Saccharomyces cerevisiae* in populations growing at different rates. Proc. Natl. Acad. Sci. USA 74(9), 3850-3854.

Stabenau, E., Kotun, K., 2012. Salinity and Hydrology of Florida Bay: Status and Trends 1990 - 2009., National Park Service, Everglades National Park, South Florida Natural Resources Center, Homestead, FL. Status and Trends Report. SFNRC Technical Series 2012:1, p. 39.

Swift, E., Durbin, E.G., 1972. The phased division and cytological characteristics of *Pyrocystis* spp. can be used to estimate doubling times of their populations in the sea. Deep Sea Res. 19(3), 189-198.

Taroncher-Oldenburg, G., Kulis, D.M., Anderson, D.M., 1999. Coupling of saxitoxin biosynthesis to the G1 phase of the cell cycle in the dinoflagellate *Alexandrium fundyense*: temperature and nutrient effects. Nat. Toxins 7(5), 207-219.

Tengs, T., Bowers, H.A., Ziman, A.P., Stoecker, D.K., Oldach, D.W., 2001. Genetic polymorphism in *Gymnodinium galatheanum* chloroplast DNA sequences and development of a molecular detection assay. Mol. Ecol. 10, 515 - 523.

Van Dolah, F., Leighfield, T.A., Sugg, L.M., 1996. Cell cycle regulation in the dinoflagellate *Gambierdiscus toxicus*: Mitosis is coupled to the diurnal cycle by a blue light dependent signal. Bull. Mount Desert Island Biol. Lab. 35, 98 - 100.

Van Wagoner, R.M., Deeds, J.R., Satake, M., Ribeiro, A.A., Place, A.R., Wright, J.L.C., 2008. Isolation and characterization of karlotoxin 1, a new amphipathic toxin from *Karlodinium veneficum*. Tetrahedron Lett. 49(45), 6457-6461.

Vanoni, M., Vai, M., Frascotti, G., 1984. Effects of temperature on the yeast cell cycle analyzed by flow cytometry. Cytometry 5, 530 - 533.

Vaulot, D., 1992. Estimate of phytoplankton division rates by the mitotic index method: The fmax approach revisited. Limnol. Oceanogr. 37(3), 644-649.

Vaulot, D., 1994. The cell cycle of phytoplankton: Coupling cell growth to population growth, In: Joint, I. (Ed.), Molecular ecology of aquatic microbes. NATO ASI Series. Springer-Verlag, Berlin, Germany, pp. 303 - 322.

Videau, C., 1987. Primary production and physiological state of phytoplankton at the Ushant tidal front (west coast of Brittany, France). Mar. Ecol. Prog. Ser. 35(1/2), 141-151.

Videau, C., Partensky, F., 1990. Variability in the growth characteristics of *Gymnodinium cf. nagasakiense* (Dinophyceae) and its consequences for the determination of *in situ* growth rates. J. Exp. Mar. Biol. and Ecol. 142(3), 169-182.

Weiler, C.S., Eppley, R.W., 1979. Temporal pattern of division in the dinoflagellate genus *Ceratium* and its application to the determination of growth rate. J. Exp. Mar. Biol. and Ecol. 39(1), 1-24.

Wetzel, R.G., Likens, G.E., 1991. Limnological Analyses, 2nd ed. Springer New York, NY, Springer-Verlag New York.

Wood, A.M., Leatham, T., 1992. The species concept in phytoplankton ecology. J. Phycol. 28, 723 - 729.

Table 3.1 Percentage of total cell cycle spent in each phase for *K. veneficum* strains grown asynchronously at 15 °C, 20 °C, and 25 °C.

Strain	**Temperature**	**Percent (± SD) of Cell Cycle Spent in**		
		G1	S	G2 + M
CCMP 1975	15 °C	56.8 ± 17.3	4.0 ± 1.2	39.2 ± 11.9
	20 °C	56.1 ± 14.5	4.5 ± 1.2	39.5 ± 10.2
	25 °C	57 ± 32.4	4 ± 2.2	40 ± 22.7
2010 IH	15 °C	65.3 ± 16.9	7.4 ± 1.9	27.4 ± 7.1
	20 °C	72.1 ± 27.8	6.6 ± 2.5	21.3 ± 8.2
	25 °C	72.2 ± 20.9	8.3 ± 2.4	19.6 ± 7.4
CCMP 426	15 °C	71.6 ± 71.9	3.5 ± 3.6	24.8 ± 24.9
	20 °C	70.3 ± 15.5	5.3 ± 1.2	24.5 ± 5.4
	25 °C	70.5 ± 10.0	6.1 ± 0.9	23.4 ± 3.3

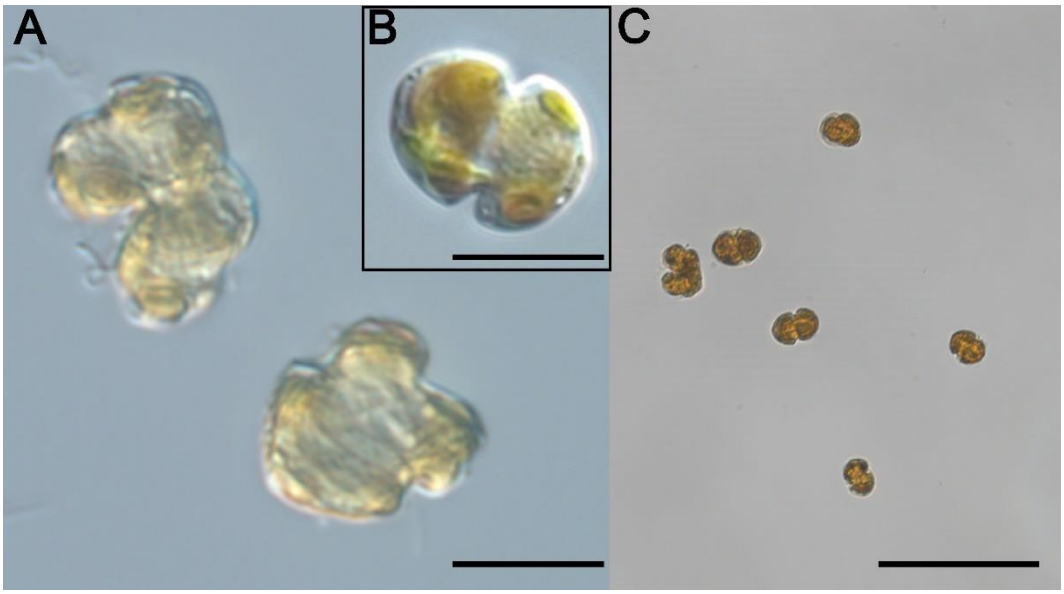

Figure 3.1 Brightfield images of *K. veneficum*. (A) Two dividing cells and a (B) non-dividing cell (bars = 10 μm). (C) Dividing and non-dividing cells together in a field of view exhibiting a mitotic index of 1/6 = 0.17 (bar = 50 μm).

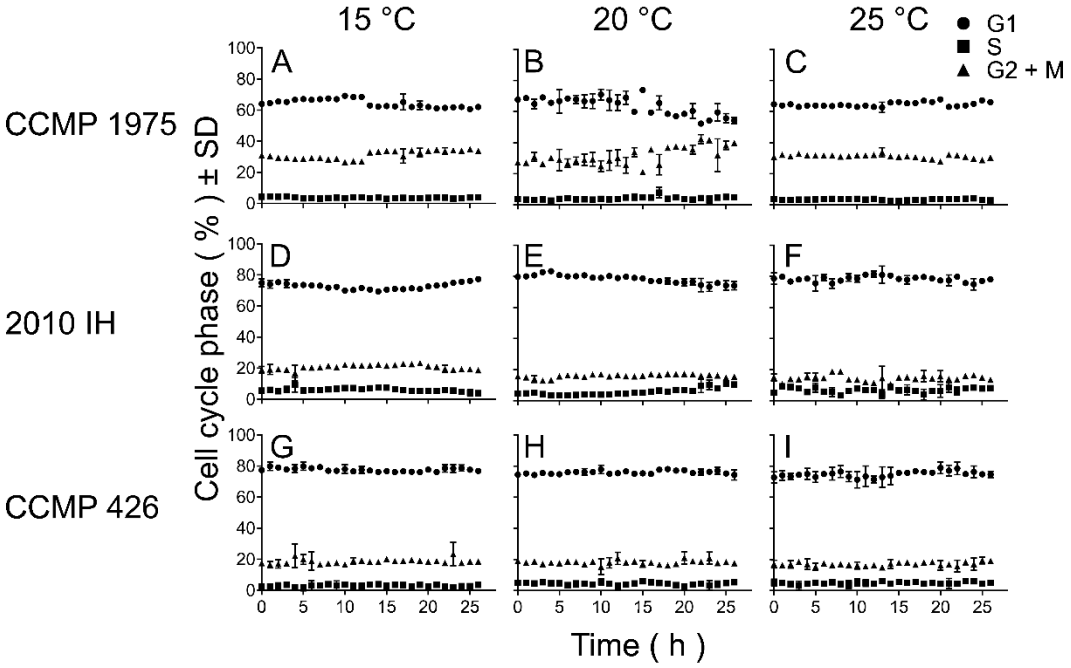

Figure 3.2 Cell cycle phase distribution diagrams for *K. veneficum* strains growing asynchronously at 15 °C, 20 °C, and 25 °C. Data points and error bars represent mean and standard deviation of n = 3. Data for non – growing CCMP 426 at 15 °C included for integrality.

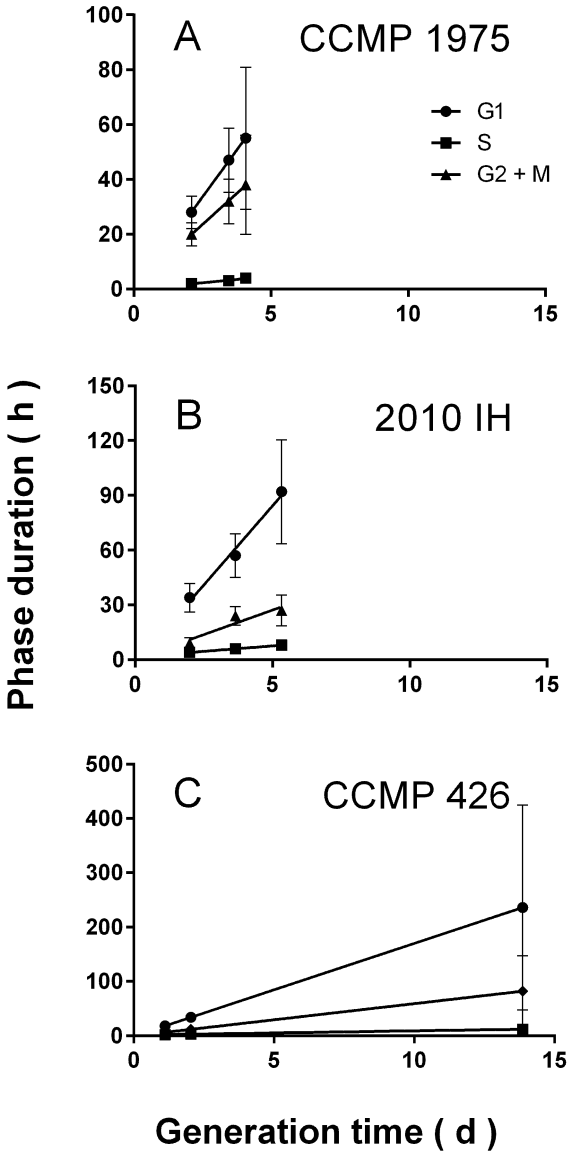

Figure 3.3 Cell cycle phase durations calculated for strains growing asynchronously. Lines represent least-squares linear regressions. Note that growth rates have been converted to generation time by dividing Ln 2 (0.693) by μ. Data points and error bars represent mean and standard deviation of n = 3. Data for non – growing CCMP 426 at 15 °C included for integrality.

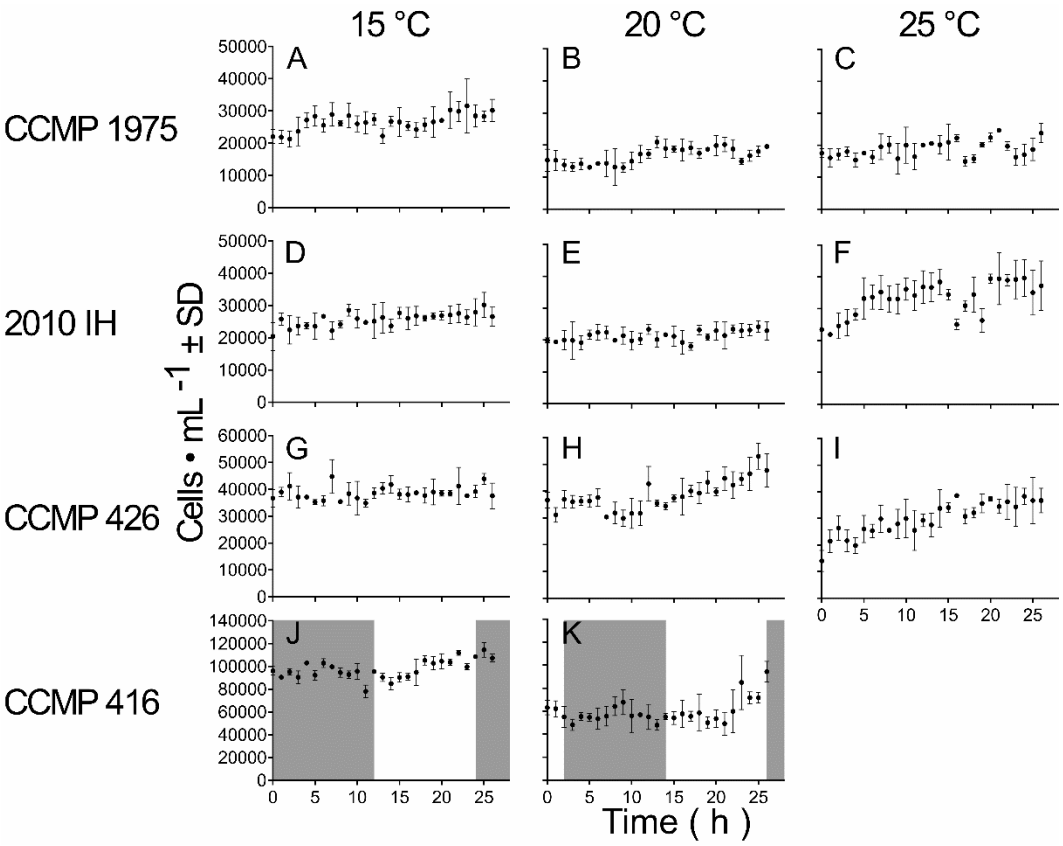

Figure 3.4 Mid-log growth curves for *K. veneficum* strains at 15 °C, 20 °C, and 25 °C. Shaded regions denote dark periods for strain CCMP 416, grown under 12:12 L:D. Note that sampling for CCMP 416 at 20 °C began two hours before onset of the dark period. Data points and error bars represent mean and standard deviation of n = 3. Data for non – growing CCMP 426 at 15 °C included for integrality.

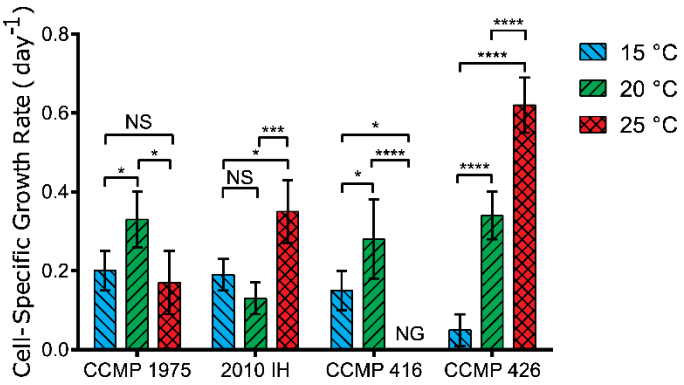

Figure 3.5 Specific growth rates for strains of *K. veneficum* grown at 15 °C, 20 °C, and 25 °C. Significance levels indicated by number of asterisks. *P* – value < 0.05 (*), *p* – value < 0.01 (**), *p* – value < 0.001 (***), *p* – value < 0.0001 (****). Error bars represent standard deviation of n = 3. Data for non – growing CCMP 426 at 15 °C included for integrality.

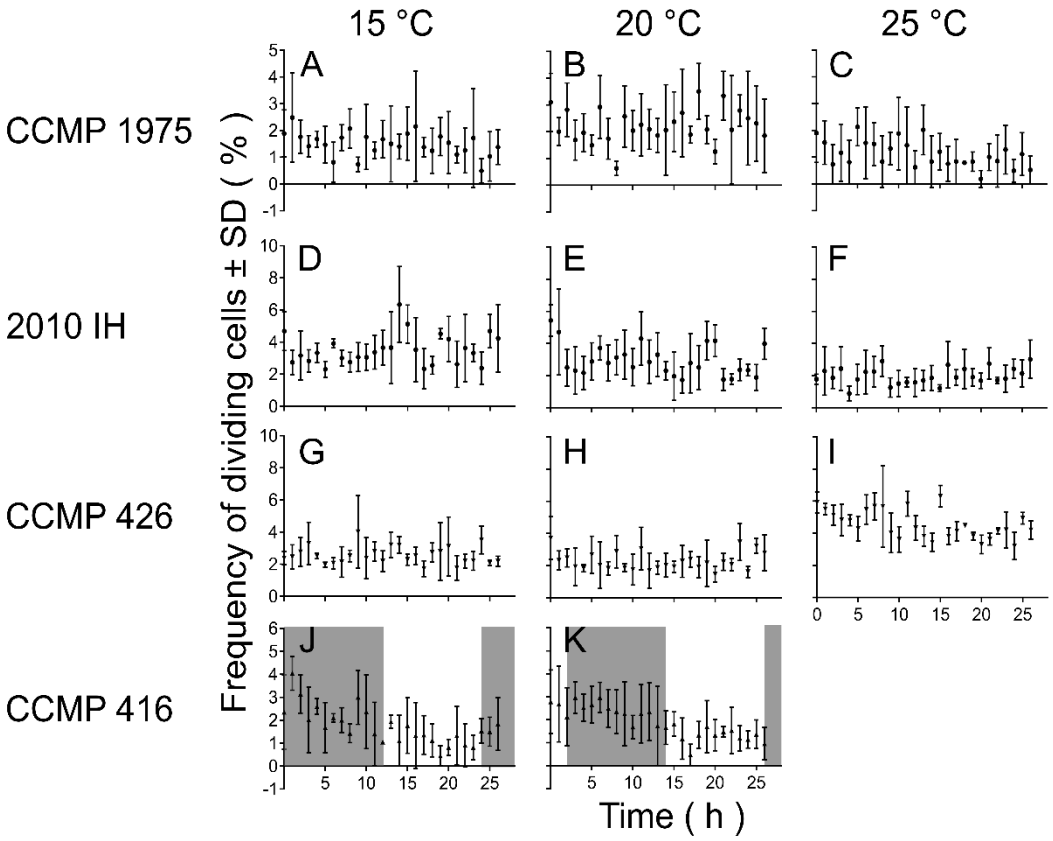

Figure 3.6 Mitotic indices measured for *K. veneficum* strains grown at 15 °C, 20 °C, and 25 °C. Shaded regions denote dark periods for strain CCMP 416, grown under 12:12 L:D. Note that sampling for CCMP 416 at 20 °C began two hours before onset of the dark period. Data points and error bars represent mean and standard deviation of n = 3. Data for non – growing CCMP 426 at 15 °C included for integrality.

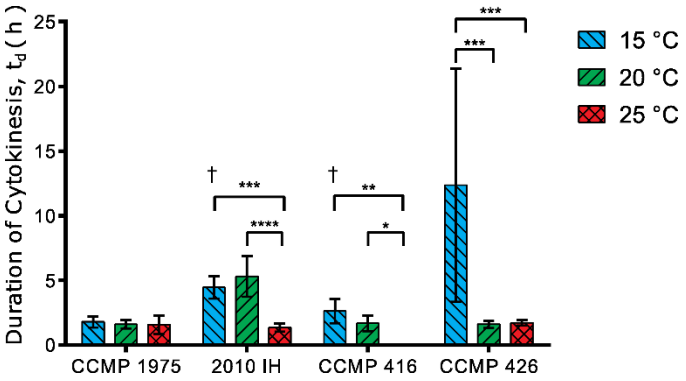

Figure 3.7 Duration of cytokinesis (t_d) determined for *K. veneficum* strains grown at 15 °C, 20 °C, and 25 °C. Significance levels indicated by number of asterisks. P – value < 0.05 (*), p – value < 0.01 (**), p – value < 0.001 (***), p – value < 0.0001 (****). † Significance for strains 2010 IH and CCMP 416 calculated by Two – way ANOVA excluding CCMP 426. Error bars represent standard deviation of n = 3. Data for non – growing CCMP 426 at 15 °C included for integrality.

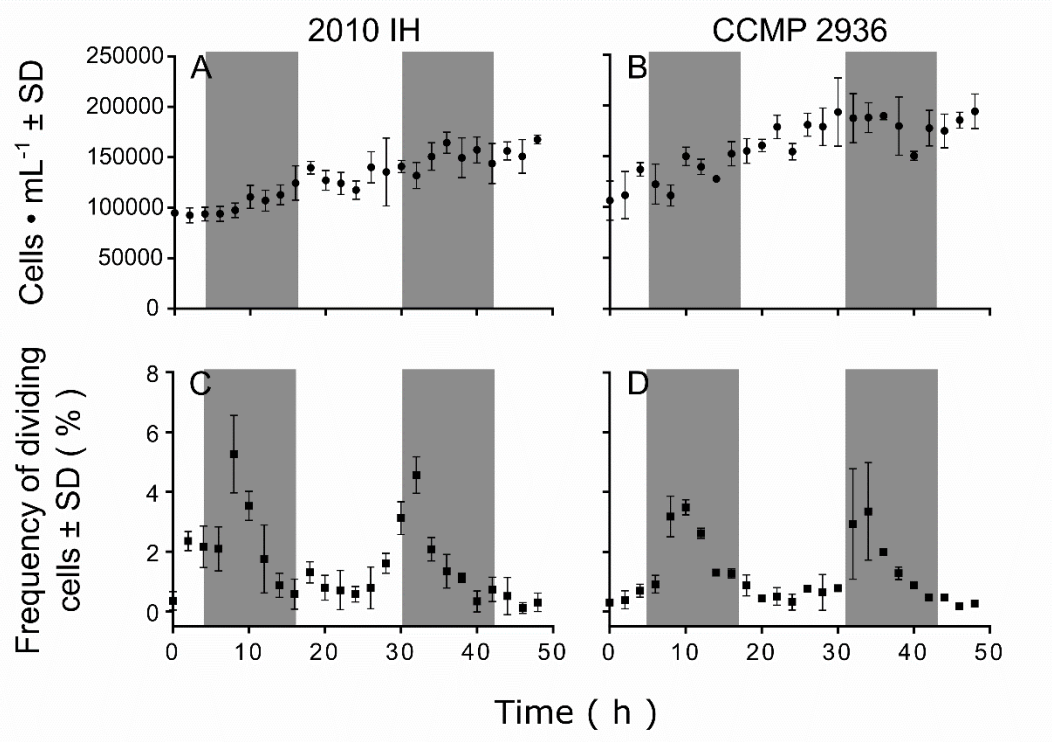

Figure 3.8 Midlog growth curves (A and B) and mitotic indices (C and D) for *K. veneficum* strains 2010 IH and CCMP 2936, respectively. Cultures grown under 12:12 L:D and sampling carried out every two hours for 48 hours. Shaded regions denote periods of dark. Data points and error bars represent mean and standard deviation of n = 3.

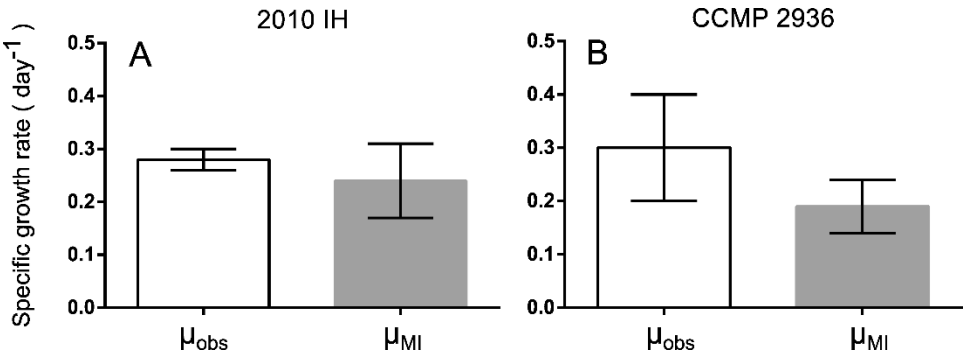

Figure 3.9 Specific growth rates for *K. veneficum* strains 2010 IH (A) and CCMP 2936 (B) calculated based on cell density (μ_{obs}) and mitotic index (μ_{MI}). Rates were compared within strains over the entire 48. Error bars represent standard deviation of n = 3.

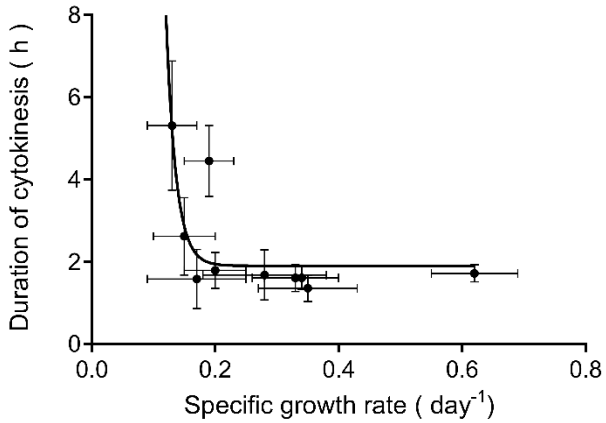

Figure 3.10 Duration of cytokinesis (t_d) vs. specific growth rate for all growing strains of *K. veneficum* used herein. Line represents least-squares fit exponential regression. Data points and error bars represent mean and standard deviation of n = 3.

CHAPTER 4

THE INFLUENCE OF MIXOTROPHY ON CELL CYCLE PHASE DURATION AND CORRELATION OF KARLOTOXIN SYNTHESIS WITH G1 PHASE IN *KARLODINIUM VENEFICUM*

Erik L. J. E. Broemsen, Jens Wira, Allen R. Place, Matthew W. Parrow

Abstract:

Karlodinium veneficum forms toxic fish killing blooms in estuaries worldwide. The toxicity of these blooms is variable and thought to be connected to bloom stage and *in situ* growth rates. Methods for measuring *in situ* growth rates rely on the assumption that cell cycle progression is phased to the diel photocycle, which is true for phototrophic cultures where G1 phase occurs during light hours and S and G2 + M phases occur during dark hours. However, *K. veneficum* is a facultative mixotroph, and the effects of mixotrophy on cell cycle synchrony are unknown. Furthermore, toxicity in laboratory cultures is inversely related to growth rate and is light dependent, suggesting synchrony between the cell cycle and karlotoxin synthesis. To test this possibility the cell cycle phase distribution and cellular toxin content for phototrophic and mixotrophic cultures were monitored hourly for a full diel cycle. The results demonstrated that mixotrophic cultures maintained a synchronous cell, despite increased growth rates. The faster growth rates were attributed to a shortened duration of G1 phase in mixotrophic cultures relative to phototrophic cultures (30.8 ± 9.2 hours vs 69.4 ± 21.5 hours, respectively). Meanwhile, toxin production was observed only during light hours, consistent with synthesis initiating with the photorespiratory byproduct, glycolate. Cellular toxin content had a

significant positive correlation with the percentage of G1 phase cells and a significant negative correlation with the percentage of S phase cells. These results indicate a clear role of the diel photocycle in synchronizing the cell and karlotoxin synthetic cycles.

Introduction

Mixotrophy (herein referring to the combination of phototrophic and phagotrophic nutritional modes) is a common trait amongst dinoflagellates, and particularly, harmful algal bloom (HAB) species (Stoecker, 1999; Burkholder et al., 2008; Jeong et al., 2010). This nutritional mode has traditionally been considered most important for survival in oligotrophic environments, where dissolved nutrients are scarce and particulate sources offer a means of supplementation. However, many HAB species associated with eutrophic environments are also capable of mixotrophy (Burkholder et al., 2008). In these environments these taxa can be at a competitive disadvantage when acquiring dissolved nutrients as compared to strict phototrophs. Many HAB species have lower affinities for dissolved nitrogen and phosphorous sources than co-occurring strict phototrophs and mixotrophy may only initiate under limited nutrient conditions or stoichiometric imbalances (Smayda, 1997). Therefore, seasonal cycles in eutrophic habitats will initially favor growth of strict phototrophs, but favor blooms of mixotrophic phytoplankton when dissolved nutrients become limiting (Stoecker et al., 2017).

The dinoflagellate *Karlodinium veneficum* is a common mixotrophic HAB species found in eutrophic estuaries around the globe, where it is often present at low background concentrations (~ 10^2 cells mL^{-1}; Place et al., 2012). Occasionally *K. veneficum* can

quickly bloom to high cell densities (> 10^5 cells mL^{-1}) that have the potential to cause massive fish mortality events (Deeds et al., 2002; Adolf et al., 2015). These blooms are often preceded by blooms of benign cryptophyte microalgae which can act to trigger *K. veneficum* bloom formation (Adolf et al., 2008). As a preferred prey, cryptophytes can contribute significantly to *K. veneficum* nutrition and in laboratory cultures they increase growth rates by two to three-fold (Li et al., 1999; Adolf et al., 2006b). Capture of cryptophyte prey is facilitated by the production of cytotoxic and hemolytic compounds called karlotoxins (KmTx; Kempton et al., 2002; Sheng et al., 2010). The structures of which have been characterized and can be measured in cultures and field samples (Bachvaroff et al., 2008; Van Wagoner et al., 2008).

Measurement of KmTx cell quotas in both culture and field samples has revealed significant variability in toxicity. Differences between strains can be as high as 100-fold, and natural blooms can have between 5 – 100-fold more KmTx per cell than cultured isolates while also varying temporally in comparable ranges (Deeds et al., 2004; Bachvaroff et al., 2009; Adolf et al., 2015). Culture studies have also revealed that KmTx cell quotas negatively correlate with growth rates and inorganic nutrient concentrations (Adolf et al., 2009; Fu et al., 2010). While the biosynthetic pathway for KmTx production is unknown it is light dependent and begins with glycolate, a byproduct of photorespiration (Adolf et al., 2020). The structure of KmTx also lacks N and P atoms, and therefore could continue even under nutrient deplete growth limitation.

The above described observations allude to a strong connection between the cell cycle and the KmTx biosynthetic cycle. In the few studies to explore interactions between the cell cycle and toxin biosynthesis in other HAB species, production has been observed

to occur during defined periods of the cell cycle (Taroncher-Oldenburg et al., 1997; Pan et al., 1999; Eschbach et al., 2005; Jia et al., 2019). These observations remain outstanding for *K. veneficum*, however, cell cycle studies have revealed a cell cycle that is tightly synchronized to the diel photocycle. In logarithmically growing cultures, G1 phase coincides with daylight hours and starting in the late afternoon, cohorts of cells quickly progress through S and G2 + M phases ultimately completing division overnight (Adolf et al., 2020). Upon reaching stationary phase these cells then arrest in G1 phase. These observations suggest a model for KmTx production where-in, proliferating cells will have relatively low cellular KmTx content and upon arrest in G1 phase will experience multiple rounds of light/dark cycles and light dependent KmTx synthesis cycles. Thus resulting in increased cellular toxicity. This model would require, over the course of at least a single diel photocycle, a positive correlation between the proportion of G1 phase cells and cellular KmTx content.

If this model is true for natural populations, it could explain the observed variability in bloom toxicity. However, it is not known if the strong synchrony between the diel photocycle and cell cycle in *K. veneficum* is retained under mixotrophic nutrition, a metabolic state likely prevalent in natural populations (Li et al., 2000b). Furthermore, testing this model in nature requires measurement of *in situ* growth rates, the methods for doing so require synchrony between the cell cycle and diel photocycle (McDuff and Chisholm, 1982; Carpenter and Chang, 1988). Therefore, in this study we aim to not only determine the effects of mixotrophic nutrition on cell cycle synchrony, but also simultaneously test our proposed model of KmTx production in laboratory cultures of *K. veneficum*. Our data demonstrate that cultures under mixotrophic conditions maintain

synchrony with diel photocycles and that KmTx production is confined to G1 phase of the cell cycle.

Materials and methods

Culture maintenance

Prior to experimentation all stock algal strains were maintained at 20 °C and 30 µE m^{-2} s^{-2} on a 12:12 L:D cycle. *K. veneficum* strain CCMP 2936 was grown in an artificial seawater medium adapted from Lopez-Rosales et al. (2015) modified with 1 mM HEPES buffer. Prey cultures of *Storeatula major* were grown in f/2 medium prepared in 15 ppt artificial seawater.

Experimental design

When provided alternating light:dark cycles *K. veneficum* exhibits synchronous cell division (Adolf et al., 2020). This entrainment can be overridden by continuous illumination leading to complete asynchrony, thus underscoring the importance of light:dark cycles in controlling cell division synchrony (chapter 3). Therefore, in order to understand the impact of mixotrophic nutrition on cell cycle synchrony, phototrophic and mixotrophic cultures were grown under identical light schedules. Cultures of both nutritional modes were acclimated (by serial transfer over the course of two weeks) to a 12:12 L:D cycle with 180 µE m^{-2} s^{-2} light intensity at 24 °C and bubbled with house air at

a rate of approximately 10 bubbles per second. Additionally, mixotrophic cultures were supplemented with daily additions of *S. major* as the mixotrophic prey source (provided approximately four to five hours prior to the beginning of the dark period). Prey cells were harvested by centrifugation at 3,000 x g for 10 minutes, resuspended in the Lopez-Rosales medium, and then added to mixotrophic *K. veneficum* cultures at a final prey:predator ratio of at least 3:1. Prey cell supplementation continued throughout the entirety of the experiment.

Following the acclimation period, cultures were split into triplicate flasks and grown to mid-log concentrations at which point sampling commenced. In order to ensure optimal mixotrophic conditions during the sampling period, *S. major* cells were additionally supplemented (prey:predator ratio of 3:1) four hours after the beginning of the dark period preceding the day of sampling. During the mid-log sampling period, triplicate cultures were sampled hourly for 27 hours for cell cycle analysis, cell density, mitotic index, and total karlotoxin content.

Mitotic index and cell density

Samples collected for cell density and mitotic index were fixed with 1 % acidic Lugol's solution (final concentration). Palmer-Maloney counting chambers (Wetzel and Likens, 1991) were used to determine the cell density and mitotic index simultaneously for each sample from a minimum of 300 cells per sample. Mitotic indices were determined from fraction of paired (dividing) cells as detailed in chapter 3.

Flow cytometry and cell cycle analysis

Cell cycle analysis samples were fixed overnight at 4 °C in the dark following addition of 5 % formalin and 0.1 % Tween 80 (final concentrations). Samples were prepared for nucleic acid staining and flow cytometry by centrifugation at 3000 x g for 10 min, followed by resuspension in an equal volume of 70 % methanol, and subsequent incubation at 4 °C overnight in the dark. Following this methanol treatment samples were centrifuged at 2000 x g for 10 min and cells resuspended in 500 uL TE (10 mM Tris-HCl and 1 mM EDTA) with 0.1 % Tween 80. Cells were then stained with 4', 6 – diamidino – 2 – phenylindole (DAPI) at a final concentration of 1 µg mL^{-1}.

All flow cytometry was conducted using a BD LSRFortessa™ flow cytometer (BD Biosciences) equipped with 405 and 488 nm 50 mW solid – state lasers following methods of Kremp and Parrow (2006). DNA histograms were generated from fluorescence emission (450 nm) of DAPI stained cells excited by the 405 nm laser. While the 488 nm laser was used to verify phagocytosis of *S. major* prey cells by detecting phycoerythrin fluorescence at 575 nm. Microscopically, phagocytosed *S. major* cells appear within mixotrophic *K. veneficum* cells as orange fluorescent inclusions (OFI). This has been useful in previous *K. veneficum* mixotrophy studies for calculating ingestion and digestion rates (Li et al., 1996; Li et al., 1999; Li et al., 2000a; Adolf et al., 2006b; Adolf et al., 2008). Similarly using flow cytometry these OFIs can be detected fluorescently at 575 nm. Based on this principle the percentage of mixotrophic *K. veneficum* cells was measured for each time point. This was then verified microscopically for time points 0, 7, 8, 12, and 24 hours at 200x magnification using a Zeiss Axio

Observer A1 inverted microscope (Carl Zeiss Microscopy GmbH, Jena Germany) equipped with an HBO 103 W/2 mercury short-arc lamp and a Zeiss filter set 15 (excitation: 546/12 nm, emission: 590 nm LP, beam splitter: 580 nm) following Li et al. (1996).

Analysis of flow cytometric data was carried out using FlowJo V10.8 (FlowJo). Initial gating excluded unconsumed cryptophyte prey cells and contaminating bacteria by forward and side scatter gating of only *K. veneficum* cells. Doublet cells were then excluded by gating DNA fluorescence peak height versus peak area (Parrow et al., 2002). Cell cycle analysis was then performed by deconvolution of triplicate DNA histograms for both phototrophic and mixotrophic samples using the Watson-Pragmatic model in FlowJo (Watson et al., 1987). Additionally, for determination of the percentage of mixotrophic *K. veneficum* cells a threshold gate was established for the minimum phycoerythrin intensity for classification of mixotrophic cells (Fig. 1). This gate was set based on phycoerythrin fluorescence vs DNA fluorescence cytograms of phototrophic samples (Fig. 1A). All *K. veneficum* cells with phycoerythrin intensity greater than this threshold were considered mixotrophic positive (Fig. 1B). This was necessary due to spillover of endogenous *K. veneficum* autofluorescence into the phycoerythrin channel.

Statistics and rate calculations

All rate calculations and means were determined using Microsoft® Excel® software 2013 (Microsoft Corporation). All other statistical analyses and hypothesis testing were performed using GraphPad Prism 6 (Graphpad Software). Growth rates were

calculated from cell density data from two time points that were 24 hours apart using the formula:

$$\mu = \frac{ln\,{}^{N_1}/_{N_0}}{T_1 - T_0}$$

where N_1 and N_0 are cell concentrations at respective times T_1 and T_0. Regression analysis of cell density data was performed by least squares fitting of a three segment piecewise linear regression. Initial break points were defined as hours 12 and 19, based on manual estimation. Polynomial regressions of the fourth order were fitted to the cell cycle phase distributions and mitotic index data.

Toxin analysis

Filters were eluted for analysis with methanol (Alfa Aesar, LC-MS Grade 99.8%+). One milliliter followed by 500µL was passed over the filter into a 1.5mL amber vial. Eluent was dried down to 150µL, a 10-fold concentration under vacuum (Savant, Environmental Speedvac System) and transferred to glass inserts with polypropylene springs. Analysis was carried out with an Agilent G6470A QQQ MS/MS equipped with AJS in multiple reaction mode (MRM). 10µL of sample was injected, and separation was carried out using an Agilent Infinity 1260 UPLC with reversed-phase C18 (Agilent Poroshell 120 EC-C18 2.7µm, 3.0 x 100mm) column held at 35oC. The mobile phase was a mix of 18MΩ water (Millipore) and LC-MS grade methanol, amended with 0.1% formic acid by volume. The elution gradient started at 30% (vol/vol) methanol for 2

min, increasing to 98% in 3 min, holding for 5min, before returning to 30% for a 2 min post-time before the next injection at a flowrate of 0.6mL/s. MS/MS ionization and MRM parameters are listed in Table 1 and 2 respectively. Retention times of KmTx 1,3 were compared with extracts from a separately isolated strain of *Karlodinium veneficum*, which produces the two KmTx congeners.

Results

Confirmation of mixotrophic activity

The gating approach used to estimate the percentage of cells actively phagocytosing prey in the mixotrophic cultures proved to be conservative. All microscopic estimates of the percentage of OFI containing cells were significantly higher than the respective flow cytometric estimates (paired T – test, p – value = 0.005), with hours zero and eight having 39.57 ± 3.84 % and 38.79 ± 3.37 %, respectively. Therefore, this gating approach was used to track the percent of actively mixotrophic cells (Fig. 2). The percentage of mixotrophic cells declined linearly between hour zero and seven (slope = -2.91 ± 0.24 % h^{-1}, p – value < 0.0001), and at the eighth hour spiked to 23.27 ± 2.46 % due to ingestion of new *S. major* prey cells added at hour seven. The ingestion rate calculated between hours seven and eight based on microscopic observation was 0.26 ± 0.05 *S. major K. veneficum*$^{-1}$ h^{-1}. The decline then continued at the same rate until hour 12 (F – test, p – value = 0.52) where piecewise regression indicated that the rate then slowed (slope = -1.00 ± 0.06 % h^{-1}, p – value < 0.0001). Interestingly, digestion rates calculated

from microscopic OFI observations similarly declined between light and dark (0.054 ± 0.011 *S. major K. veneficum*$^{-1}$ h^{-1} and 0.028 ± 0.003 *S. major K. veneficum*$^{-1}$ h^{-1}, respectively; T – test, p – value = 0.02).

Growth rate and cell division synchrony

Simple linear regression analysis revealed significantly positive slopes for both the phototrophic and mixotrophic cell density data (data not shown; F – test, p – value < 0.0001 and p – value < 0.0001, respectively). The specific growth rates for the phototrophic cultures were 0.17 ± 0.05 days^{-1}, which was significantly slower than the mixotrophic cultures at 0.42 ± 0.12 days^{-1} (T – test, p – value = 0.03). To more precisely evaluate the timing of population growth a piecewise linear regression was fit to both cell density data sets (Fig. 3). Piecewise regression analysis estimates for the first break point were 12.00 ± 1.46 hours and 8.62 ± 1.88 hours for the phototrophic and mixotrophic conditions respectively. The second break point was estimated at 16.79 ± 1.65 hours for the phototrophic cultures and 17.00 ± 1.41 hours for the mixotrophic cultures. Comparison between the two regressions did not find significant differences between the initial break points or between the second break points (F – test; p – value = 0.11 and p – value = 0.86, respectively). Only the middle segments of both the phototrophic and mixotrophic regressions had significantly positive slopes (F – test; p – value < 0.001 and 0.01, respectively).

To further explore the synchrony of cell division, dividing cell frequencies were determined for each time point. The distribution of dividing cells over the time course

had a parabolic shape for both the phototrophic and mixotrophic conditions (Fig. 4). The maximum percentage of dividing cells occurred at hour 15 for the phototrophic cultures and hour 14 for the mixotrophic cultures. Additionally, the frequency of dividing cells was significantly higher for the phototrophic cultures than the mixotrophic cultures (2.90 ± 0.10 % and 2.27 ± 0.35 %, respectively; T – test, p – value = 0.04). However, the average frequency of dividing cells in the phototrophic cultures over the entire 27 hours was significantly lower than in the mixotrophic cultures (0.83 ± 0.63 % and 1.1 ± 0.49 %, respectively; T – test, p – value = 0.04). Additionally the average frequency of dividing cells for the first 13 timepoints was significantly higher in the mixotrophic cultures than the phototrophic cultures (1.16 ± 0.39 % vs 0.73 ± 0.32 %, respectively; T – test, p – value < 0.01).

Cell cycle phase synchronization and duration

All cell cycle phases for both phototrophic and mixotrophic cultures oscillated during the diel period (Fig. 5A – F). The minimum percent of G1 phase cells for the phototrophic cultures occurred near the transition from light to dark, while for the mixotrophic cultures the G1 minimum occurred seven hours earlier, shortly after lights on. Timing of the G1 peak maxima were similar for both growth conditions, occurring early in the morning several hours before the dark to light transition (Fig. 5A and D). The timing of the S phase peak maxima was discongruent between the two culture conditions with the phototrophic S phase percentage reaching its maximum around hour nine, while the mixotrophic S phase percentage reached maximum about three hours earlier (Fig. 5B

and E). By the middle of the dark period the daily cohort of dividing cells for both conditions had finished transition from S phase. As for G2 + M phase timing, the mixotrophic cultures reached their maximum percentage early around hour three. Whereas the phototrophic cultures peaked approximately nine hours later at the light to dark transition (Fig. 5C and D). For both conditions the daily cohort of dividing cells finished dividing just before the onset of the next light period.

Following the methods of Slater et al. (1977) the durations of each cell cycle phase were calculated from the measured cell cycle proportions and cell division rates (Fig. 6). Two – way ANOVA comparison indicated a significant interaction between cell cycle phase and trophic condition (p – value = 0.03). Multiple comparisons between trophic conditions found that only the duration of G1 phase differed significantly, with the mixotrophic G1 phase duration being less than half the length of the phototrophic G1 phase duration (p – value < 0.01).

Karlotoxin content

Karlotoxin was below the detection limit in phototrophic cultures. However, the congener KmTx 3 was detectable in the mixotrophic cultures, but concentrations were too low for mass quantification. Comparison of log transformed integration values indicated that production of KmTx 3 occurred only during the light hours (Fig. 7; slope = 0.067 ± 0.028, p – value = 0.03). The production began approximately 3 to 4 hours into the light period and continued until the transition to the dark period at hour 12. Cellular KmTx 3 content did not change during the dark period (p – value = 0.92). Regression

analysis between cell cycle phases and KmTx 3 content during the light hours did indicate significant linear relationships (Fig. 8). There was a positive relationship with G1 phase cells (Fig. 8A; slope = 0.075 ± 0.032, p – value = 0.02), a negative linear relationship with the percentage of S phase cells (Fig. 8B; slope = - 0.201 ± 0.066, p – value < 0.01), and no detectable relationship with the percentage of G2 + M phase cells (Fig. 8C; p – value = 0.15).

Discussion

Understanding the mechanism by which mixotrophic nutrition in *K. veneficum* effects cell cycle progression provides important insight into the underlying factors that contribute to bloom dynamics, such as the role of cryptophyte microalgae in bloom initiation and development. This is important for modeling and monitoring of toxic blooms where toxicity can potentially be regulated by cell cycle progression and linked to defined cell cycle stages. Thus improved understanding of how *K. veneficum* cell cycle progression is regulated can lead to improved modeling of bloom dynamics and toxicity. Data presented here clearly demonstrates that mixotrophic nutrition increases cellular growth rates by shortening the duration of G1 phase of the cell cycle. Furthermore, cellular toxin data shows a significant correlation with the percentage of cells in G1 phase of the cell cycle, supporting our proposed model for regulation of Karlotoxin production.

Mixotrophic activity

Mixotrophic behavior in *K. veneficum* is variable with influence from both physical and biological factors. Both increases in light intensity and decreases in dissolved inorganic nutrients (N and P) lead to increased prey ingestion rates (Li et al., 1999; Li et al., 2000a). Other factors influencing ingestion rates include *K. veneficum* strain variation (e.g., toxicity), as well as prey type, abundance, and nutritional quality (Li et al., 1996; Adolf et al., 2006a; Adolf et al., 2008; Calbet et al., 2011; Lin et al., 2017). The design of this current study aimed to induce the greatest degree of mixotrophic activity while not simultaneously inhibiting phototrophic growth. As such, prey abundance and light intensity were provided at saturating levels (Li et al., 1996; Li et al., 1999), and strains of algae were selected for optimal mixotrophic performance (Adolf et al., 2008). However, dissolved inorganic nutrients were maintained at replete concentrations for both phototrophic and mixotrophic cultures.

As shown in Figure 2 these conditions successfully supported mixotrophy and maintained it throughout the experiment. Not surprisingly the flow cytometric estimation of the percentage of OFI positive cells was lower than the manual estimation. This is due to the conservative nature of the gating approach used to identify OFI positive cells (Fig. 1) which excludes *K. veneficum* cells containing fewer and/or smaller OFIs (i.e., cells less fluorescently intense at 540 nm). Unfortunately, the maximum percentage of mixotrophic cells observed here (~ 40 %) was lower than the highest reported maxima (~ 60 %) in other *K. veneficum* mixotrophy studies (Li et al., 1996; Adolf et al., 2008). These studies likewise provided saturating prey concentrations and comparable prey:predator ratios.

However, these studies were *in situ* feeding experiments using natural plankton assemblages and likely contained mixed populations of multiple *K. veneficum* strains and morphologically similar species. As has been demonstrated by Calbet et al. (2011) mixotrophic capacity can vary widely between *K. veneficum* strains, even amongst those isolated from the same bloom event. Therefore, this difference in percentage of mixotrophic *K. veneficum* cells can be readily attributed to strain variation. Furthermore, the ingestion rate calculated between hours seven and eight (6.32 ± 2.22 prey $K.v.^{-1}d^{-1}$) is comparable to or higher than most rates reported by other studies (Li et al., 1999; Adolf et al., 2008; Calbet et al., 2011). In fact, it is only exceeded by a rate (~ 9.6 prey $K.v.^{-1}d^{-1}$) measured for cultures under N and P limitation (Li et al., 2000a). Regardless of the variation in mixotrophic performance as compared to other studies a sizeable proportion of the cultured population was actively mixotrophic and rapidly ingested the supplemented *S. major* cells.

Cell division synchrony

Cell division in both the phototrophic and mixotrophic cultures was synchronized. This is illustrated in Figure 3 where the cell density curve exhibits a stepped pattern. This is a typical pattern observed in synchronously dividing cultures with radian or infradian growth rates (Sweeney and Hastings, 1958; Edmunds, 1964; Bruce, 1970; Chisholm and Brand, 1981; Taroncher-Oldenburg et al., 1997). Interestingly, piecewise linear regression estimated an earlier initial break point for mixotrophic cultures, possibly indicating an earlier onset of cell division. This would suggest there was a longer window

of opportunity during which cell division would be occurring for mixotrophic cultures than for phototrophic cultures (~8 hours vs ~ 5 hours, respectively). However, the initial break points of both treatments were not significantly different. On the other hand, the distribution of mitotic indices were significantly different, particularly during the light period (Fig. 4). The average mitotic index for mixotrophic cultures during these hours was 1.6 times higher than the corresponding time points for the phototrophic cultures. Given that the mitotic index is a direct measure of the proportion of cells progressing through the terminal stage of the cell division cycle (i.e., cytokinesis), this is strong evidence of a broadening of the cell division window. Unfortunately, changes in cell density and mitotic index are only measures of the end product of cell cycle progression and the terminal stage of it, respectively. Therefore, these metrics do not provide insight into other stages of the cell cycle (i.e., G1, S, G2 + M).

Cell cycle synchrony and duration

The dinoflagellate cell cycle follows the typical Eukaryotic G1 – S – G2 – M sequence (Bhaud et al., 1991). Usually, these phases are restricted to discrete periods during a 24 hr photoperiod with division often occurring during the dark and early morning hours (Chisholm, 1981; Cetta and Anderson, 1990; Taroncher-Oldenburg et al., 1997; Van Dolah and Leighfield, 1999; Salgado et al., 2017; Jia et al., 2019). Previous work with *K. veneficum* has demonstrated similar patterns of cell cycle progression with strong phasing to the diel period. In exponentially growing cultures, S phase begins in the latter part of the light period with the proportion of S phase cells peaking near the light to

dark transition. During the dark period cells enter G2 + M phase and subsequently complete cell division prior to the transition from dark to light (Adolf et al., 2020). Field populations of *K. veneficum* (initially identified as *Gyrodinium corsicum*) in Alfacs Bay have slightly different timing; with S phase proportions reaching maximum in the middle of the dark period and G2 + M peaks also occurring in the dark period or near the transition from dark to light (Garcés et al., 1999; Garcés et al., 2006). The cell cycle patterns observed in the current study similarly exhibited synchrony and phasing of the cell cycle to the photocycle (Fig. 5).

Interestingly, for both the phototrophic and mixotrophic cultures the proportion of G2 + M cells never fell below ~ 12 % and ~ 9 %, respectively. This constant persistence of G2 + M cells throughout the cell cycle has been previously observed for strain CCMP 2936. In Pokrzywinski et al. (2017), using this strain, the proportion of G2 + M cells in untreated control cultures remained present throughout the entire photocycle, albeit at a much lower percentage (~ 5 %), with little variation. This has also been observed for *Alexandrium minutum, Protoceratium reticulatum,* and two species of *Scrippsiella,* where as much as 20 % of cells remaining throughout a photocycle had 2C DNA content (Figueroa et al., 2007; Figueroa et al., 2015; Salgado et al., 2017; Fagin et al., 2019). This observation is most likely attributable to the presence of 2C planozygotes. In fact, Figueroa et al. (2015) found 2C cells persisting throughout the entire photocycle of both clonal and crossed cultures of *A. minutum*. The proportion of 2C cells persisting was higher in crossed cultures than clonal cultures, suggesting these remaining 2C cells to be planozygotes. Additionally, phased populations of 4C planozygotes have been observed in many *K. veneficum* cultures (Adolf et al., 2020). Similarly, a phased population of cells

with > 2C DNA content was detected in both the phototrophic and mixotrophic cultures, though their occurrence remained below 1 % (data not shown). It is possible that a sizeable proportion of 2C zygotes temporarily arrest at this stage and proceed through multiple photocycles before entering meiotic S phase. Alternatively, these retained G2 + M phase cells could be G2 cells which have failed to finish mitosis in a single light:dark cycle.

The timing of cell cycle phases did differ between the phototrophic and mixotrophic cultures. Under phototrophic conditions the S phase proportion peaked in the late afternoon prior to the light to dark transition, while the G2 + M proportion reached its maximum just at the light to dark transition. However, under mixotrophic conditions the maximum S phase and G2 + M phase proportions were shifted several hours earlier (three and nine hours sooner, respectively) but maintained a synchronous oscillation. Shifts in the timing of S phase entry have been reported previously in *Karenia brevis* cultures exposed to blue light. Typically for *K. brevis* entry into S phase is cued by the dawn and begins approximately 6 hours after the transition with G2 + M phase beginning 8 – 10 hours later after S phase (Van Dolah and Leighfield, 1999). However, when cultures grown in white light are moved to either red or blue light, on the same photoperiod, entry into S phase occurs earlier under blue light but does not change under red light (Brunelle et al., 2007). The light regime (i.e. schedule and color) provided in the current study was identical between mixotrophic and phototrophic cultures, and therefore these shifts observed in the *K. veneficum* cell cycle can only be attributed to mixotrophic nutrition.

Interestingly, the cell cycle patterns observed in this study (Fig. 5) indicate that the cell cycle remains entrained with the diel cycle under mixotrophic conditions. It is possible that the dawn cue functions to entrain the cell cycle of *K. veneficum* as reported in other dinoflagellates (Van Dolah and Leighfield, 1999; Leighfield and Van Dolah, 2001) and continues to do so under mixotrophy. Interestingly, previous research in our lab has demonstrated that the dawn cue is not necessary for cell division, and several strains of *K. veneficum* can be induced into asynchronous cell division by culturing under continuous illumination (Broemsen et al In review). This has also recently been demonstrated for *K. brevis* under continuous illumination (Gao and Erdner, 2022). In contrast, pulses of limiting nutrients have been shown to entrain cell division. Olson and Chisholm (1983) demonstrated that pulses of ammonium in N – limited cultures of *Amphidinium carteri* (grown in continuous light) phased cell division to occur approximately 18 hours after the pulse. During acclimation of the mixotrophic *K. veneficum* cultures, prey cells were provided daily in the mid – afternoon. There was no attempt made to follow a strict schedule of feeding other than to supplement prey during a two hour window. Therefore, there is a possibility that prey supplementation is acting as an entraining cue. Additionally, given that prey ingestion is light dependent in *K. veneficum* (Li et al., 1999), there is an inherent coupling of mixotrophic activity to the photoperiod.

Besides entrainment cues that phase the cell cycle to the diel cycle, accumulation of necessary nutrients is also required for entry into S phase. Cells that have not acquired sufficient nutrition to progress into S phase in a single photocycle will remain in G1 phase for additional light periods until nutritional needs are met. Thus, entering S phase

after the next dawn entrainment cue. In cultures this manifests as a lengthening of the average duration of G1 phase and subsequently an increase in generation time (Olson and Chisholm, 1986; Olson et al., 1986; Van Dolah et al., 2008). The purpose of comparing mixotrophic and phototrophic *K. veneficum* cells in this current study was to explore the nutritional effects of prey supplementation on cell cycle phasing. Since cryptophyte prey can provide significant nutritional supplementation (Li et al., 2001), mixotrophic *K. veneficum* cells should not require as many light periods to reach sufficient nutrition for S phase entry as phototrophic cells. This scenario would suggest that mixotrophic nutrition shortens one or more cell cycle phases. Alternatively, mixotrophic nutrition could decouple the cell and diel cycles leading toward an asynchronous division state. The former hypothesis is supported by our data (Fig. 6), with only G1 phase being significantly shortened under mixotrophic nutrition.

Synchrony of cell cycle and karlotoxin production

Few studies have focused on the elucidation of the diel dynamics of toxin production in harmful algae. Those that have found toxin synthesis to be confined to discrete periods coinciding with specific phases of the cell cycle. In the case of *Alexandrium fundyense* saxitoxin production began shortly after dawn and continued for 8 – 10 hours during which cells were confined to G1 phase (Taroncher-Oldenburg et al., 1997). *Prorocentrum lima*, began production of DTX – 4 during G1 phase and continued shortly into S phase, whereas okadoic acid (OA) and DTX – 1 occurred later in the afternoon while cells occupied S and G + M phases (Pan et al., 1999). Similarly, DTX – 1

and OA production in *Dinophysis acuminata* was most active in S phase, and the prymnesiophyte *Chrysocromulina polylepsis* had the greatest haemolytic activity during hours occupied by G1 phase (Eschbach et al., 2005; Jia et al., 2019). Toxin production and the coinciding cell cycle phases for these three microalgae were restricted to the light hours of the photocycle. Likewise, here in this study KmTx production was only observed during light hours (Fig. 7). This is consistent with previous observations that KmTx synthesis is light dependent (Adolf et al., 2020). Furthermore, production was delayed until approximately three hours after dawn (Fig. 7), coinciding with the timing of the peak percentage of G2 + M phase cells (Fig. 5F). This event marks the point at which cells have stopped entering G2 + M phase and begin to re-enter G1 phase. This timing suggests an association between KmTx production and G1 phase, which is further shown by a significant positive linear relationship between the percentage of G1 phase cells and the cellular KmTx content (Fig. 8A). In fact, our data suggests that KmTx production is strictly confined to G1 phase. The negative correlation and absence of correlation with S and G2 + M phases, respectively, is a strong indication that KmTx production in these phases has either ceased or at minimal levels (Fig. 8B and C).

Unfortunately, the phototrophic cultures grown in these experiments failed to produce detectable levels of KmTx. We suspect this is likely attributed to our choice in *K. veneficum* strain. Strain CCMP 2936 is known to not only produce KmTx 1 and 3, typically produced by Chesapeake Bay strains, but also KmTx 2 produced in strains isolated from south of the Chesapeake Bay (Van Wagoner et al., 2010). Furthermore, Fu et al. (2010) demonstrated, using CCMP 2936, that alterations in both CO_2 and P conditions in culture can lead to alterations in the level of and congener of KmTx

produced. Changes in karlotoxin cell quotas and congener produced have also been observed in other phototrophic cultures grown over many generations, with a trend of reduced karlotoxin cell quotas over time (Bachvaroff et al., 2009). These changes were reported as permanent as single cell re-isolation from the cultures did not return the original toxin phenotype. These past observations do not detract from our arguments, however, they do offer some insight into the source of variability observed in the experiments conducted here.

Conclusion

This study represents the first comparison of phototrophic and mixotrophic cell cycles in a HAB species, and for the first time reveals the discrete period during which KmTx synthesis occurs. Our data demonstrate that increases in growth rate for mixotrophic *K. veneficum* cultures are due solely to the shortening of G1 phase of the cell cycle. Furthermore, we show that KmTx synthesis occurs during light hours which coincide with G1 phase of the cell cycle. Unfortunately, the results from this study do not provide insight into the specific mechanisms by which mixotrophy shortens G1 phase. However, nutritional gating of S phase entry is a probable explanation. Nutritionally, cryptophyte prey are a significant source of N and P supplementation (Li et al., 2001), and can have significant effects on *K. veneficum* growth rates (Li et al., 1999; Adolf et al., 2006b). As well, a recent study has shown that prey nutritional quality (i.e. N:P stoichiometry) can have significant impacts on both growth and mixotrophy rates (Lin et al., 2017). Reciprocally, in the case of several phototrophic dinoflagellate species P

limitation has been observed to cause arrest in G1 phase, which would manifest as a lengthening of G1 phase duration (Lei and Lu, 2011; Zhang et al., 2014; Li et al., 2015; Li et al., 2016). Considering these past studies in concert with the data presented here, indicates that alterations in prey nutritional quality should lead to congruent changes in G1 phase durations. Furthermore, the relationship observed here between KmTx and G1 phase is only correlational. As such, experiments exploring the relationship between variability in G1 phase duration and cellular toxicity are necessary to determine if accumulation of cellular KmTx is related to the time spent in G1 phase. Such a relationship has been observed previously in *A. fundyense*, therefore we expect a similar relationship in *K. veneficum* (Taroncher-Oldenburg et al., 1999). The current findings will also be useful for future field studies aimed at measuring *in situ* growth rates and testing our proposed model of KmTx production in natural populations of *K. veneficum*. This study establishes that the diel phasing of the *K. veneficum* cell cycle is not lost under mixotrophic conditions, which is important as the methods for determining *in situ* growth rates rely upon the assumption that cell division is in phase with the natural L:D cycle (McDuff and Chisholm, 1982; Carpenter and Chang, 1988). Furthermore, the utility of our model for toxicity forecasting during development and maintenance of natural blooms would be minimalized if the cell cycle, KmTx biosynthesis cycle, and diurnal cycle were decoupled under mixotrophic growth conditions. Therefore, this study significantly contributes towards improved modeling and monitoring of *K. veneficum* blooms.

References

Adolf, J.E., Bachvaroff, T., Place, A.R., 2008. Can cryptophyte abundance trigger toxic *Karlodinium veneficum* blooms in eutrophic estuaries? Harmful Algae 8(1), 119-128.

Adolf, J.E., Bachvaroff, T.R., Deeds, J.R., Place, A.R., 2015. Ichthyotoxic *Karlodinium veneficum* (Ballantine) J Larsen in the Upper Swan River Estuary (Western Australia): Ecological conditions leading to a fish kill. Harmful Algae 48, 83-93.

Adolf, J.E., Bachvaroff, T.R., Krupatkina, D.N., Nonogaki, H., Brown, P.J.P., Lewitus, A.J., Harvey, H.R., Place, A.R., 2006a. Species specificity and potential roles of *Karlodinium micrum* toxin. African Journal of Marine Science 28(2), 415-419.

Adolf, J.E., Bachvaroff, T.R., Place, A.R., 2009. Environmental modulation of karlotoxin levels in strains of the cosmopolitan dinoflagellate, *Karlodinium veneficum* (Dinophyceae). J. Phycol. 45(1), 176-192.

Adolf, J.E., Parrow, M.W., Place, A.R., 2020. *Karlodinium veneficum*: Still blooming and toxic sixty-two years later, In: Subba Rao, V.D. (Ed.), Dinoflagellates. Nova Science Publishers, Inc., pp. 355 - 402.

Adolf, J.E., Stoecker, D.K., Harding, J.L.W., 2006b. The balance of autotrophy and heterotrophy during mixotrophic growth of *Karlodinium micrum* (Dinophyceae). Journal of Plankton Research 28(8), 737-751.

Bachvaroff, T.R., Adolf, J.E., Place, A.R., 2009. Strain variation in *Karlodinium veneficum* (Dinophyceae): Toxin profiles, pigments, and growth characteristics. Journal of Phycology 45(1), 137-153.

Bachvaroff, T.R., Adolf, J.E., Squier, A.H., Harvey, H.R., Place, A.R., 2008. Characterization and quantification of karlotoxins by liquid chromatography-mass spectrometry. Harmful Algae 7(4), 473-484.

Bhaud, Y., Salmon, J.-M., Soyer-Gobillard, M.-O., 1991. The complex cell cycle of the dinoflagellate protoctist *Crypthecodinium cohnii* as studied *in vivo* and by cytofluorimetry. Journal of Cell Science 100(3), 675-682.

Bruce, V.G., 1970. The biological clock in *Chlamydomonas reinhardi*. The Journal of Protozoology 17(2), 328-334.

Brunelle, S.A., Hazard, E.S., Sotka, E.E., Dolah, F.M.V., 2007. Characterization of a dinoflagellate cryptochrome blue-light receptor with a possible role in circadian control of the cell cycle. Journal of Phycology 43(3), 509-518.

Burkholder, J.M., Glibert, P.M., Skelton, H.M., 2008. Mixotrophy, a major mode of nutrition for harmful algal species in eutrophic waters. Harmful Algae 8(1), 77-93.

Calbet, A., Bertos, M., Fuentes-Grünewald, C., Alacid, E., Figueroa, R., Renom, B., Garcés, E., 2011. Intraspecific variability in *Karlodinium veneficum*: Growth rates, mixotrophy, and lipid composition. Harmful Algae 10(6), 654-667.

Carpenter, E.J., Chang, J., 1988. Species-specific phytoplankton growth rates via diel DNA synthesis cycles. I. Concept of the method. Marine Ecology Progress Series 43(1/2), 105-111.

Cetta, C.M., Anderson, D.M., 1990. Cell cycle studies of the dinoflagellates *Gonyaulax polyedra* Stein and *Gyrodinium uncatenum* Hulburt during asexual and sexual reproduction. Journal of Experimental Marine Biology and Ecology 135(1), 69-83.

Chisholm, S.W., 1981. Temporal patterns of cell division in unicellular algae. Canadian Bulletin of Fisheries and Aquatic Sciences 210, 150 - 181.

Chisholm, S.W., Brand, L.E., 1981. Persistence of cell division phasing in marine phytoplankton in continuous light after entrainment to light:dark cycles. Journal of Experimental Marine Biology and Ecology 51, 107 - 118.

Deeds, J.R., Kibler, S.R., Tester, P.A., Place, A.R., 2004. Geographic strain variation in toxin production in *Karlodinium micrum* (Dinophyceae) from southeastern United States, In: Steidinger, K.A., Landsberg, J.H., Tomas, C.R., Vargo, G.A. (Eds.), Harmful Algae 2002, IOC-UNESCO, Florida, pp. 145-147.

Deeds, J.R., Terlizzi, D.E., Adolf, J.E., Stoecker, D.K., Place, A.R., 2002. Toxic activity from cultures of *Karlodinium micrum* (=*Gyrodinium galatheanum*) (Dinophyceae)—a dinoflagellate associated with fish mortalities in an estuarine aquaculture facility. Harmful Algae 1(2), 169-189.

Edmunds, L.N., 1964. Replication of DNA and cell division in synchronously dividing cultures of *Euglena gracilis*. Science 145(3629), 266-268.

Eschbach, E., John, U., Reckermann, M., Cembella, A.D., Edvardsen, B., Medlin, L.K., 2005. Cell cycle dependent expression of toxicity by the ichthyotoxic prymnesiophyte *Chrysochromulina polylepis*. Aquatic Microbial Ecology 39(1), 85-95.

Fagin, E., Bravo, I., Garrido, J.L., Rodriguez, F., Figueroa, R.I., 2019. *Scrippsiella acuminata* versus *Scrippsiella ramonii*: A Physiological Comparison. Cytometry A 95(9), 985-996.

Figueroa, R.I., Dapena, C., Bravo, I., Cuadrado, A., 2015. The hidden sexuality of *Alexandrium minutum*: An example of overlooked sex in dinoflagellates. PLOS ONE 10(11), e0142667.

Figueroa, R.I., Garcés, E., Bravo, I., 2007. Comparative study of the life cycles of *Alexandrium tamutum* and *Alexandrium minutum* (Gonyaulacales, Dinophyceae) in culture. Journal of Phycology 43(5), 1039-1053.

Fu, F.X., Place, A.R., Garcia, N.S., Hutchins, D.A., 2010. CO2 and phosphate availability control the toxicity of the harmful bloom dinoflagellate *Karlodinium veneficum*. Aquatic Microbial Ecology 59(1), 55-65.

Gao, Y., Erdner, D.L., 2022. Dynamics of cell death across growth stages and the diel cycle in the dinoflagellate *Karenia brevis*. Journal of Eukaryotic Microbiology 69(1), e12874.

Garcés, E., Delgado, M., Masó, M., Camp, J., 1999. *In situ* growth rate and distribution of the ichthyotoxic dinoflagellate *Gyrodinium corsicum* Paulmier in an estuarine embayment (Alfacs Bay, NW Mediterranean Sea). Journal of Plankton Research 21(10), 1977-1991.

Garcés, E., Fernandez, M., Penna, A., Van Lenning, K., Gutierrez, A., Camp, J., Zapata, M., 2006. Characterization of NW Mediterranean *Karlodinium* spp. (Dinophyceae)

strains using morphological, molecular, chemical, and physiological methodologies. Journal of Phycology 42(5), 1096-1112.

Jeong, H.J., Yoo, Y.D., Kim, J.S., Seong, K.A., Kang, N.S., Kim, T.H., 2010. Growth, feeding and ecological roles of the mixotrophic and heterotrophic dinoflagellates in marine planktonic food webs. Ocean Science Journal 45(2), 65-91.

Jia, Y., Gao, H., Tong, M., Anderson, D.M., 2019. Cell cycle regulation of the mixotrophic dinoflagellate *Dinophysis acuminata*: Growth, photosynthetic efficiency and toxin production. Harmful Algae 89, 101672.

Kempton, J.W., Lewitus, A.J., Deeds, J.R., Law, J.M., Place, A.R., 2002. Toxicity of *Karlodinium micrum* (Dinophyceae) associated with a fish kill in a South Carolina brackish retention pond. Harmful Algae 1(2), 233-241.

Kremp, A., Parrow, M.W., 2006. Evidence for asexual resting cysts in the life cycle of the marine peridinoid dinoflagellate, *Scrippsiella hangoei*. Journal of Phycology 42(2), 400-409.

Lei, Q.-Y., Lu, S.-H., 2011. Molecular ecological responses of the dinoflagellate *Karenia mikimotoi* to phosphate stress. Harmful Algae 12, 39-45.

Leighfield, T.A., Van Dolah, F.M., 2001. Cell cycle regulation in a dinoflagellate, *Amphidinium operculatum*: identification of the diel entraining cue and a possible role for cyclic AMP. Journal of Experimental Marine Biology and Ecology 262(2), 177-197.

Li, A., Stoecker, D.K., Adolf, J.E., 1999. Feeding, pigmentation, photosynthesis and growth of the mixotrophic dinoflagellate *Gyrodinium galatheanum*. Aquatic Microbial Ecology 19(2), 163-176.

Li, A., Stoecker, D.K., Coats, D.W., 2000a. Mixotrophy in *Gyrodinium galatheanum* (DINOPHYCEAE): grazing responses to light intensity and inorganic nutrients*. Journal of Phycology 36(1), 33-45.

Li, A., Stoecker, D.K., Coats, D.W., 2000b. Spatial and temporal aspects of *Gyrodinium galatheanum* in Chesapeake Bay: distribution and mixotrophy. Journal of Plankton Research 22(11), 2105-2124.

Li, A., Stoecker, D.K., Coats, D.W., 2001. Use of the ‘food vacuole content ’method to estimate grazing by the mixotrophic dinoflagellate *Gyrodinium galatheanum* on cryptophytes. Journal of Plankton Research 23(3), 303-318.

Li, A., Stoecker, D.K., Coats, D.W., Adam, E.J., 1996. Ingestion of fluorescently labeled and phycoerythrin-containing prey by mixotrophic dinoflagellates. Aquatic Microbial Ecology 10(2), 139-147.

Li, M., Li, L., Shi, X., Lin, L., Lin, S., 2015. Effects of phosphorus deficiency and adenosine 5′-triphosphate (ATP) on growth and cell cycle of the dinoflagellate *Prorocentrum donghaiense*. Harmful Algae 47, 35-41.

Li, M., Shi, X., Guo, C., Lin, S., 2016. Phosphorus deficiency inhibits cell division but not growth in the dinoflagellate *Amphidinium carterae*. Front Microbiol 7, 826.

Lin, C.H., Accoroni, S., Glibert, P.M., 2017. *Karlodinium veneficum* feeding responses and effects on larvae of the eastern oyster *Crassostrea virginica* under variable nitrogen:phosphorus stoichiometry. Aquatic Microbial Ecology 79(2), 101-114.

López-Rosales, L., García-Camacho, F., Sánchez-Mirón, A., Chisti, Y., 2015. An optimal culture medium for growing *Karlodinium veneficum*: Progress towards a microalgal dinoflagellate-based bioprocess. Algal Research 10, 177-182.

McDuff, R.E., Chisholm, S.W., 1982. The calculation of *in situ* growth rates of phytoplankton populations from fractions of cells undergoing mitosis: A clarification. Limnology and Oceanography 27(4), 783-788.

Olson, R.J., Chisholm, S.W., 1983. Effects of photocycles and periodic ammonium supply on three marine phytoplankton species. I. Cell division patterns. Journal of Phycology 19, 522 - 528.

Olson, R.J., Chisholm, S.W., 1986. Effects of light and nitrogen limitation on the cell cycle of the dinoflagellate *Amphidinium carteri*. Journal of Plankton Research 8, 785 - 793.

Olson, R.J., Vaulot, D., Chisholm, S.W., 1986. Effects of environmental stresses on the cell cycle of two marine phytoplankton species. Plant Physiology 80, 918 - 925.

Pan, Y., Cembella, D.A., Quilliam, A.M., 1999. Cell cycle and toxin production in the benthic dinoflagellate *Prorocentrum lima*. Marine Biology 134(3), 541-549.

Parrow, M., Burkholder, J.M., Deamer, N.J., Zhang, C., 2002. Vegetative and sexual reproduction in *Pfiesteria* spp. (Dinophyceae) cultured with algal prey, and inferences for their classification. Harmful Algae 1(1), 5-33.

Place, A.R., Bowers, H.A., Bachvaroff, T.R., Adolf, J.E., Deeds, J.R., Sheng, J., 2012. *Karlodinium veneficum*—The little dinoflagellate with a big bite. Harmful Algae 14, 179-195.

Pokrzywinski, K.L., Tilney, C.L., Warner, M.E., Coyne, K.J., 2017. Cell cycle arrest and biochemical changes accompanying cell death in harmful dinoflagellates following exposure to bacterial algicide IRI-160AA. Sci Rep 7, 45102.

Salgado, P., Figueroa, R.I., Ramilo, I., Bravo, I., 2017. The life history of the toxic marine dinoflagellate *Protoceratium reticulatum* (Gonyaulacales) in culture. Harmful Algae 68, 67-81.

Sheng, J., Malkiel, E., Katz, J., Adolf, J.E., Place, A.R., 2010. A dinoflagellate exploits toxins to immobilize prey prior to ingestion. Proceedings of the National Academy of Sciences 107(5), 2082-2087.

Slater, M.L., Sharrow, S.O., Gart, J.J., 1977. Cell cycle of *Saccharomyces cerevisiae* in populations growing at different rates. Proceedings of the National Academy of Sciences 74(9), 3850-3854.

Smayda, T.J., 1997. Harmful algal blooms: Their ecophysiology and general relevance to phytoplankton blooms in the sea. Limnology and Oceanography 42(5part2), 1137-1153.

Stoecker, D.K., 1999. Mixotrophy among Dinoflagellates. Journal of Eukaryotic Microbiology 46(4), 397-401.

Stoecker, D.K., Hansen, P.J., Caron, D.A., Mitra, A., 2017. Mixotrophy in the Marine Plankton. Annual Review of Marine Science 9(1), 311-335.

Sweeney, B.M., Hastings, J.W., 1958. Rhythmic cell division in populations of *Gonyaulax polyedra**†‡. The Journal of Protozoology 5(3), 217-224.

Taroncher-Oldenburg, G., Kulis, D.M., Anderson, D.M., 1997. Toxin variability during the cell cycle of the dinoflagellate Alexandrium fundyense. Limnology and Oceanography 42(5part2), 1178-1188.

Taroncher-Oldenburg, G., Kulis, D.M., Anderson, D.M., 1999. Coupling of saxitoxin biosynthesis to the G1 phase of the cell cycle in the dinoflagellate *Alexandrin fundyense*: temperature and nutrient effects. Natural Toxins 7(5), 207-219.

Van Dolah, F.M., Leighfield, T.A., 1999. Diel phasing of the cell-cycle in the florida red tide Dinoflagellate, *Gymnodinium breve*. Journal of Phycology 35(6), 1404-1411.

Van Dolah, F.M., Leighfield, T.A., Kamykowski, D., Kirkpatrick, G.J., 2008. Cell cycle behavior of laboratory and field populations of the Florida red tide dinoflagellate, *Karenia brevis*. Continental Shelf Research 28(1), 11-23.

Van Wagoner, R.M., Deeds, J.R., Satake, M., Ribeiro, A.A., Place, A.R., Wright, J.L.C., 2008. Isolation and characterization of karlotoxin 1, a new amphipathic toxin from *Karlodinium veneficum*. Tetrahedron Letters 49(45), 6457-6461.

Van Wagoner, R.M., Deeds, J.R., Tatters, A.O., Place, A.R., Tomas, C.R., Wright, J.L.C., 2010. Structure and relative potency of several karlotoxins from *Karlodinium veneficum*. Journal of Natural Products 73(8), 1360-1365.

Watson, J.V., Chambers, S.H., Smith, P.J., 1987. A pragmatic approach to the analysis of DNA histograms with a definable G1 peak. Cytometry 8(1), 1-8.

Wetzel, R.G., Likens, G.E., 1991. Limnological Analyses, 2nd ed. Springer New York, NY, Springer-Verlag New York.

Zhang, C., Lin, S., Huang, L., Lu, W., Li, M., Liu, S., 2014. Suppression subtraction hybridization analysis revealed regulation of some cell cycle and toxin genes in *Alexandrium catenella* by phosphate limitation. Harmful Algae 39, 26-39.

Table 4.1 Agilent Jet System source and MRM parameters for MS/MS analysis

Parameter	
Gas Temp (ºC)	250
Gas Flow (L/min)	11
Nebulizer (psi)	45
Sheath Gas Temp (ºC)	350
Sheath Gas Flow (L/min)	12
Capillary Voltage (V)	6000
Nozzle Voltage (V)	2000

Table 4.2 MRM parameters for MS/MS analysis.

Parameter			
Dwell Time (ms)	100	Collision Energy (V)	120
Fragmentor Voltage (V)	135	Cell Accelerator Voltage (V)	7

MRM Scan Segments

Compound	**Polarity**	**Precursor Ion (m/z)**	**Product Ion (m/z)**
KmTx1 + Na	+	1361.8	937.6
KmTx1 + Na	+	1361.8	877.6
KmTx3 + Na	+	1347.8	937.6
KmTx3 + Na	+	1347.8	877.6

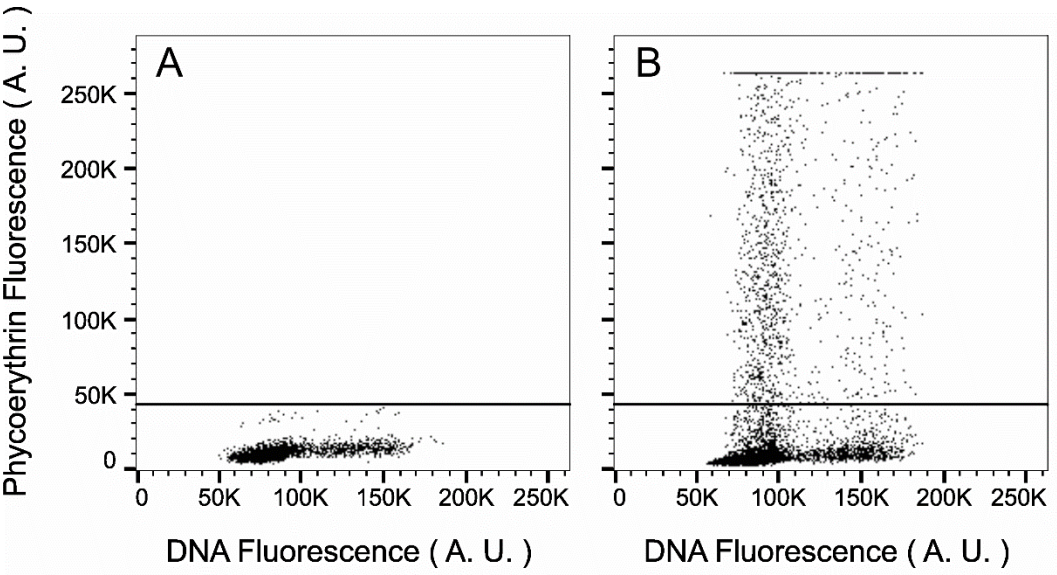

Figure 4.1 Phycoerythrin versus DNA fluorescence cytograms of (A) phototrophic and (B) mixotrophic samples. Solid lines indicate phycoerythrin threshold intensity for delineating cellular mixotrophic status. Data points and error bars represent mean and standard deviation of n = 3.

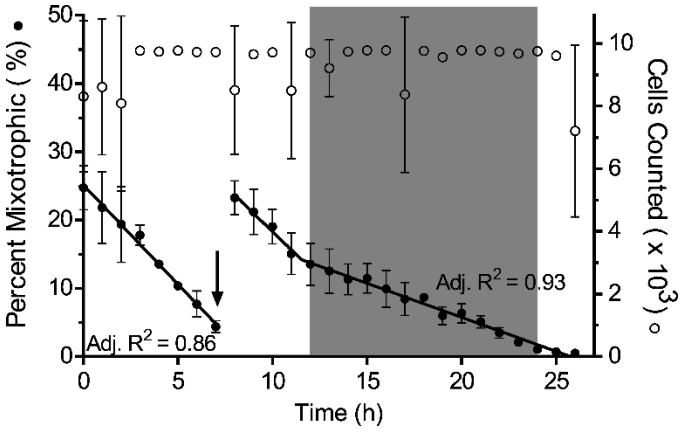

Figure 4.2 Percentage of mixotrophically active *K. veneficum* cells (●) during mid – log sampling and cells counted (○). Arrow indicates addition of prey cells following sample collection. Shaded regions represent dark hours. Data points and error bars represent mean and standard deviation of n = 3. Missing error bars are smaller than symbol.

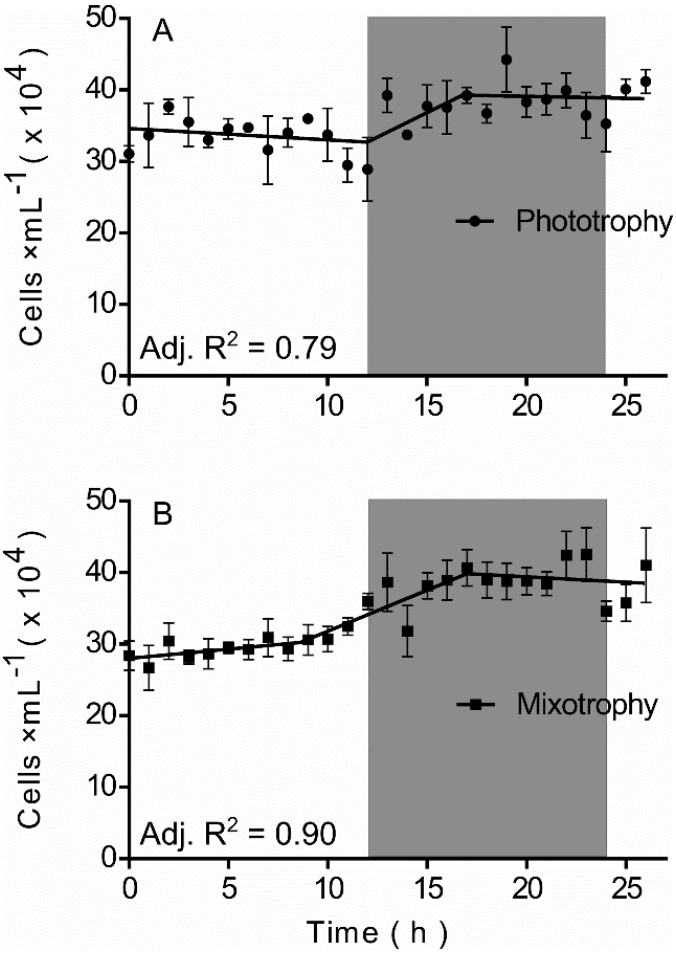

Figure 4.3 Hourly cell density for phototrophic (A) and mixotrophic (B) cultures. Shaded regions represent dark hours. Line represents least – squares piecewise linear regression. Data points and error bars represent mean and standard deviation of n = 3.

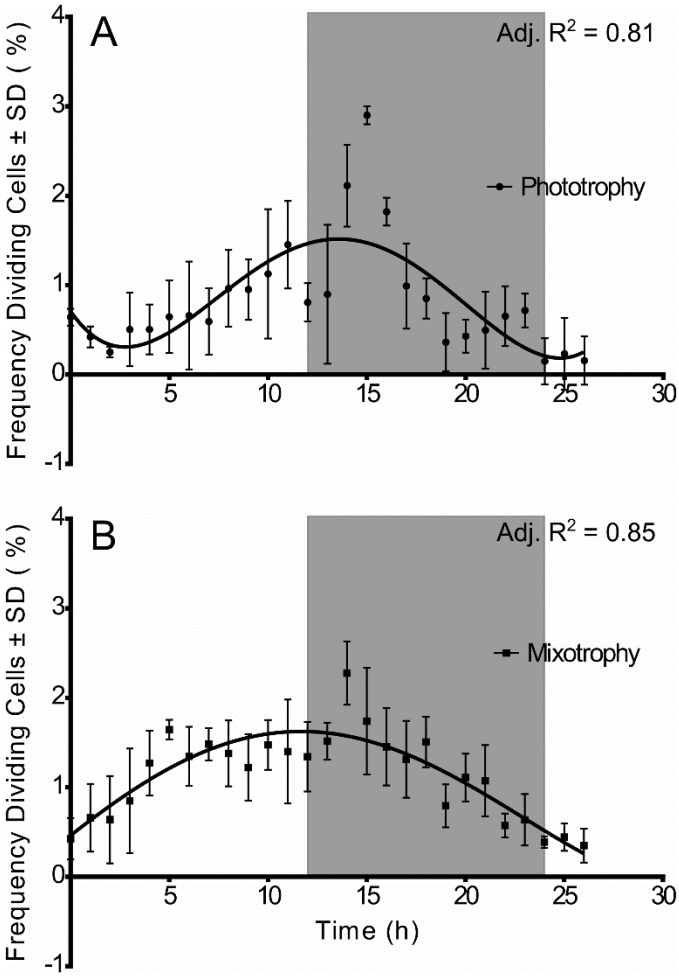

Figure 4.4 Mitotic indices for phototrophic (A) and mixotrophic (B) cultures. Shaded regions represent dark hours. Lines represent least – squares fourth order polynomial regressions. Data points and error bars represent mean and standard deviation of n = 3.

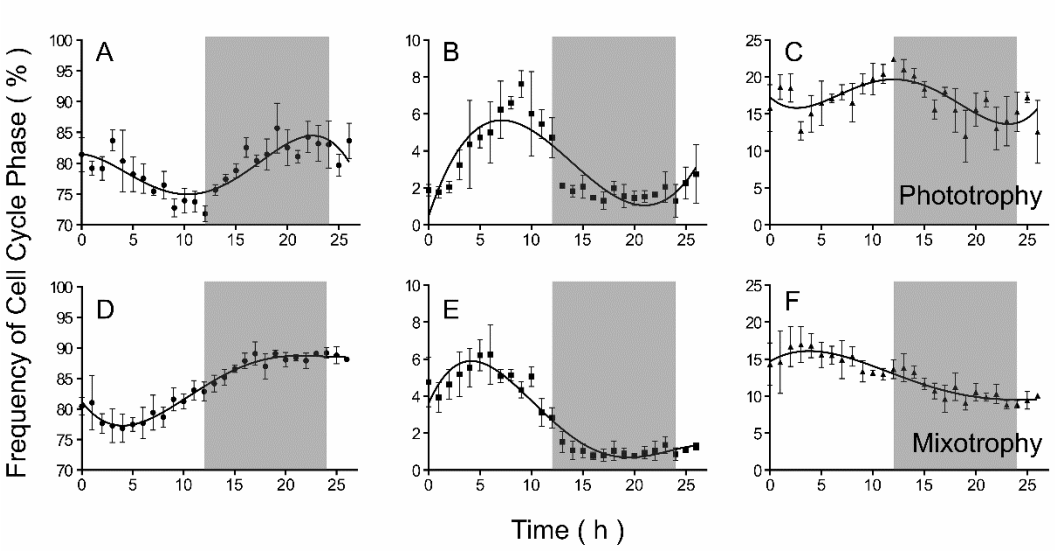

Figure 4.5 Cell cycle phase distribution diagrams for phototrophic (A, B, and C) and mixotrophic (D, E, and F) *K. veneficum* cultures. The frequency of G1 (circles), S (squares), and G2 + M (triangles) phases were measured hourly for 27 hours. Shaded regions represent dark hours. Lines represent least – squares fourth order polynomial regressions. Data points and error bars represent mean and standard deviation of n = 3.

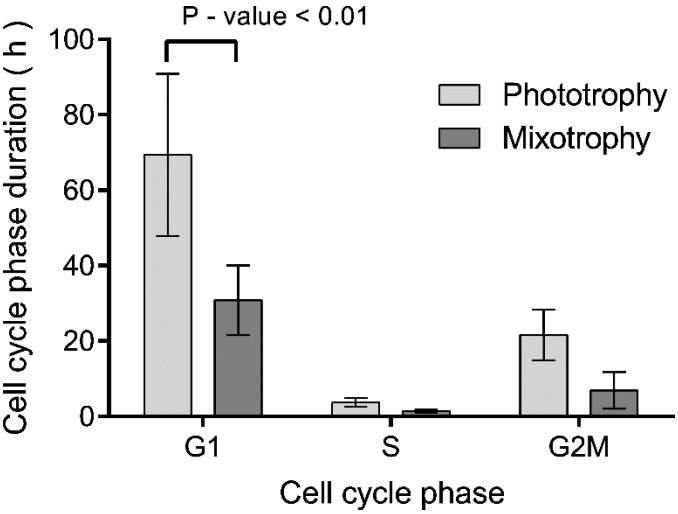

Figure 4.6 Cell cycle phase durations calculated for phototrophic (light gray) and mixotrophic (dark gray) *K. veneficum* cultures. Error bars represent standard deviation of n = 3.

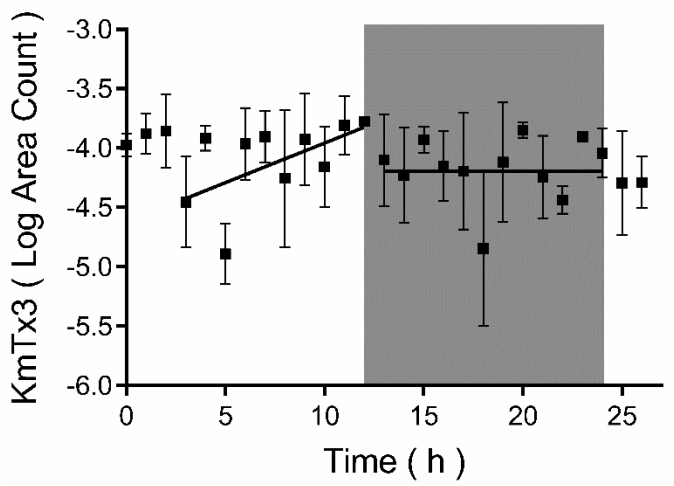

Figure 4.7 Hourly log transformed cellular karlotoxin content. Shaded regions represent dark hours. Lines represent least – squares linear regressions during light and dark hours. Data points and error bars represent mean and standard deviation of n = 3, with the exception of hours 0, 4, 12, 13, and 25 calculated from n = 2 and hour 23 calculated form n = 1.

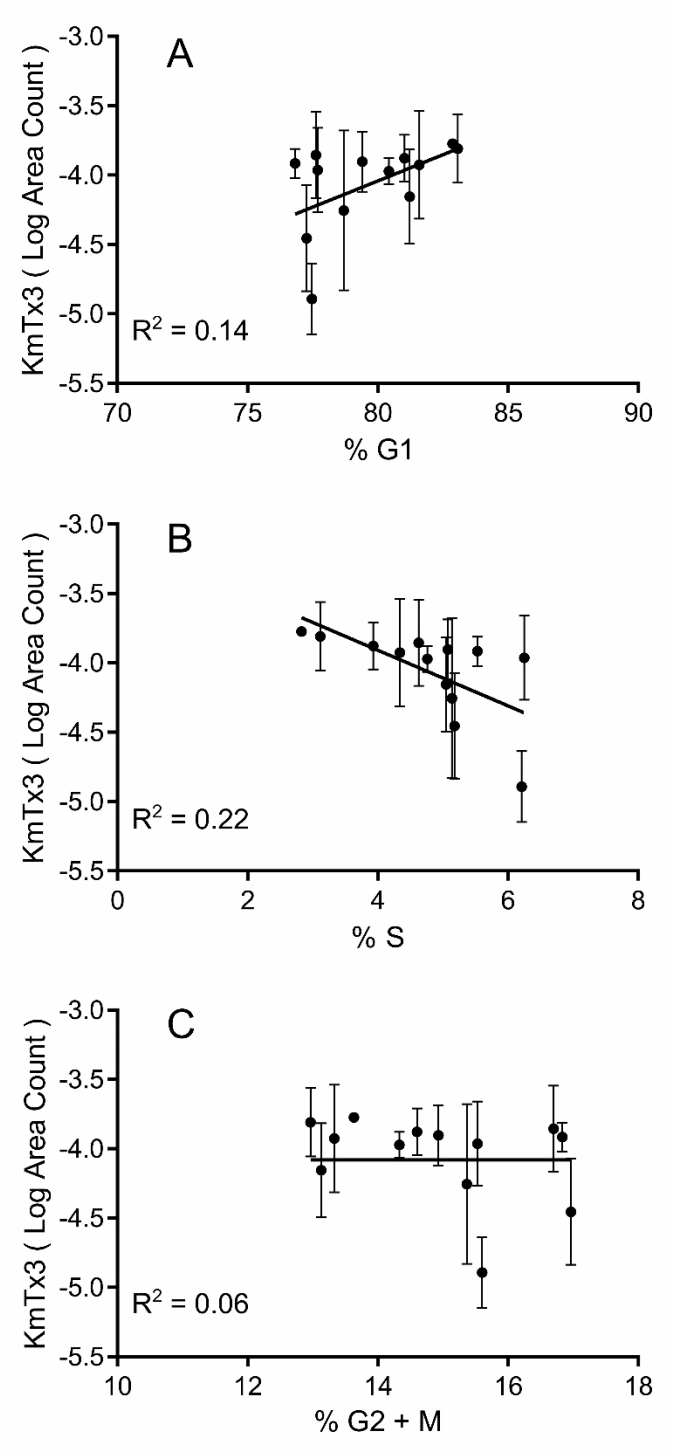

Figure 4.8 Correlational analysis of cell cycle phases and cellular karlotoxin content during light hours for G1 phase (A), S phase (B), and G2 + M phase (C). Lines represent least – squares linear regressions. Data points and error bars represent mean and standard deviation of n = 3, with the exception of hours 0, 4, 12, 13, and 25 calculated from n = 2 and hour 23 calculated form n = 1.

CHAPTER 5

SUMMARY AND FUTURE DIRECTIONS

The main goals of this work were to 1) optimize methodologies for measuring *in situ* growth rates, 2) test the model for predicting *K. veneficum* bloom toxicity described in chapter 1 section 1.4 in a laboratory setting, and 3) determine the impact of mixotrophic nutrition on cell cycle synchrony. These goals are important for public agencies and private stakeholders (e.g. aquaculture industry) as the tools described and optimized in chapters 2 and 3 offer an accessible means of monitoring aquatic systems and the observations from chapter 4 contribute to our existing knowledge of *K. veneficum* ecophysiology which will be invaluable for bloom modeling. As a whole the results presented in this dissertation will facilitate and guide future field studies, helping to improve coastal resource monitoring and management.

In chapter 2 we described the adaptation and optimization of image cytometry for quantification of nuclear DNA content and cell cycle analysis of *K. veneficum*. Experiments therein found the precision for measurement of nuclear DNA content to be influenced by several factors, which include selection of DNA staining fluorophore, selection of objective magnification power, and selection of sample staining buffer. The best precision (CV = 5.4 %) was achieved using DAPI to stain *K. veneficum* cells suspended in Milli Q – H_2O and image acquisition to be carried out using a lower powered objective (10x). In order to facilitate cell identification and selection the small *K. veneficum* cells, a 20x objective was chosen as the preferred objective, though this reduced the precision (CV = 6.6 %). Cell cycle analysis via image cytometry and flow

cytometry of *K. veneficum* cultures were in close agreement ($p = 0.93$), however, analysis of field samples were similar but not identical ($p < 0.001$). The results of this study indicate that image cytometry can be a useful tool for cell cycle analysis of microalgae in cultured and natural populations.

Chapter 3 sought to determine the t_d for four geographically distinct strains of *K. veneficum* at three relevant temperatures. The work presented in this chapter demonstrated that t_d for all strains was 1.6 ± 0.1 h, and corresponds to a nearly four – fold range of growth rates. Furthermore, the temperatures that yield this value and the highest growth rates varied amongst strains, corresponding to the average temperatures reported in their respective habitats of origin. This illustrates the existences of thermal ecotypes in the *K. veneficum* species. These findings will be useful in future field studies focused on elucidating the relationship between toxicity and *in situ* growth rates, and may benefit modeling and management efforts.

The work presented in chapter 4 detailed experiments to determine the influence of mixotrophic nutrition on cell cycle synchrony and determined correlations between karlotoxin synthesis and cell cycle phases. These experiments found cell cycle synchrony to be retained in mixotrophic cultures despite a two – fold increase in growth rate relative to strictly phototrophic cultures. The increased growth rate was attributed to a compression of the duration of the mixotrophic G1 phase to approximately half of that of the photorophic G1 phase. While durations of S phase and G2 + M phases were not significantly different between mixotrophic and phototrophic cultures. Toxin analysis revealed that karlotoxin synthesis occurred only during light hours and had a significant positive correlation with G1 phase cells and significant negative correlation with S phase

cells. Restriction of karlotoxin synthesis is consistent with the use of glycolate, a byproduct of photorespiration, as a precursor molecule.

Future directions

While the results from chapter 4 experiments support the proposed model for predicting *K. veneficum* bloom toxicity described in chapter 1 section 1.4, extrapolation to field populations should be done with caution. There is no guarantee that laboratory strains of *K. veneficum* are representative of populations in nature. In fact it is expected that all microalgae isolates maintained in laboratory cultures will over time come to genotypically and phenotypically deviate from the populations from which they were originally isolated (Lakeman et al 2009). Therefore, it is necessary to test this model in natural bloom populations of *K. veneficum*, and with the tools and observations described in chapters 1 and 2 this is achievable. Furthermore, the mechanism for how mixotrophic nutrition leads to shortened G1 phase durations remains speculative, but we suspect it is nutrient dependent. Therefore, a test of the effect of varying prey nutritional quality on G1 phase durations is necessary.

INTRODUCTION REFERENCES

Abbott, B.C., Ballantine, D., 1957. The toxin from *Gymnodinium veneficum* Ballantine. J. Mar. Biol. Assoc. U.K. 36(01), 169.

Adolf, J.E., Bachvaroff, T., Place, A.R., 2008. Can cryptophyte abundance trigger toxic *Karlodinium veneficum* blooms in eutrophic estuaries? Harmful Algae 8(1), 119-128.

Adolf, J.E., Bachvaroff, T.R., Deeds, J.R., Place, A.R., 2015. Ichthyotoxic *Karlodinium veneficum* (Ballantine) J Larsen in the Upper Swan River Estuary (Western Australia): Ecological conditions leading to a fish kill. Harmful Algae 48, 83-93.

Adolf, J.E., Bachvaroff, T.R., Krupatkina, D.N., Nonogaki, H., Brown, P.J.P., Lewitus, A.J., Harvey, H.R., Place, A.R., 2006a. Species specificity and potential roles of *Karlodinium micrum* toxin. Afr. J. Mar. Sci. 28(2), 415-419.

Adolf, J.E., Bachvaroff, T.R., Place, A.R., 2009. Environmental modulation of karlotoxin levels in strains of the cosmopolitan dinoflagellate, *Karlodinium veneficum* (Dinophyceae). J. Phycol. 45(1), 176-192.

Adolf, J.E., Krupatkina, D., Bachvaroff, T., Place, A.R., 2007. Karlotoxin mediates grazing by *Oxyrrhis marina* on strains of *Karlodinium veneficum*. Harmful Algae 6(3), 400-412.

Adolf, J.E., Parrow, M.W., Place, A.R., 2020. *Karlodinium veneficum*: Still blooming and toxic sixty-two years later, In: Subba Rao, V.D. (Ed.), Dinoflagellates. Nova Science Publishers, Inc., pp. 355 - 402.

Adolf, J.E., Stoecker, D.K., Harding, J.L.W., 2006b. The balance of autotrophy and heterotrophy during mixotrophic growth of *Karlodinium micrum* (Dinophyceae). J. Plankton Res. 28(8), 737-751.

Bachvaroff, T.R., Adolf, J.E., Place, A.R., 2009. Strain variation in *Karlodinium veneficum* (Dinophyceae): Toxin profiles, pigments, and growth characteristics. J. Phycol. 45(1), 137-153.

Bachvaroff, T.R., Adolf, J.E., Squier, A.H., Harvey, H.R., Place, A.R., 2008. Characterization and quantification of karlotoxins by liquid chromatography-mass spectrometry. Harmful Algae 7(4), 473-484.

Bainbridge, R., 1953. Studies on the Interrelationships of Zooplankton and Phytoplankton. J. Mar. Biol. Assoc. U.K. 32(2), 385-447.

Ballantine, D., 1956. Two new marine species of *Gymnodinium* isolated from the Plymouth area. J. Mar. Biol. Assoc. U.K. 35(3), 467-474.

Bergholtz, T., Daugbjerg, N., Moestrup, Ø., Fernández-Tejedor, M., 2006. On the identity of *Karlodinium veneficum* and description of *Karlodinium armiger* sp. nov. (dinophyceae), based on light and electron microscopy, nuclear-encoded lsu rdna, and pigment composition. J. Phycol. 42(1), 170-193.

Bjørnland, T., Tangen, K., 1979. Pigmentation and morphology of a marine *Gyrodinium* (DINOPHYCEAE) with a major carotenoid different from peridinin and fucoxanthin. J. Phycol. 15, 457 - 463.

Braarud, T., 1957. A red water organism from Walvis Bay. Galathea Report 1, 137 - 138.

Burkholder, J.M., Glibert, P.M., Skelton, H.M., 2008. Mixotrophy, a major mode of nutrition for harmful algal species in eutrophic waters. Harmful Algae 8(1), 77-93.

Cai, P., He, S., Zhou, C., Place, A.R., Haq, S., Ding, L., Chen, H., Jiang, Y., Guo, C., Xu, Y., Zhang, J., Yan, X., 2016. Two new karlotoxins found in *Karlodinium veneficum* (strain GM2) from the East China Sea. Harmful Algae 58, 66-73.

Calbet, A., Bertos, M., Fuentes-Grünewald, C., Alacid, E., Figueroa, R., Renom, B., Garcés, E., 2011. Intraspecific variability in *Karlodinium veneficum*: Growth rates, mixotrophy, and lipid composition. Harmful Algae 10(6), 654-667.

Carpenter, E.J., Chang, J., 1988. Species-specific phytoplankton growth rates via diel DNA synthesis cycles. I. Concept of the method. Mar. Ecol. Prog. Ser. 43(1/2), 105-111.

Copenhagen, W.J., Fisheries, S.A.D.O.S., 1953. The periodic mortality of fish in the walvis region: A phenomenon within the Benguela current. Division of Sea Fisheries.

Daugbjerg, N., Hansen, G., Larsen, J., Moestrup, Ø., 2000. Phylogeny of some of the major genera of dinoflagellates based on ultrastructure and partial LSU rDNA sequence data, including the erection of three new genera of unarmoured dinoflagellates. Phycologia 39(4), 302-317.

Deeds, J.R., Hoesch, R.E., Place, A.R., Kao, J.P., 2015. The cytotoxic mechanism of karlotoxin 2 (KmTx 2) from *Karlodinium veneficum* (Dinophyceae). Aquat. Toxicol. 159, 148-155.

Deeds, J.R., Kibler, S.R., Tester, P.A., Place, A.R., 2004. Geographic strain variation in toxin production in *Karlodinium micrum* (Dinophyceae) from southeastern United States, In: Steidinger, K.A., Landsberg, J.H., Tomas, C.R., Vargo, G.A. (Eds.), Harmful Algae 2002, IOC-UNESCO, Florida, pp. 145-147.

Deeds, J.R., Place, A.R., 2006. Sterol-specific membrane interactions with the toxins from *Karlodinium micrum* (Dinophyceae) — a strategy for self-protection? Afr. J. Mar. Sci. 28(2), 421-425.

Deeds, J.R., Reimschuessel, R., Place, A.R., 2006. Histopathological Effects in Fish Exposed to the Toxins from *Karlodinium micrum*. J. Aquat. Anim. Health 18(2), 136-148.

Deeds, J.R., Terlizzi, D.E., Adolf, J.E., Stoecker, D.K., Place, A.R., 2002. Toxic activity from cultures of *Karlodinium micrum* (=*Gyrodinium galatheanum*) (Dinophyceae)—a dinoflagellate associated with fish mortalities in an estuarine aquaculture facility. Harmful Algae 1(2), 169-189.

Delgado, M., Alcaraz, M., 1999. Interactions between red tide microalgae and herbivorous zooplankton: the noxious effects of *Gyrodinium corsicum* (Dinophyceae) on *Acartia grani* (Copepoda: Calanoida). J. Plankton Res. 21(12), 2361-2371.

Eschbach, E., John, U., Reckermann, M., Cembella, A.D., Edvardsen, B., Medlin, L.K., 2005. Cell cycle dependent expression of toxicity by the ichthyotoxic prymnesiophyte *Chrysochromulina polylepis*. Aquat. Microb. Ecol. 39(1), 85-95.

Fu, F.X., Place, A.R., Garcia, N.S., Hutchins, D.A., 2010. CO2 and phosphate availability control the toxicity of the harmful bloom dinoflagellate *Karlodinium veneficum*. Aquat. Microb. Ecol. 59(1), 55-65.

Garcés, E., Fernandez, M., Penna, A., Van Lenning, K., Gutierrez, A., Camp, J., Zapata, M., 2006. Characterization of NW Mediterranean *Karlodinium* spp. (Dinophyceae) strains using morphological, molecular, chemical, and physiological methodologies. J. Phycol. 42(5), 1096-1112.

Glibert, P.M., Terlizzi, D.E., 1999. Cooccurrence of elevated urea levels and dinoflagellate blooms in temperate estuarine aquaculture ponds. Appl. Environ. Microbiol. 65(12), 5594-5596.

Houdai, T., Matsuoka, S., Matsumori, N., Murata, M., 2004. Membrane-permeabilizing activities of amphidinol 3, polyene-polyhydroxy antifungal from a marine dinoflagellate. Biochim. Biophys. Acta 1667(1), 91-100.

Hulburt, E.M., 1957. The Taxonomy of Unarmored Dinophyceae of Shallow Embayments on Cape Cod, Massachusetts. Biological Bulletin 112(2), 196-219.

Jeong, H.J., Yoo, Y.D., Kim, J.S., Seong, K.A., Kang, N.S., Kim, T.H., 2010. Growth, feeding and ecological roles of the mixotrophic and heterotrophic dinoflagellates in marine planktonic food webs. Ocean Science Journal 45(2), 65-91.

Kempton, J.W., Lewitus, A.J., Deeds, J.R., Law, J.M., Place, A.R., 2002. Toxicity of *Karlodinium micrum* (Dinophyceae) associated with a fish kill in a South Carolina brackish retention pond. Harmful Algae 1(2), 233-241.

Krock, B., Busch, J.A., Tillmann, U., García-Camacho, F., Sánchez-Mirón, A., Gallardo-Rodríguez, J.J., López-Rosales, L., Andree, K.B., Fernández-Tejedor, M., Witt, M., Cembella, A.D., Place, A.R., 2017. LC-MS/MS Detection of karlotoxins reveals new variants in strains of the marine dinoflagellate *Karlodinium veneficum* from the Ebro Delta (NW Mediterranean). Mar. Drugs 15(12), 391.

Lakeman, M.B., von Dassow, P., Cattolico, R.A., 2009. The strain concept in phytoplankton ecology. Harmful Algae 8(5), 746-758.

Leadbeater, B., Dodge, J.D., 1966. The fine structure of *Woloszynskia micra* Sp.Nov., a new marine dinoflagellate. British Phycological Bulletin 3(1), 1-17.

Leadbeater, B., Dodge, J.D., 1967. An electron microscope study of nuclear and cell division in a dinoflagellate. Archiv für Mikrobiologie 57(3), 239-254.

Lewitus, A.J., Schmidt, L.B., Mason, L.J., Kempton, J.W., Wilde, S.B., Wolny, J.L., Williams, B.J., Hayes, K.C., Hymel, S.N., Keppler, C.J., Ringwood, A.H., 2003. Harmful Algal Blooms in South Carolina Residential and Golf Course Ponds. Population and Environment 24(5), 387-413.

Li, A., Stoecker, D.K., Adolf, J.E., 1999. Feeding, pigmentation, photosynthesis and growth of the mixotrophic dinoflagellate *Gyrodinium galatheanum*. Aquat. Microb. Ecol. 19(2), 163-176.

Li, A., Stoecker, D.K., Coats, D.W., 2000a. Mixotrophy in *Gyrodinium galatheanum* (DINOPHYCEAE): grazing responses to light intensity and inorganic nutrients*. J. Phycol. 36(1), 33-45.

Li, A., Stoecker, D.K., Coats, D.W., 2000b. Spatial and temporal aspects of *Gyrodinium galatheanum* in Chesapeake Bay: distribution and mixotrophy. J. Plankton Res. 22(11), 2105-2124.

Li, A., Stoecker, D.K., Coats, D.W., 2001. Use of the 'food vacuole content' method to estimate grazing by the mixotrophic dinoflagellate *Gyrodinium galatheanum* on cryptophytes. J. Plankton Res. 23(3), 303-318.

Li, A., Stoecker, D.K., Coats, D.W., Adam, E.J., 1996. Ingestion of fluorescently labeled and phycoerythrin-containing prey by mixotrophic dinoflagellates. Aquat. Microb. Ecol. 10(2), 139-147.

Lin, C.-H., Flynn, K.J., Mitra, A., Glibert, P.M., 2018. Simulating effects of variable stoichiometry and temperature on mixotrophy in the harmful dinoflagellate *Karlodinium veneficum*. Frontiers in Marine Science 5.

Lin, S., Jeng, C., Carpenter, E.J., 1995. Growth characteristics of phytoplankton determined by cell cycle proteins: PCNA immunostaining of *Dunaliella tertiolecta* (Chlorophyceae). J. Phycol. 31(3), 388-395.

Liu, J., Jiao, N., Hong, H., Luo, T., Cai, H., 2005. Proliferating cell nuclear antigen (PCNA) as a marker of cell proliferation in the marine dinoflagellate *Prorocentrum donghaiense* Lu and the green alga *Dunaliella salina* Teodoresco. J. Appl. Phycol. 17(4), 323-330.

Loeblich A, R., III, 1970. The amphiesma or dinoflagellate cell covering. Proceedings of the North American Paleontology Convention ; September 1969, Chicago.

Marshall, H.G., 1980. Seasonal phytoplankton composition in the lower Chesapeake Bay and old plantation Creek, Cape Charles, Virginia. Estuaries 3(3), 207-216.

Marshall, S.M., Orr, A.P., 1955. On the biology of *Calanus finmarchicus* VIII. Food uptake, assimilation and excretion in adult and Stage V *Calanus*. J. Mar. Biol. Assoc. U.K. 34(3), 495-529.

McDuff, R.E., Chisholm, S.W., 1982. The calculation of *in situ* growth rates of phytoplankton populations from fractions of cells undergoing mitosis: A clarification. Limnol. Oceanogr. 27(4), 783-788.

Morsy, N., Houdai, T., Konoki, K., Matsumori, N., Oishi, T., Murata, M., 2008. Effects of lipid constituents on membrane-permeabilizing activity of amphidinols. Bioorganic & Medicinal Chemistry 16(6), 3084-3090.

Nielsen, M.V., 1993. Toxic effect of the marine dinoflagellate *Gymnodinium galatheanum* on juvenile cod Gadus morhua. Mar. Ecol. Prog. Ser. 95(3), 273-277.

Nielsen, M.V., 1996. Growth and chemical composition of the toxic dinoflagellate *Gymnodinium galatheanum* in relation to irradiance, temperature and salinity. Mar. Ecol. Prog. Ser. 136, 205 - 211.

Nielsen, M.V., Strømgren, T., 1991. Shell growth response of mussels (*Mytilus edulis*) exposed to toxic microalgae. Mar. Biol. 108(2), 263-267.

Pan, Y., Cembella, D.A., Quilliam, A.M., 1999. Cell cycle and toxin production in the benthic dinoflagellate *Prorocentrum lima*. Mar. Biol. 134(3), 541-549.

Paul, G.K., Matsumori, N., Murata, M., Tachibana, K., 1995. Isolation and chemical structure of amphidinol 2, a potent hemolytic compound from marine dinoflagellate *Amphidinium klebsii*. Tetrahedron Lett. 36(35), 6279-6282.

Paulmier, G., Berland, B., Billard, C., Nezan, E., 1995. *Gyrodinium corsicum* nov. sp. (Gymnodiniales, Dinophycées), organisme responsable d'une ‘‘eau verte’’ dans l'étang marin de Diana (Corse), en avril 1994. Cryptogamie Algol. 16, 77.

Peng, J., Place, A.R., Yoshida, W., Anklin, C., Hamann, M.T., 2010. Structure and Absolute Configuration of Karlotoxin-2, an Ichthyotoxin from the Marine Dinoflagellate *Karlodinium veneficum*. J. Am. Chem. Soc. 132(10), 3277-3279.

Place, A.R., Bowers, H.A., Bachvaroff, T.R., Adolf, J.E., Deeds, J.R., Sheng, J., 2012. *Karlodinium veneficum*—The little dinoflagellate with a big bite. Harmful Algae 14, 179-195.

Richardson, T.L., Pinckney, J.L., Walker, E.A., Marshalonis, D.M., 2006. Photopigment radiolabelling as a tool for determining *in situ* growth rates of the toxic dinoflagellate *Karenia brevis* (Dinophyceae). Eur. J. Phycol. 41(4), 415-423.

Rivkin, R.B., Seliger, H.H., 1981. Liquid scintillation counting for 14C uptake of single algal cells isolated from natural samples. Limnol. Oceanogr. 26(4), 780-785.

Sheng, J., Malkiel, E., Katz, J., Adolf, J.E., Place, A.R., 2010. A dinoflagellate exploits toxins to immobilize prey prior to ingestion. Proceedings of the National Academy of Sciences 107(5), 2082-2087.

Smayda, T.J., 1997. Harmful algal blooms: Their ecophysiology and general relevance to phytoplankton blooms in the sea. Limnol. Oceanogr. 42(5part2), 1137-1153.

Steemann Nielsen, E., Jensen, E.A., 1957. Primary oceanic production. The autorophic production of organic matter in the oceans. Galathea Report 1, 49 - 136.

Stoecker, D.K., 1999. Mixotrophy among Dinoflagellates. J. Eukaryot. Microbiol. 46(4), 397-401.

Swasono, R.T., Mouri, R., Morsy, N., Matsumori, N., Oishi, T., Murata, M., 2010. Sterol effect on interaction between amphidinol 3 and liposomal membrane as evidenced by surface plasmon resonance. Bioorganic & Medicinal Chemistry Letters 20(7), 2215-2218.

Taroncher-Oldenburg, G., Kulis, D.M., Anderson, D.M., 1997. Toxin variability during the cell cycle of the dinoflagellate *Alexandrium fundyense*. Limnol. Oceanogr. 42(5part2), 1178-1188.

Van Wagoner, R.M., Deeds, J.R., Satake, M., Ribeiro, A.A., Place, A.R., Wright, J.L.C., 2008. Isolation and characterization of karlotoxin 1, a new amphipathic toxin from *Karlodinium veneficum*. Tetrahedron Lett. 49(45), 6457-6461.

Videau, C., 1987. Primary production and physiological state of phytoplankton at the Ushant tidal front (west coast of Brittany, France). Mar. Ecol. Prog. Ser. 35(1/2), 141-151.

Waggett, R.J., Tester, P.A., Place, A.R., 2008. Anti-grazing properties of the toxic dinoflagellate *Karlodinium veneficum* during predator–prey interactions with the copepod *Acartia tonsa*. Mar. Ecol. Prog. Ser. 366, 31-42.

Waters, A.L., Oh, J., Place, A.R., Hamann, M.T., 2015. Stereochemical Studies of the Karlotoxin Class Using NMR Spectroscopy and DP4 Chemical-Shift Analysis: Insights into their Mechanism of Action. Angewandte Chemie 127(52), 15931-15936.

Yang, H., Hu, Z., Shang, L., Deng, Y., Tang, Y.Z., 2020. A strain of the toxic dinoflagellate *Karlodinium veneficum* isolated from the East China Sea is an omnivorous phagotroph. Harmful Algae 93, 101775.